US010335072B2

(12) **United States Patent**
Al-Ali et al.

(10) **Patent No.: US 10,335,072 B2**
(45) **Date of Patent: *Jul. 2, 2019**

(54) **PHYSIOLOGICAL MONITOR**

(71) Applicant: **Masimo Corporation**, Irvine, CA (US)

(72) Inventors: **Ammar Al-Ali**, Tustin, CA (US); **Mohamed K. Diab**, Ladera Ranch, CA (US); **Massi E. Kiani**, Laguna Niguel, CA (US); **Robert James Kopotic**, Jamul, CA (US); **David Tobler**, Westminster, CO (US)

(73) Assignee: **MASIMO CORPORATION**, Irvine, CA (US)

(*) Notice: Subject to any disclaimer, the term of this patent is extended or adjusted under 35 U.S.C. 154(b) by 0 days.

This patent is subject to a terminal disclaimer.

(21) Appl. No.: **15/351,181**

(22) Filed: **Nov. 14, 2016**

(65) **Prior Publication Data**

US 2017/0188919 A1 Jul. 6, 2017

Related U.S. Application Data

(63) Continuation of application No. 14/275,691, filed on May 12, 2014, now Pat. No. 9,492,110, which is a continuation of application No. 13/745,590, filed on Jan. 18, 2013, now Pat. No. 8,721,541, which is a continuation of application No. 11/417,931, filed on

(Continued)

(51) **Int. Cl.**

A61B 5/1455	(2006.01)
A61B 5/00	(2006.01)
A61B 5/0205	(2006.01)
A61B 5/1459	(2006.01)

(Continued)

(52) **U.S. Cl.**

CPC ***A61B 5/14551*** (2013.01); ***A61B 5/0205*** (2013.01); ***A61B 5/1459*** (2013.01); ***A61B 5/6814*** (2013.01); ***A61B 5/6815*** (2013.01); ***A61B 5/6819*** (2013.01); ***A61B 5/6825*** (2013.01); ***A61B 5/6826*** (2013.01); ***A61B 5/6829*** (2013.01); ***A61B 5/6838*** (2013.01); ***A61B 5/742*** (2013.01); ***A61B 5/746*** (2013.01); *A61B 5/02416* (2013.01);

(Continued)

(58) **Field of Classification Search**

None

See application file for complete search history.

(56) **References Cited**

U.S. PATENT DOCUMENTS

3,704,706 A 12/1972 Herczfeld et al.
3,847,483 A 11/1974 Shaw et al.

(Continued)

FOREIGN PATENT DOCUMENTS

EP 0 555 553 8/1993
EP 0 807 402 11/1997

(Continued)

OTHER PUBLICATIONS

US 8,845,543 B2, 09/2014, Diab et al. (withdrawn)

(Continued)

Primary Examiner — Etsub D Berhanu

(74) *Attorney, Agent, or Firm* — Knobbe, Martens, Olson & Bear, LLP

(57) **ABSTRACT**

A patient monitor has multiple sensors adapted to attach to tissue sites of a living subject. The sensors generate sensor signals that are responsive to at least two wavelengths of optical radiation after attenuation by pulsatile blood within the tissue sites.

15 Claims, 25 Drawing Sheets

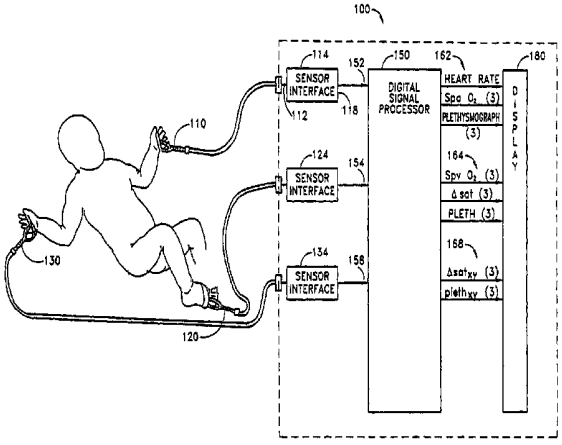

Related U.S. Application Data

May 3, 2006, now Pat. No. 8,364,223, which is a continuation of application No. 11/104,720, filed on Apr. 13, 2005, now Pat. No. 7,761,128, which is a continuation of application No. 10/668,487, filed on Sep. 22, 2003, now Pat. No. 6,898,452, which is a continuation of application No. 10/026,013, filed on Dec. 21, 2001, now Pat. No. 6,714,804, which is a continuation of application No. 09/323,176, filed on May 27, 1999, now Pat. No. 6,334,065.

(60) Provisional application No. 60/087,802, filed on Jun. 3, 1998.

(51) **Int. Cl.**
A61B 5/024 (2006.01)
A61M 16/00 (2006.01)

(52) **U.S. Cl.**
CPC *A61M 16/00* (2013.01); *A61M 16/021* (2017.08); *A61M 2230/205* (2013.01)

(56) **References Cited**

U.S. PATENT DOCUMENTS

4,109,643 A 8/1978 Bond et al.
4,446,715 A 5/1984 Bailey
4,653,498 A 3/1987 New, Jr. et al.
4,854,699 A 8/1989 Edgar, Jr.
4,869,253 A 9/1989 Craig, Jr. et al.
4,911,167 A 3/1990 Corenman et al.
4,927,264 A 5/1990 Shiga et al.
4,934,372 A 6/1990 Corenman et al.
4,960,128 A 10/1990 Gordon et al.
4,964,408 A 10/1990 Hink et al.
5,020,516 A 6/1991 Biondi et al.
5,041,187 A 8/1991 Hink et al.
5,069,213 A 12/1991 Polczynski
5,078,136 A 1/1992 Stone et al.
5,163,438 A 11/1992 Gordon et al.
5,218,962 A 6/1993 Mannheimer et al.
5,233,991 A 8/1993 Wright
5,251,632 A 10/1993 Delpy
5,253,645 A 10/1993 Friedman et al.
5,273,036 A 12/1993 Kronberg et al.
5,308,919 A 5/1994 Minnich
5,319,355 A 6/1994 Russek
5,337,744 A 8/1994 Branigan
5,341,805 A 8/1994 Stavridi et al.
D353,195 S 12/1994 Savage et al.
D353,196 S 12/1994 Savage et al.
5,377,676 A 1/1995 Vari et al.
5,385,144 A 1/1995 Yamanishi et al.
5,396,893 A 3/1995 Oberg et al.
D359,546 S 6/1995 Savage et al.
5,431,170 A 7/1995 Mathews
D361,840 S 8/1995 Savage et al.
D362,063 S 9/1995 Savage et al.
5,448,991 A 9/1995 Polson et al.
5,448,999 A 9/1995 Teare et al.
5,452,717 A 9/1995 Branigan et al.
D363,120 S 10/1995 Savage et al.
5,456,252 A 10/1995 Vari et al.
5,479,934 A 1/1996 Imran
5,482,036 A 1/1996 Diab et al.
5,490,505 A 2/1996 Diab et al.
5,494,043 A 2/1996 O'Sullivan et al.
5,533,511 A 7/1996 Kaspari et al.
5,534,851 A 7/1996 Russek
5,542,421 A 8/1996 Erdman
5,561,275 A 10/1996 Savage et al.
5,562,002 A 10/1996 Lalin
5,575,284 A 11/1996 Athan et al.
5,590,649 A 1/1997 Caro et al.
5,602,924 A 2/1997 Durand et al.
5,632,272 A 5/1997 Diab et al.
5,638,816 A 6/1997 Kiani-Azarbayjany et al.
5,638,818 A 6/1997 Diab et al.
5,645,440 A 7/1997 Tobler et al.
5,647,359 A 7/1997 Kohno et al.
5,682,877 A 11/1997 Mondry
5,685,299 A 11/1997 Diab et al.
5,715,816 A 2/1998 Mainiero et al.
D393,830 S 4/1998 Tobler et al.
5,743,261 A 4/1998 Mainiero et al.
5,743,262 A 4/1998 Lepper, Jr. et al.
5,743,857 A 4/1998 Shinoda et al.
5,758,644 A 6/1998 Diab et al.
5,760,910 A 6/1998 Lepper, Jr. et al.
5,769,785 A 6/1998 Diab et al.
5,782,757 A 7/1998 Diab et al.
5,785,659 A 7/1998 Caro et al.
5,791,347 A 8/1998 Flaherty et al.
5,810,734 A 9/1998 Caro et al.
5,823,950 A 10/1998 Diab et al.
5,827,181 A 10/1998 Dias et al.
5,827,196 A 10/1998 Yeo et al.
5,830,131 A 11/1998 Caro et al.
5,830,135 A 11/1998 Bosque et al.
5,833,618 A 11/1998 Caro et al.
5,846,190 A 12/1998 Woehrle
5,860,919 A 1/1999 Kiani-Azarbayjany et al.
5,876,335 A 3/1999 Handy et al.
5,890,929 A 4/1999 Mills et al.
5,904,654 A 5/1999 Wohltmann et al.
5,919,134 A 7/1999 Diab
5,934,925 A 8/1999 Tobler et al.
5,940,182 A 8/1999 Lepper, Jr. et al.
5,954,053 A 9/1999 Chance et al.
5,987,343 A 11/1999 Kinast
5,995,855 A 11/1999 Kiani et al.
5,997,343 A 12/1999 Mills et al.
6,002,952 A 12/1999 Diab et al.
6,011,986 A 1/2000 Diab et al.
6,027,452 A 2/2000 Flaherty et al.
6,036,642 A 3/2000 Diab et al.
6,045,509 A 4/2000 Caro et al.
6,067,462 A 5/2000 Diab et al.
6,081,735 A 6/2000 Diab et al.
6,083,172 A 7/2000 Baker, Jr. et al.
6,088,607 A 7/2000 Diab et al.
6,094,592 A 7/2000 Yorkey et al.
6,110,522 A 8/2000 Lepper, Jr. et al.
6,122,535 A 9/2000 Kaestle et al.
6,124,597 A 9/2000 Shehada et al.
6,128,521 A 10/2000 Marro et al.
6,129,675 A 10/2000 Jay
6,144,868 A 11/2000 Parker
6,151,516 A 11/2000 Kiani-Azarbayjany et al.
6,152,754 A 11/2000 Gerhardt et al.
6,157,850 A 12/2000 Diab et al.
6,165,005 A 12/2000 Mills et al.
6,184,521 B1 2/2001 Coffin et al.
6,206,830 B1 3/2001 Diab et al.
6,229,856 B1 5/2001 Diab et al.
6,232,609 B1 5/2001 Snyder et al.
6,236,872 B1 5/2001 Diab et al.
6,241,683 B1 6/2001 Macklem et al.
6,253,097 B1 6/2001 Aronow et al.
6,256,523 B1 7/2001 Diab et al.
6,263,222 B1 7/2001 Diab et al.
6,278,522 B1 8/2001 Lepper, Jr. et al.
6,280,213 B1 8/2001 Tobler et al.
6,285,896 B1 9/2001 Tobler et al.
6,301,493 B1 10/2001 Marro et al.
6,308,089 B1 10/2001 von der Ruhr et al.
6,317,627 B1 11/2001 Ennen et al.
6,321,100 B1 11/2001 Parker
6,325,761 B1 12/2001 Jay
6,334,065 B1 12/2001 Al-Ali et al.
6,343,224 B1 1/2002 Parker
6,349,228 B1 2/2002 Kiani et al.
6,360,114 B1 3/2002 Diab et al.
6,368,283 B1 4/2002 Xu et al.

(56) **References Cited**

U.S. PATENT DOCUMENTS

6,371,921 B1 4/2002 Caro et al.
6,377,829 B1 4/2002 Al-Ali
6,388,240 B2 5/2002 Schulz et al.
6,397,091 B2 5/2002 Diab et al.
6,430,437 B1 8/2002 Marro
6,430,525 B1 8/2002 Weber et al.
6,463,311 B1 10/2002 Diab
6,470,199 B1 10/2002 Kopotic et al.
6,501,975 B2 12/2002 Diab et al.
6,505,059 B1 1/2003 Kollias et al.
6,515,273 B2 2/2003 Al-Ali
6,519,487 B1 2/2003 Parker
6,525,386 B1 2/2003 Mills et al.
6,526,300 B1 2/2003 Kiani et al.
6,541,756 B2 4/2003 Schulz et al.
6,542,764 B1 4/2003 Al-Ali et al.
6,580,086 B1 6/2003 Schulz et al.
6,584,336 B1 6/2003 Ali et al.
6,595,316 B2 7/2003 Cybulski et al.
6,597,932 B2 7/2003 Tian et al.
6,597,933 B2 7/2003 Kiani et al.
6,606,511 B1 8/2003 Ali et al.
6,632,181 B2 10/2003 Flaherty et al.
6,639,668 B1 10/2003 Trepagnier
6,640,116 B2 10/2003 Diab
6,643,530 B2 11/2003 Diab et al.
6,650,917 B2 11/2003 Diab et al.
6,654,624 B2 11/2003 Diab et al.
6,658,276 B2 12/2003 Kiani et al.
6,661,161 B1 12/2003 Lanzo et al.
6,671,531 B2 12/2003 Al-Ali et al.
6,678,543 B2 1/2004 Diab et al.
6,684,090 B2 1/2004 Ali et al.
6,684,091 B2 1/2004 Parker
6,697,656 B1 2/2004 Al-Ali
6,697,657 B1 2/2004 Shehada et al.
6,697,658 B2 2/2004 Al-Ali
RE38,476 E 3/2004 Diab et al.
6,699,194 B1 3/2004 Diab et al.
6,714,804 B2 3/2004 Al-Ali et al.
RE38,492 E 4/2004 Diab et al.
6,721,582 B2 4/2004 Trepagnier et al.
6,721,585 B1 4/2004 Parker
6,725,075 B2 4/2004 Al-Ali
6,728,560 B2 4/2004 Kollias et al.
6,735,459 B2 5/2004 Parker
6,745,060 B2 6/2004 Diab et al.
6,760,607 B2 7/2004 Al-Ali
6,770,028 B1 8/2004 Ali et al.
6,771,994 B2 8/2004 Kiani et al.
6,792,300 B1 9/2004 Diab et al.
6,813,511 B2 11/2004 Diab et al.
6,816,741 B2 11/2004 Diab
6,822,564 B2 11/2004 Al-Ali
6,826,419 B2 11/2004 Diab et al.
6,830,711 B2 12/2004 Mills et al.
6,850,787 B2 2/2005 Weber et al.
6,850,788 B2 2/2005 Al-Ali
6,852,083 B2 2/2005 Caro et al.
6,861,639 B2 3/2005 Al-Ali
6,898,452 B2 5/2005 Al-Ali et al.
6,920,345 B2 7/2005 Al-Ali et al.
6,931,268 B1 8/2005 Kiani-Azarbayjany et al.
6,934,570 B2 8/2005 Kiani et al.
6,939,305 B2 9/2005 Flaherty et al.
6,943,348 B1 9/2005 Coffin, IV
6,950,687 B2 9/2005 Al-Ali
6,961,598 B2 11/2005 Diab
6,970,792 B1 11/2005 Diab
6,979,812 B2 12/2005 Al-Ali
6,985,764 B2 1/2006 Mason et al.
6,993,371 B2 1/2006 Kiani et al.
6,996,427 B2 2/2006 Ali et al.
6,999,904 B2 2/2006 Weber et al.
7,003,338 B2 2/2006 Weber et al.
7,003,339 B2 2/2006 Diab et al.
7,015,451 B2 3/2006 Dalke et al.
7,024,233 B2 4/2006 Ali et al.
7,027,849 B2 4/2006 Al-Ali
7,030,749 B2 4/2006 Al-Ali
7,039,449 B2 5/2006 Al-Ali
7,041,060 B2 5/2006 Flaherty et al.
7,044,918 B2 5/2006 Diab
7,048,687 B1 5/2006 Reuss et al.
7,067,893 B2 6/2006 Mills et al.
7,096,052 B2 8/2006 Mason et al.
7,096,054 B2 8/2006 Abdul-Hafiz et al.
7,132,641 B2 11/2006 Schulz et al.
7,142,901 B2 11/2006 Kiani et al.
7,149,561 B2 12/2006 Diab
7,186,966 B2 3/2007 Al-Ali
7,190,261 B2 3/2007 Al-Ali
7,215,984 B2 5/2007 Diab et al.
7,215,986 B2 5/2007 Diab et al.
7,221,971 B2 5/2007 Diab et al.
7,225,006 B2 5/2007 Al-Ali et al.
7,225,007 B2 5/2007 Al-Ali et al.
RE39,672 E 6/2007 Shehada et al.
7,239,905 B2 7/2007 Kiani-Azarbayjany et al.
7,245,953 B1 7/2007 Parker
7,254,429 B2 8/2007 Schurman et al.
7,254,431 B2 8/2007 Al-Ali et al.
7,254,433 B2 8/2007 Diab et al.
7,254,434 B2 8/2007 Schulz et al.
7,272,425 B2 9/2007 Al-Ali
7,274,955 B2 9/2007 Kiani et al.
D554,263 S 10/2007 Al-Ali
7,280,858 B2 10/2007 Al-Ali et al.
7,289,835 B2 10/2007 Mansfield et al.
7,292,883 B2 11/2007 De Felice et al.
7,295,866 B2 11/2007 Al-Ali
7,328,053 B1 2/2008 Diab et al.
7,332,784 B2 2/2008 Mills et al.
7,340,287 B2 3/2008 Mason et al.
7,341,559 B2 3/2008 Schulz et al.
7,343,186 B2 3/2008 Lamego et al.
D566,282 S 4/2008 Al-Ali et al.
7,355,512 B1 4/2008 Al-Ali
7,356,365 B2 4/2008 Schurman
7,371,981 B2 5/2008 Abdul-Hafiz
7,373,193 B2 5/2008 Al-Ali et al.
7,373,194 B2 5/2008 Weber et al.
7,376,453 B1 5/2008 Diab et al.
7,377,794 B2 5/2008 Al-Ali et al.
7,377,899 B2 5/2008 Weber et al.
7,383,070 B2 6/2008 Diab et al.
7,415,297 B2 8/2008 Al-Ali et al.
7,428,432 B2 9/2008 Ali et al.
7,438,683 B2 10/2008 Al-Ali et al.
7,440,787 B2 10/2008 Diab
7,454,240 B2 11/2008 Diab et al.
7,467,002 B2 12/2008 Weber et al.
7,469,157 B2 12/2008 Diab et al.
7,471,969 B2 12/2008 Diab et al.
7,471,971 B2 12/2008 Diab et al.
7,483,729 B2 1/2009 Al-Ali et al.
7,483,730 B2 1/2009 Diab et al.
7,489,958 B2 2/2009 Diab et al.
7,496,391 B2 2/2009 Diab et al.
7,496,393 B2 2/2009 Diab et al.
D587,657 S 3/2009 Al-Ali et al.
7,499,741 B2 3/2009 Diab et al.
7,499,835 B2 3/2009 Weber et al.
7,500,950 B2 3/2009 Al-Ali et al.
7,509,154 B2 3/2009 Diab et al.
7,509,494 B2 3/2009 Al-Ali
7,510,849 B2 3/2009 Schurman et al.
7,526,328 B2 4/2009 Diab et al.
7,530,942 B1 5/2009 Diab
7,530,949 B2 5/2009 Al Ali et al.
7,530,955 B2 5/2009 Diab et al.
7,563,110 B2 7/2009 Al-Ali et al.
7,596,398 B2 9/2009 Al-Ali et al.
7,618,375 B2 11/2009 Flaherty et al.

(56) **References Cited**

U.S. PATENT DOCUMENTS

D606,659 S 12/2009 Kiani et al.
7,647,083 B2 1/2010 Al-Ali et al.
D609,193 S 2/2010 Al-Ali et al.
D614,305 S 4/2010 Al-Ali et al.
RE41,317 E 5/2010 Parker
7,729,733 B2 6/2010 Al-Ali et al.
7,734,320 B2 6/2010 Al-Ali
7,761,127 B2 7/2010 Al-Ali et al.
7,761,128 B2 7/2010 Al-Ali et al.
7,764,982 B2 7/2010 Dalke et al.
D621,516 S 8/2010 Kiani et al.
7,791,155 B2 9/2010 Diab
7,801,581 B2 9/2010 Diab
7,822,452 B2 10/2010 Schurman et al.
RE41,912 E 11/2010 Parker
7,844,313 B2 11/2010 Kiani et al.
7,844,314 B2 11/2010 Al-Ali
7,844,315 B2 11/2010 Al-Ali
7,865,222 B2 1/2011 Weber et al.
7,873,497 B2 1/2011 Weber et al.
7,880,606 B2 2/2011 Al-Ali
7,880,626 B2 2/2011 Al-Ali et al.
7,891,355 B2 2/2011 Al-Ali et al.
7,894,868 B2 2/2011 Al-Ali et al.
7,899,507 B2 3/2011 Al-Ali et al.
7,899,518 B2 3/2011 Trepagnier et al.
7,904,132 B2 3/2011 Weber et al.
7,909,772 B2 3/2011 Popov et al.
7,910,875 B2 3/2011 Al-Ali
7,919,713 B2 4/2011 Al-Ali et al.
7,937,128 B2 5/2011 Al-Ali
7,937,129 B2 5/2011 Mason et al.
7,937,130 B2 5/2011 Diab et al.
7,941,199 B2 5/2011 Kiani
7,942,824 B1 5/2011 Kayyali et al.
7,951,086 B2 5/2011 Flaherty et al.
7,957,780 B2 6/2011 Lamego et al.
7,962,188 B2 6/2011 Kiani et al.
7,962,190 B1 6/2011 Diab et al.
7,976,472 B2 7/2011 Kiani
7,988,637 B2 8/2011 Diab
7,990,382 B2 8/2011 Kiani
7,991,446 B2 8/2011 Al-Ali et al.
8,000,761 B2 8/2011 Al-Ali
8,008,088 B2 8/2011 Bellott et al.
RE42,753 E 9/2011 Kiani-Azarbayjany et al.
8,019,400 B2 9/2011 Diab et al.
8,028,701 B2 10/2011 Al-Ali et al.
8,029,765 B2 10/2011 Bellott et al.
8,036,727 B2 10/2011 Schurman et al.
8,036,728 B2 10/2011 Diab et al.
8,046,040 B2 10/2011 Ali et al.
8,046,041 B2 10/2011 Diab et al.
8,046,042 B2 10/2011 Diab et al.
8,048,040 B2 11/2011 Kiani
8,050,728 B2 11/2011 Al-Ali et al.
RE43,169 E 2/2012 Parker
8,118,620 B2 2/2012 Al-Ali et al.
8,126,528 B2 2/2012 Diab et al.
8,128,572 B2 3/2012 Diab et al.
8,130,105 B2 3/2012 Al-Ali et al.
8,145,287 B2 3/2012 Diab et al.
8,150,487 B2 4/2012 Diab et al.
8,175,672 B2 5/2012 Parker
8,180,420 B2 5/2012 Diab et al.
8,182,443 B1 5/2012 Kiani
8,185,180 B2 5/2012 Diab et al.
8,190,223 B2 5/2012 Al-Ali et al.
8,190,227 B2 5/2012 Diab et al.
8,203,438 B2 6/2012 Kiani et al.
8,203,704 B2 6/2012 Merritt et al.
8,204,566 B2 6/2012 Schurman et al.
8,219,172 B2 7/2012 Schurman et al.
8,224,411 B2 7/2012 Al-Ali et al.
8,228,181 B2 7/2012 Al-Ali
8,229,533 B2 7/2012 Diab et al.
8,233,955 B2 7/2012 Al-Ali et al.
8,244,325 B2 8/2012 Al-Ali et al.
8,255,026 B1 8/2012 Al-Ali
8,255,027 B2 8/2012 Al-Ali et al.
8,255,028 B2 8/2012 Al-Ali et al.
8,260,577 B2 9/2012 Weber et al.
8,265,723 B1 9/2012 McHale et al.
8,274,360 B2 9/2012 Sampath et al.
8,280,473 B2 10/2012 Al-Ali
8,301,217 B2 10/2012 Al-Ali et al.
8,306,596 B2 11/2012 Schurman et al.
8,310,336 B2 11/2012 Muhsin et al.
8,315,683 B2 11/2012 Al-Ali et al.
RE43,860 E 12/2012 Parker
8,337,403 B2 12/2012 Al-Ali et al.
8,346,330 B2 1/2013 Lamego
8,353,842 B2 1/2013 Al-Ali et al.
8,355,766 B2 1/2013 MacNeish, III et al.
8,359,080 B2 1/2013 Diab et al.
8,364,223 B2 1/2013 Al-Ali et al.
8,364,226 B2 1/2013 Diab et al.
8,374,665 B2 2/2013 Lamego
8,385,995 B2 2/2013 Al-Ali et al.
8,385,996 B2 2/2013 Dalke et al.
8,388,353 B2 3/2013 Kiani et al.
8,399,822 B2 3/2013 Al-Ali
8,401,602 B2 3/2013 Kiani
8,405,608 B2 3/2013 Al-Ali et al.
8,414,499 B2 4/2013 Al-Ali et al.
8,418,524 B2 4/2013 Al-Ali
8,423,106 B2 4/2013 Lamego et al.
8,428,967 B2 4/2013 Olsen et al.
8,430,817 B1 4/2013 Al-Ali et al.
8,437,825 B2 5/2013 Dalvi et al.
8,455,290 B2 6/2013 Siskavich
8,457,703 B2 6/2013 Al-Ali
8,457,707 B2 6/2013 Kiani
8,463,349 B2 6/2013 Diab et al.
8,466,286 B2 6/2013 Bellott et al.
8,471,713 B2 6/2013 Poeze et al.
8,473,020 B2 6/2013 Kiani et al.
8,483,787 B2 7/2013 Al-Ali et al.
8,489,364 B2 7/2013 Weber et al.
8,498,684 B2 7/2013 Weber et al.
8,504,128 B2 8/2013 Blank et al.
8,509,867 B2 8/2013 Workman et al.
8,515,509 B2 8/2013 Bruinsma et al.
8,523,781 B2 9/2013 Al-Ali
8,529,301 B2 9/2013 Al-Ali et al.
8,532,727 B2 9/2013 Al-Ali et al.
8,532,728 B2 9/2013 Diab et al.
D692,145 S 10/2013 Al-Ali et al.
8,547,209 B2 10/2013 Kiani et al.
8,548,548 B2 10/2013 Al-Ali
8,548,549 B2 10/2013 Schurman et al.
8,548,550 B2 10/2013 Al-Ali et al.
8,560,032 B2 10/2013 Al-Ali et al.
8,560,034 B1 10/2013 Diab et al.
8,570,167 B2 10/2013 Al-Ali
8,570,503 B2 10/2013 Vo et al.
8,571,617 B2 10/2013 Reichgott et al.
8,571,618 B1 10/2013 Lamego et al.
8,571,619 B2 10/2013 Al-Ali et al.
8,584,345 B2 10/2013 Al-Ali et al.
8,577,431 B2 11/2013 Lamego et al.
8,581,732 B2 11/2013 Al-Ali et al.
8,588,880 B2 11/2013 Abdul-Hafiz et al.
8,600,467 B2 12/2013 Al-Ali et al.
8,606,342 B2 12/2013 Diab
8,626,255 B2 1/2014 Al-Ali et al.
8,630,691 B2 1/2014 Lamego et al.
8,634,889 B2 1/2014 Al-Ali et al.
8,641,631 B2 2/2014 Sierra et al.
8,652,060 B2 2/2014 Al-Ali
8,663,107 B2 3/2014 Kiani
8,666,468 B1 3/2014 Al-Ali
8,667,967 B2 3/2014 Al-Ali et al.
8,670,811 B2 3/2014 O'Reilly

(56) **References Cited**

U.S. PATENT DOCUMENTS

8,670,814 B2 3/2014 Diab et al.
8,676,286 B2 3/2014 Weber et al.
8,682,407 B2 3/2014 Al-Ali
RE44,823 E 4/2014 Parker
RE44,875 E 4/2014 Kiani et al.
8,690,799 B2 4/2014 Telfort et al.
8,700,112 B2 4/2014 Kiani
8,702,627 B2 4/2014 Telfort et al.
8,706,179 B2 4/2014 Parker
8,712,494 B1 4/2014 MacNeish, III et al.
8,715,206 B2 5/2014 Telfort et al.
8,718,735 B2 5/2014 Lamego et al.
8,718,737 B2 5/2014 Diab et al.
8,718,738 B2 5/2014 Blank et al.
8,720,249 B2 5/2014 Al-Ali
8,721,541 B2 5/2014 Al-Ali et al.
8,721,542 B2 5/2014 Al-Ali et al.
8,723,677 B1 5/2014 Kiani
8,740,792 B1 6/2014 Kiani et al.
8,754,776 B2 6/2014 Poeze et al.
8,755,535 B2 6/2014 Telfort et al.
8,755,856 B2 6/2014 Diab et al.
8,755,872 B1 6/2014 Marinow
8,761,850 B2 6/2014 Lamego
8,764,671 B2 7/2014 Kiani
8,768,423 B2 7/2014 Shakespeare et al.
8,771,204 B2 7/2014 Telfort et al.
8,777,634 B2 7/2014 Kiani et al.
8,781,543 B2 7/2014 Diab et al.
8,781,544 B2 7/2014 Al-Ali et al.
8,781,549 B2 7/2014 Al-Ali et al.
8,788,003 B2 7/2014 Schurman et al.
8,790,268 B2 7/2014 Al-Ali
8,801,613 B2 8/2014 Al-Ali et al.
8,821,397 B2 9/2014 Al-Ali et al.
8,821,415 B2 9/2014 Al-Ali et al.
8,830,449 B1 9/2014 Lamego et al.
8,831,700 B2 9/2014 Schurman et al.
8,840,549 B2 9/2014 Al-Ali et al.
8,847,740 B2 9/2014 Kiani et al.
8,849,365 B2 9/2014 Smith et al.
8,852,094 B2 10/2014 Al-Ali et al.
8,852,994 B2 10/2014 Wojtczuk et al.
8,868,147 B2 10/2014 Stippick et al.
8,868,150 B2 10/2014 Al-Ali et al.
8,870,792 B2 10/2014 Al-Ali et al.
8,886,271 B2 11/2014 Kiani et al.
8,888,539 B2 11/2014 Al-Ali et al.
8,888,708 B2 11/2014 Diab et al.
8,892,180 B2 11/2014 Weber et al.
8,897,847 B2 11/2014 Al-Ali
8,909,310 B2 12/2014 Lamego et al.
8,911,377 B2 12/2014 Al-Ali
8,912,909 B2 12/2014 Al-Ali et al.
8,920,317 B2 12/2014 Al-Ali et al.
8,921,699 B2 12/2014 Al-Ali et al.
8,922,382 B2 12/2014 Al-Ali et al.
8,929,964 B2 1/2015 Al-Ali et al.
8,942,777 B2 1/2015 Diab et al.
8,948,834 B2 2/2015 Diab et al.
8,948,835 B2 2/2015 Diab
8,965,471 B2 2/2015 Lamego
8,983,564 B2 3/2015 Al-Ali
8,989,831 B2 3/2015 Al-Ali et al.
8,996,085 B2 3/2015 Kiani et al.
8,998,809 B2 4/2015 Kiani
9,028,429 B2 5/2015 Telfort et al.
9,037,207 B2 5/2015 Al-Ali et al.
9,060,721 B2 6/2015 Reichgott et al.
9,066,666 B2 6/2015 Kiani
9,066,680 B1 6/2015 Al-Ali et al.
9,072,474 B2 7/2015 Al-Ali et al.
9,078,560 B2 7/2015 Schurman et al.
9,084,569 B2 7/2015 Weber et al.
9,095,316 B2 8/2015 Welch et al.
9,106,038 B2 8/2015 Telfort et al.
9,107,625 B2 8/2015 Telfort et al.
9,107,626 B2 8/2015 Al-Ali et al.
9,113,831 B2 8/2015 Al-Ali
9,113,832 B2 8/2015 Al-Ali
9,119,595 B2 9/2015 Lamego
9,131,881 B2 9/2015 Diab et al.
9,131,882 B2 9/2015 Al-Ali et al.
9,131,883 B2 9/2015 Al-Ali
9,131,917 B2 9/2015 Telfort et al.
9,138,180 B1 9/2015 Coverston et al.
9,138,182 B2 9/2015 Al-Ali et al.
9,138,192 B2 9/2015 Weber et al.
9,142,117 B2 9/2015 Muhsin et al.
9,153,112 B1 10/2015 Kiani et al.
9,153,121 B2 10/2015 Kiani et al.
9,161,696 B2 10/2015 Al-Ali et al.
9,161,713 B2 10/2015 Al-Ali et al.
9,167,995 B2 10/2015 Lamego et al.
9,176,141 B2 11/2015 Al-Ali et al.
9,186,102 B2 11/2015 Bruinsma et al.
9,192,312 B2 11/2015 Al-Ali
9,192,329 B2 11/2015 Al-Ali
9,192,351 B1 11/2015 Telfort et al.
9,195,385 B2 11/2015 Al-Ali et al.
9,211,072 B2 12/2015 Kiani
9,211,095 B1 12/2015 Al-Ali
9,218,454 B2 12/2015 Kiani et al.
9,226,696 B2 1/2016 Kiani
9,241,662 B2 1/2016 Al-Ali et al.
9,245,668 B1 1/2016 Vo et al.
9,259,185 B2 2/2016 Abdul-Hafiz et al.
9,267,572 B2 2/2016 Barker et al.
9,277,880 B2 3/2016 Poeze et al.
9,289,167 B2 3/2016 Diab et al.
9,295,421 B2 3/2016 Kiani et al.
9,307,928 B1 4/2016 Al-Ali et al.
9,323,894 B2 4/2016 Kiani
D755,392 S 5/2016 Hwang et al.
9,326,712 B1 5/2016 Kiani
9,333,316 B2 5/2016 Kiani
9,339,220 B2 5/2016 Lamego et al.
9,341,565 B2 5/2016 Lamego et al.
9,351,673 B2 5/2016 Diab et al.
9,351,675 B2 5/2016 Al-Ali et al.
9,364,181 B2 6/2016 Kiani et al.
9,368,671 B2 6/2016 Wojtczuk et al.
9,370,325 B2 6/2016 Al-Ali et al.
9,370,326 B2 6/2016 McHale et al.
9,370,335 B2 6/2016 Al-ali et al.
9,375,185 B2 6/2016 Ali et al.
9,386,953 B2 7/2016 Al-Ali
9,386,961 B2 7/2016 Al-Ali et al.
9,392,945 B2 7/2016 Al-Ali et al.
9,397,448 B2 7/2016 Al-Ali et al.
9,408,542 B1 8/2016 Kinast et al.
9,436,645 B2 9/2016 Al-Ali et al.
9,445,759 B1 9/2016 Lamego et al.
9,466,919 B2 10/2016 Kiani et al.
9,474,474 B2 10/2016 Lamego et al.
9,480,422 B2 11/2016 Al-Ali
9,480,435 B2 11/2016 Olsen
9,492,110 B2 11/2016 Al-Ali et al.
9,510,779 B2 12/2016 Poeze et al.
9,517,024 B2 12/2016 Kiani et al.
9,532,722 B2 1/2017 Lamego et al.
9,538,949 B2 1/2017 Al-Ali et al.
9,538,980 B2 1/2017 Telfort et al.
9,549,696 B2 1/2017 Lamego et al.
9,554,737 B2 1/2017 Schurman et al.
9,560,996 B2 2/2017 Kiani
9,560,998 B2 2/2017 Al-Ali et al.
9,566,019 B2 2/2017 Al-Ali et al.
9,579,039 B2 2/2017 Jansen et al.
9,591,975 B2 3/2017 Dalvi et al.
9,622,692 B2 4/2017 Lamego et al.
9,622,693 B2 4/2017 Diab
D788,312 S 5/2017 Al-Ali et al.
9,636,055 B2 5/2017 Al-Ali et al.

(56) **References Cited**

U.S. PATENT DOCUMENTS

9,636,056 B2 5/2017 Al-Ali
9,649,054 B2 5/2017 Lamego et al.
9,662,052 B2 5/2017 Al-Ali et al.
9,668,679 B2 6/2017 Schurman et al.
9,668,680 B2 6/2017 Bruinsma et al.
9,668,703 B2 6/2017 Al-Ali
9,675,286 B2 6/2017 Diab
9,687,160 B2 6/2017 Kiani
9,693,719 B2 7/2017 Al-Ali et al.
9,693,737 B2 7/2017 Al-Ali
9,697,928 B2 7/2017 Al-Ali et al.
9,717,425 B2 8/2017 Kiani et al.
9,717,458 B2 8/2017 Lamego et al.
9,724,016 B1 8/2017 Al-Ali et al.
9,724,024 B2 8/2017 Al-Ali
9,724,025 B1 8/2017 Kiani et al.
9,730,640 B2 8/2017 Diab et al.
9,743,887 B2 8/2017 Al-Ali et al.
9,749,232 B2 8/2017 Sampath et al.
9,750,442 B2 9/2017 Olsen
9,750,443 B2 9/2017 Smith et al.
9,750,461 B1 9/2017 Telfort
9,775,545 B2 10/2017 Al-Ali et al.
9,775,546 B2 10/2017 Diab et al.
9,775,570 B2 10/2017 Al-Ali
9,778,079 B1 10/2017 Al-Ali et al.
9,782,077 B2 10/2017 Lamego et al.
9,782,110 B2 10/2017 Kiani
9,787,568 B2 10/2017 Lamego et al.
9,788,735 B2 10/2017 Al-Ali
9,788,768 B2 10/2017 Al-Ali et al.
9,795,300 B2 10/2017 Al-Ali
9,795,310 B2 10/2017 Al-Ali
9,795,358 B2 10/2017 Telfort et al.
9,795,739 B2 10/2017 Al-Ali et al.
9,801,556 B2 10/2017 Kiani
9,801,588 B2 10/2017 Weber et al.
9,808,188 B1 11/2017 Perea et al.
9,814,418 B2 11/2017 Weber et al.
9,820,691 B2 11/2017 Kiani
9,833,152 B2 12/2017 Kiani et al.
9,833,180 B2 12/2017 Shakespeare et al.
9,839,379 B2 12/2017 Al-Ali et al.
9,839,381 B1 12/2017 Weber et al.
9,847,002 B2 12/2017 Kiani et al.
9,847,749 B2 12/2017 Kiani et al.
9,848,800 B1 12/2017 Lee et al.
9,848,806 B2 12/2017 Al-Ali et al.
9,848,807 B2 12/2017 Lamego
9,861,298 B2 1/2018 Eckerbom et al.
9,861,304 B2 1/2018 Al-Ali et al.
9,861,305 B1 1/2018 Weber et al.
9,867,578 B2 1/2018 Al-Ali et al.
9,872,623 B2 1/2018 Al-Ali
9,876,320 B2 1/2018 Coverston et al.
9,877,650 B2 1/2018 Muhsin et al.
9,877,686 B2 1/2018 Al-Ali et al.
9,891,079 B2 2/2018 Dalvi
9,895,107 B2 2/2018 Al-Ali et al.
9,913,617 B2 3/2018 Al-Ali et al.
9,924,893 B2 3/2018 Schurman et al.
9,924,897 B1 3/2018 Abdul-Hafiz
9,936,917 B2 4/2018 Poeze et al.
9,943,269 B2 4/2018 Muhsin et al.
9,949,676 B2 4/2018 Al-Ali
9,955,937 B2 5/2018 Telfort
9,965,946 B2 5/2018 Al-Ali
9,980,667 B2 5/2018 Kiani et al.
D820,865 S 6/2018 Muhsin et al.
9,986,919 B2 6/2018 Lamego et al.
9,986,952 B2 6/2018 Dalvi et al.
9,989,560 B2 6/2018 Poeze et al.
9,993,207 B2 6/2018 Al-Ali et al.
10,007,758 B2 6/2018 Al-Ali et al.
D822,215 S 7/2018 Al-Ali et al.
D822,216 S 7/2018 Barker et al.
10,010,276 B2 7/2018 Al-Ali et al.
10,032,002 B2 7/2018 Kiani et al.
10,039,482 B2 8/2018 Al-Ali et al.
10,052,037 B2 8/2018 Kinast et al.
10,058,275 B2 8/2018 Al-Ali et al.
10,064,562 B2 9/2018 Al-Ali
10,086,138 B1 10/2018 Novak, Jr.
10,092,200 B2 10/2018 Al-Ali et al.
10,092,249 B2 10/2018 Kiani et al.
10,098,550 B2 10/2018 Al-Ali et al.
10,098,591 B2 10/2018 Al-Ali et al.
10,098,610 B2 10/2018 Al-Ali et al.
D833,624 S 11/2018 DeJong et al.
10,123,726 B2 11/2018 Al-Ali et al.
10,130,291 B2 11/2018 Schurman et al.
D835,282 S 12/2018 Barker et al.
D835,283 S 12/2018 Barker et al.
D835,284 S 12/2018 Barker et al.
D835,285 S 12/2018 Barker et al.
10,149,616 B2 12/2018 Al-Ali et al.
10,154,815 B2 12/2018 Al-Ali et al.
10,159,412 B2 12/2018 Lamego et al.
2004/0054261 A1 3/2004 Kamataki et al.
2004/0097797 A1 5/2004 Porges et al.
2006/0161054 A1 7/2006 Reuss et al.
2007/0282478 A1 12/2007 Al-Ali et al.
2009/0247984 A1 10/2009 Lamego et al.
2009/0275813 A1 11/2009 Davis
2009/0275844 A1 11/2009 Al-Ali
2009/0299157 A1 12/2009 Telfort et al.
2010/0004518 A1 1/2010 Vo et al.
2010/0030040 A1 2/2010 Poeze et al.
2010/0261979 A1 10/2010 Kiani
2011/0001605 A1 1/2011 Kiani et al.
2011/0082711 A1 4/2011 Poeze et al.
2011/0087083 A1 4/2011 Poeze et al.
2011/0105854 A1 5/2011 Kiani et al.
2011/0125060 A1 5/2011 Telfort et al.
2011/0208015 A1 8/2011 Welch et al.
2011/0209915 A1 9/2011 Telfort et al.
2011/0213212 A1 9/2011 Al-Ali
2011/0230733 A1 9/2011 Al-Ali
2011/0237911 A1 9/2011 Lamego et al.
2011/0237969 A1 9/2011 Eckerbom et al.
2011/0288383 A1 11/2011 Diab
2011/0301444 A1 12/2011 Al-Ali
2012/0041316 A1 2/2012 Al-Ali et al.
2012/0046557 A1 2/2012 Kiani
2012/0059267 A1 3/2012 Lamego et al.
2012/0088984 A1 4/2012 Al-Ali et al.
2012/0116175 A1 5/2012 Al-Ali et al.
2012/0165629 A1 6/2012 Merritt et al.
2012/0179006 A1 7/2012 Jansen et al.
2012/0209082 A1 8/2012 Al-Ali
2012/0209084 A1 8/2012 Olsen et al.
2012/0227739 A1 9/2012 Kiani
2012/0265039 A1 10/2012 Kiani
2012/0283524 A1 11/2012 Kiani et al.
2012/0286955 A1 11/2012 Welch et al.
2012/0296178 A1 11/2012 Lamego et al.
2012/0319816 A1 12/2012 Al-Ali
2012/0330112 A1 12/2012 Lamego et al.
2013/0023775 A1 1/2013 Lamego et al.
2013/0045685 A1 2/2013 Kiani
2013/0046204 A1 2/2013 Lamego et al.
2013/0041591 A1 3/2013 Lamego
2013/0060108 A1 3/2013 Schurman et al.
2013/0060147 A1 3/2013 Welch et al.
2013/0096405 A1 4/2013 Garfio
2013/0096936 A1 4/2013 Sampath et al.
2013/0109935 A1 5/2013 Al-Ali et al.
2013/0162433 A1 6/2013 Muhsin et al.
2013/0190581 A1 7/2013 Al-Ali et al.
2013/0197328 A1 8/2013 Diab et al.
2013/0211214 A1 8/2013 Olsen
2013/0243021 A1 9/2013 Siskavich
2013/0253334 A1 9/2013 Al-Ali et al.
2013/0262730 A1 10/2013 Al-Ali et al.

(56) **References Cited**

U.S. PATENT DOCUMENTS

2013/0267804 A1 10/2013 Al-Ali
2013/0274571 A1 10/2013 Diab et al.
2013/0274572 A1 10/2013 Al-Ali et al.
2013/0296672 A1 11/2013 O'Neil et al.
2013/0296713 A1 11/2013 Al-Ali et al.
2013/0317370 A1 11/2013 Dalvi et al.
2013/0324808 A1 12/2013 Al-Ali et al.
2013/0331660 A1 12/2013 Al-Ali et al.
2013/0331670 A1 12/2013 Kiani
2013/0338461 A1 12/2013 Lamego et al.
2014/0012100 A1 1/2014 Al-Ali et al.
2014/0025306 A1 1/2014 Weber et al.
2014/0034353 A1 2/2014 Al-Ali et al.
2014/0051952 A1 2/2014 Reichgott et al.
2014/0051953 A1 2/2014 Lamego et al.
2014/0051954 A1 2/2014 Al-Ali et al.
2014/0058230 A1 2/2014 Abdul-Hafiz et al.
2014/0066783 A1 3/2014 Kiani et al.
2014/0077956 A1 3/2014 Sampath et al.
2014/0081100 A1 3/2014 Muhsin et al.
2014/0081175 A1 3/2014 Telfort
2014/0094667 A1 4/2014 Schurman et al.
2014/0100434 A1 4/2014 Diab et al.
2014/0114199 A1 4/2014 Lamego et al.
2014/0120564 A1 5/2014 Workman et al.
2014/0121482 A1 5/2014 Merritt et al.
2014/0121483 A1 5/2014 Kiani
2014/0125495 A1 5/2014 Al-Ali
2014/0127137 A1 5/2014 Bellott et al.
2014/0128696 A1 5/2014 Al-Ali
2014/0128699 A1 5/2014 Al-Ali et al.
2014/0129702 A1 5/2014 Lamego et al.
2014/0135588 A1 5/2014 Al-Ali et al.
2014/0142401 A1 5/2014 Al-Ali et al.
2014/0142402 A1 5/2014 Al-Ali et al.
2014/0163344 A1 6/2014 Al-Ali
2014/0163402 A1 6/2014 Lamego et al.
2014/0166076 A1 6/2014 Kiani et al.
2014/0171763 A1 6/2014 Diab
2014/0180038 A1 6/2014 Kiani
2014/0180154 A1 6/2014 Sierra et al.
2014/0180160 A1 6/2014 Brown et al.
2014/0187973 A1 7/2014 Brown et al.
2014/0194709 A1 7/2014 Al-Ali et al.
2014/0194711 A1 7/2014 Al-Ali
2014/0194766 A1 7/2014 Al-Ali et al.
2014/0200420 A1 7/2014 Al-Ali
2014/0200422 A1 7/2014 Weber et al.
2014/0206963 A1 7/2014 Al-Ali
2014/0213864 A1 7/2014 Abdul-Hafiz et al.
2014/0243627 A1 8/2014 Diab et al.
2014/0266790 A1 9/2014 Al-Ali et al.
2014/0275808 A1 9/2014 Poeze et al.
2014/0275835 A1 9/2014 Lamego et al.
2014/0275871 A1 9/2014 Lamego et al.
2014/0275872 A1 9/2014 Merritt et al.
2014/0275881 A1 9/2014 Lamego et al.
2014/0276115 A1 9/2014 Dalvi et al.
2014/0288400 A1 9/2014 Diab et al.
2014/0296664 A1 10/2014 Bruinsma et al.
2014/0303520 A1 10/2014 Telfort et al.
2014/0309506 A1 10/2014 Lamego et al.
2014/0309559 A1 10/2014 Telfort et al.
2014/0316217 A1 10/2014 Purdon et al.
2014/0316218 A1 10/2014 Purdon et al.
2014/0316228 A1 10/2014 Blank et al.
2014/0323825 A1 10/2014 Al-Ali et al.
2014/0323897 A1 10/2014 Brown et al.
2014/0323898 A1 10/2014 Purdon et al.
2014/0330092 A1 11/2014 Al-Ali et al.
2014/0330098 A1 11/2014 Merritt et al.
2014/0330099 A1 11/2014 Al-Ali et al.
2014/0333440 A1 11/2014 Kiani
2014/0336481 A1 11/2014 Shakespeare et al.
2014/0343436 A1 11/2014 Kiani
2014/0357966 A1 12/2014 Al-Ali et al.
2014/0371548 A1 12/2014 Al-Ali et al.
2014/0371632 A1 12/2014 Al-Ali et al.
2014/0378784 A1 12/2014 Kiani et al.
2015/0005600 A1 1/2015 Blank et al.
2015/0011907 A1 1/2015 Purdon et al.
2015/0012231 A1 1/2015 Poeze et al.
2015/0018650 A1 1/2015 Al-Ali et al.
2015/0025406 A1 1/2015 Al-Ali
2015/0032029 A1 1/2015 Al-Ali et al.
2015/0038859 A1 2/2015 Dalvi et al.
2015/0045637 A1 2/2015 Dalvi
2015/0051462 A1 2/2015 Olsen
2015/0080754 A1 3/2015 Purdon et al.
2015/0087936 A1 3/2015 Al-Ali et al.
2015/0094546 A1 4/2015 Al-Ali
2015/0097701 A1 4/2015 Al-Ali et al.
2015/0099950 A1 4/2015 Al-Ali et al.
2015/0099951 A1 4/2015 Al-Ali et al.
2015/0099955 A1 4/2015 Al-Ali et al.
2015/0101844 A1 4/2015 Al-Ali et al.
2015/0106121 A1 4/2015 Muhsin et al.
2015/0112151 A1 4/2015 Muhsin et al.
2015/0116076 A1 4/2015 Al-Ali et al.
2015/0126830 A1 5/2015 Schurman et al.
2015/0133755 A1 5/2015 Smith et al.
2015/0140863 A1 5/2015 Al-Ali et al.
2015/0141781 A1 5/2015 Weber et al.
2015/0165312 A1 6/2015 Kiani
2015/0196237 A1 7/2015 Lamego
2015/0196249 A1 7/2015 Brown et al.
2015/0201874 A1 7/2015 Diab
2015/0208966 A1 7/2015 Al-Ali
2015/0216459 A1 8/2015 Al-Ali et al.
2015/0230755 A1 8/2015 Al-Ali et al.
2015/0238722 A1 8/2015 Al-Ali
2015/0245773 A1 9/2015 Lamego et al.
2015/0245794 A1 9/2015 Al-Ali
2015/0257689 A1 9/2015 Al-Ali et al.
2015/0272514 A1 10/2015 Kiani et al.
2015/0351697 A1 12/2015 Weber et al.
2015/0351704 A1 12/2015 Kiani et al.
2015/0359429 A1 12/2015 Al-Ali et al.
2015/0366472 A1 12/2015 Kiani
2015/0366507 A1 12/2015 Blank
2015/0374298 A1 12/2015 Al-Ali et al.
2015/0380875 A1 12/2015 Coverston et al.
2016/0000362 A1 1/2016 Diab et al.
2016/0007930 A1 1/2016 Weber et al.
2016/0029932 A1 2/2016 Al-Ali
2016/0029933 A1 2/2016 Al-Ali et al.
2016/0045118 A1 2/2016 Kiani
2016/0051205 A1 2/2016 Al-Ali et al.
2016/0058338 A1 3/2016 Schurman et al.
2016/0058347 A1 3/2016 Reichgott et al.
2016/0066823 A1 3/2016 Kind et al.
2016/0066824 A1 3/2016 Al-Ali et al.
2016/0066879 A1 3/2016 Telfort et al.
2016/0072429 A1 3/2016 Kiani et al.
2016/0073967 A1 3/2016 Lamego et al.
2016/0081552 A1 3/2016 Wojtczuk et al.
2016/0095543 A1 4/2016 Telfort et al.
2016/0095548 A1 4/2016 Al-Ali et al.
2016/0103598 A1 4/2016 Al-Ali et al.
2016/0113527 A1 4/2016 Al-Ali et al.
2016/0143548 A1 5/2016 Al-Ali
2016/0166182 A1 6/2016 Al-Ali et al.
2016/0166183 A1 6/2016 Poeze et al.
2016/0166188 A1 6/2016 Bruinsma et al.
2016/0166210 A1 6/2016 Al-Ali
2016/0192869 A1 7/2016 Kiani et al.
2016/0196388 A1 7/2016 Lamego
2016/0197436 A1 7/2016 Barker et al.
2016/0213281 A1 7/2016 Eckerbom et al.
2016/0228043 A1 8/2016 O'Neil et al.
2016/0233632 A1 8/2016 Scruggs et al.
2016/0234944 A1 8/2016 Schmidt et al.
2016/0270735 A1 9/2016 Diab et al.
2016/0283665 A1 9/2016 Sampath et al.

(56) **References Cited**

U.S. PATENT DOCUMENTS

2016/0287090 A1 10/2016 Al-Ali et al.
2016/0287786 A1 10/2016 Kiani
2016/0296169 A1 10/2016 McHale et al.
2016/0310052 A1 10/2016 Al-Ali et al.
2016/0314260 A1 10/2016 Kiani
2016/0324486 A1 11/2016 Al-Ali et al.
2016/0324488 A1 11/2016 Olsen
2016/0327984 A1 11/2016 Al-Ali et al.
2016/0328528 A1 11/2016 Al-Ali et al.
2016/0331332 A1 11/2016 Al-Ali
2016/0367173 A1 12/2016 Dalvi et al.
2017/0007134 A1 1/2017 Al-Ali et al.
2017/0007190 A1 1/2017 Al-Ali et al.
2017/0007198 A1 1/2017 Al-Ali et al.
2017/0014083 A1 1/2017 Diab et al.
2017/0014084 A1 1/2017 Al-Ali et al.
2017/0021099 A1 1/2017 Al-Ali et al.
2017/0024748 A1 1/2017 Haider
2017/0027456 A1 2/2017 Kinast et al.
2017/0042488 A1 2/2017 Muhsin
2017/0055847 A1 3/2017 Kiani et al.
2017/0055851 A1 3/2017 Al-Ali
2017/0055882 A1 3/2017 Al-Ali et al.
2017/0055887 A1 3/2017 Al-Ali
2017/0055896 A1 3/2017 Al-Ali et al.
2017/0079594 A1 3/2017 Telfort et al.
2017/0086723 A1 3/2017 Al-Ali et al.
2017/0143281 A1 5/2017 Olsen
2017/0147774 A1 5/2017 Kiani
2017/0156620 A1 6/2017 Al-Ali et al.
2017/0173632 A1 6/2017 Al-Ali
2017/0187146 A1 6/2017 Kiani et al.
2017/0196464 A1 7/2017 Jansen et al.
2017/0196470 A1 7/2017 Lamego et al.
2017/0224262 A1 8/2017 Al-Ali
2017/0228516 A1 8/2017 Sampath et al.
2017/0245790 A1 8/2017 Al-Ali et al.
2017/0251974 A1 9/2017 Shreim et al.
2017/0251975 A1 9/2017 Shreim et al.
2017/0258403 A1 9/2017 Abdul-Hafiz et al.
2017/0311891 A1 11/2017 Kiani et al.
2017/0325728 A1 11/2017 Al-Ali et al.
2017/0332976 A1 11/2017 Al-Ali et al.
2017/0340293 A1 11/2017 Al-Ali et al.
2017/0360310 A1 12/2017 Kiani et al.
2017/0367632 A1 12/2017 Al-Ali et al.
2018/0008146 A1 1/2018 Al-Ali et al.
2018/0013562 A1 1/2018 Haider et al.
2018/0014752 A1 1/2018 Al-Ali et al.
2018/0028124 A1 2/2018 Al-Ali et al.
2018/0055385 A1 3/2018 Al-Ali
2018/0055390 A1 3/2018 Kiani et al.
2018/0055430 A1 3/2018 Diab et al.
2018/0064381 A1 3/2018 Shakespeare et al.
2018/0069776 A1 3/2018 Lamego et al.
2018/0070867 A1 3/2018 Smith et al.
2018/0082767 A1 3/2018 Al-Ali et al.
2018/0085068 A1 3/2018 Telfort
2018/0087937 A1 3/2018 Al-Ali et al.
2018/0103874 A1 4/2018 Lee et al.
2018/0103905 A1 4/2018 Kiani
2018/0110478 A1 4/2018 Al-Ali
2018/0116575 A1 5/2018 Perea et al.
2018/0125368 A1 5/2018 Lamego et al.
2018/0125430 A1 5/2018 Al-Ali et al.
2018/0125445 A1 5/2018 Telfort et al.
2018/0130325 A1 5/2018 Kiani et al.
2018/0132769 A1 5/2018 Weber et al.
2018/0132770 A1 5/2018 Lamego
2018/0146901 A1 5/2018 Al-Ali et al.
2018/0146902 A1 5/2018 Kiani et al.
2018/0153442 A1 6/2018 Eckerbom et al.
2018/0153446 A1 6/2018 Kiani
2018/0153447 A1 6/2018 Al-Ali et al.
2018/0153448 A1 6/2018 Weber et al.
2018/0161499 A1 6/2018 Al-Ali et al.
2018/0168491 A1 6/2018 Al-Ali et al.
2018/0174679 A1 6/2018 Sampath et al.
2018/0174680 A1 6/2018 Sampath et al.
2018/0182484 A1 6/2018 Sampath et al.
2018/0184917 A1 7/2018 Kiani
2018/0192924 A1 7/2018 Al-Ali
2018/0192953 A1 7/2018 Shreim et al.
2018/0192955 A1 7/2018 Al-Ali et al.
2018/0199871 A1 7/2018 Pauley et al.
2018/0206795 A1 7/2018 Al-Ali
2018/0206815 A1 7/2018 Telfort
2018/0213583 A1 7/2018 Al-Ali
2018/0214031 A1 8/2018 Kiani et al.
2018/0214090 A1 8/2018 Al-Ali et al.
2018/0218792 A1 8/2018 Muhsin et al.
2018/0225960 A1 8/2018 Al-Ali et al.
2018/0238718 A1 8/2018 Dalvi
2018/0242853 A1 8/2018 Al-Ali
2018/0242921 A1 8/2018 Muhsin et al.
2018/0242923 A1 8/2018 Al-Ali et al.
2018/0242924 A1 8/2018 Barker et al.
2018/0242926 A1 8/2018 Muhsin et al.
2018/0247353 A1 8/2018 Al-Ali et al.
2018/0247712 A1 8/2018 Muhsin et al.
2018/0249933 A1 9/2018 Schurman et al.
2018/0253947 A1 9/2018 Muhsin et al.
2018/0256087 A1 9/2018 Al-Ali et al.
2018/0256113 A1 9/2018 Weber et al.
2018/0285094 A1 10/2018 Housel et al.
2018/0289325 A1 10/2018 Poeze et al.
2018/0289337 A1 10/2018 Al-Ali et al.
2018/0296161 A1 10/2018 Shreim et al.
2018/0300919 A1 10/2018 Muhsin et al.
2018/0310822 A1 11/2018 Indorf et al.
2018/0310823 A1 11/2018 Al-Ali et al.
2018/0317826 A1 11/2018 Muhsin
2018/0317841 A1 11/2018 Novak, Jr.
2018/0333055 A1 11/2018 Lamego et al.
2018/0333087 A1 11/2018 Al-Ali
2019/0000317 A1 1/2019 Muhsin et al.
2019/0000362 A1 1/2019 Kiani et al.
2019/0015023 A1 1/2019 Monfre

FOREIGN PATENT DOCUMENTS

EP 2319398 5/2011
WO WO 96/12435 5/1996

OTHER PUBLICATIONS

US 9,579,050 B2, 02/2017, Al-Ali (withdrawn)

Bartlett, "Oxygen Kinetics", Critical Care Physiology, 13th Ed., pp. 1-23.

Confidential Declaration of Michelle Armond in Support of MASIMO Corporation's Responsive Claim Construction Brief, *MASIMO Corporation* v. *Philips Electronics North America Corporation and Philips Medizin Systeme Böblingen GMBH*, (District of Delaware, Case No. 1:09-cv-00080 (LPS/MPT) dated Nov. 19, 2010.

Declaration of Perry D. Oldham in Support of MASIMO Corporation's Opening Claim Construction Brief, *MASIMO Corporation* v. *Philips Electronics North America Corporation and Philips Medizin Systeme Böblingen GMBH*, (District of Delaware, Case No. 1:09-cv-00080 (LPS/MPT) dated Oct. 19, 2010.

Declaration of Robert T. Stone in Support of Philips' Responsive Markman Brief, *MASIMO Corporation* v. *Philips Electronics North America Corporation and Philips Medizin Systeme Böblingen GMBH*, (District of Delaware, Case No. 1:09-cv-00080 (LPS/MPT) dated Nov. 15, 2010.

Dudell, Glode et al., "What Constitutes Adequate Oxygenation?" Pediatrics, Jan. 1990, pp. 39-41.

Granelli A.D., Mellander et al., "Screening for duct-dependent congenital heart disease with pulse oximetry: A critical evaluation of strategies to maximize sensitivity", Acta Paediatrica, Nov. 2005; 94:1590-1596, http://www.masimo.com/pdf/Granelli_Article.pdf, 1 page downloaded and printed from the World Wide Web.

(56) **References Cited**

OTHER PUBLICATIONS

Hoke, et al., "Oxygen Saturation as a Screening Test for Critical Congenital Heart Disease: A Preliminary Study", Pediatr Cardiol, 23(4):403-409, Jul.-Aug. 2002.

Koppel, Robert I et al., "Effective of Pulse Oximetry Screening for Congenital Heart Disease in Asymptomatic Newborns", Pediatrics, Mar. 2003, vol. 111, No. 3, 451-455.

Mallinckrodt inc. v. *Masimo Corp.*, 147 Fed. Appx. 158, 2005 WL 2139867 (Fed. Cir. 2005).

Mallinckrodt inc. v. *Masimo Corp.*, 2004 U.S. Dist. LEXIS 28518 (C.D. Cal. Jul. 12, 2004).

Mallinckrodt inc. v. *Masimo Corp.*, 254 F. Supp.2d 1140 (C.D. Cal. 2003).

Masimo Corporation v. *Philips Electronics North America Corporation and Philips Medizin Systeme Böblingen GMBH*, (District of Delaware, Case No. 09-000080(JJF)) Complaint for Patent Infringement dated Feb. 3, 2009, pp. 1-13.

Masimo Corporation v. *Philips Electronics North America Corporation and Philips Medizin Systeme Böblingen GMBH*, (District of Delaware, Case No. 09-00080(JJF)) Masimo's Answer to Philips' Counterclaims dated Jul. 9, 2009, pp. 1-68.

Masimo Corporation v. *Philips Electronics North America Corporation and Philips Medizin Systeme Böblingen GMBH*, (District of Delaware, Case No. 09-00080(JJF)) Defendant/Counterclaim-Plaintiff Philips Electronics North America Corporation Answer to Masimo's Counterclaims dated Aug. 3, 2009, pp. 1-23.

Masimo Corporation v. *Philips Electronics North America Corporation and Philips Medizin Systeme Böblingen GMBH*, (District of Delaware, Case No. 09-00080(JJF)) Defendants' Answer and Philips Electronics North America Corporation's Amended Counterclaims to Masimo's First Amended Complaint, dated Apr. 21, 2010, pp. 1-62.

Masimo Corporation v. *Philips Electronics North America Corporation and Philips Medizin Systeme Böblingen GMBH*, (District of Delaware, Case No. 09-00080(JJF)) Defendants' Answer and Philips Electronics North America Corporation's Counterclaims to Masimo's First Amended Complaint dated Jun. 15, 2009, pp. 1-65.

Masimo Corporation v. *Philips Electronics North America Corporation and Philips Medizin Systeme Böblingen GMBH*, (District of Delaware, Case No. 09-00080(JJF)) First Amended Complaint for Patent Infringement dated May 12, 2009, pp. 1-16.

Masimo Corporation v. *Philips Electronics North America Corporation and Philips Medizin Systeme Böblingen GMBH*, (District of Delaware, Case No. 09-00080(JJF)) Masimo's Answer to Philips' Amended Counterclaims, dated May 10, 2010, pp. 1-76.

Masimo Corporation v. *Philips Electronics North America Corporation and Philips Medizin Systeme Böblingen GMBH*, (District of Delaware, Case No. 09-00080(JJF)) Philips Electronics North America Corporation's Answer to Masimo's Amended Counterclaims (D.I. 102) dated May 27, 2010, pp. 1-24.

Masimo Corporation v. *Philips Electronics North America Corporation and Philips Medizin Systeme Böblingen GMBH*, (District of Delaware, Case No. 09-00080(JJF)) Philips North America Corporation and Philips Medizin Systeme Boblingen GMBH's Seventh Supplemental Objections and Responses to Masimo Corporation's First Set of Interrogatories (Nos. 1-8) dated Jun. 30, 2010, pp. 1-40 (redacted).

MASIMO Corporation's Opening Claim Construction Brief, *MASIMO Corporation* v. *Philips Electronics North America Corporation and Philips Medizin Systeme Böblingen GMBH*, (District of Delaware, Case No. 1:09-cv-00080 (LPS/MPT) dated Oct. 19, 2010.

MASIMO Corporation's Responsive Claim Construction Brief, *MASIMO Corporation* v. *Philips Electronics North America Corporation and Philips Medizin Systeme Böblingen GMBH*, (District of Delaware, Case No. 1:09-cv-00080 (LPS/MPT) dated Nov. 19, 2010 (REDACTED).

Masimo's Technical Tutorial, *MASIMO Corporation* v. *Philips Electronics North America Corporation and Philips Medizin Systeme Böblingen GMBH*, (District of Delaware, Case No. 1:09-cv-00080 (LPS/MPT) dated Dec. 1, 2010.

Murray, Willie et al., The Peripheral Pulse Wave: Information Overlooked, Journal of Clinical Monitoring, vol. 12, pp. 365-377, Sep. 1996.

Neuhof, H. et al., "Simultaneous Continuous Measurement of Arterial and Mixed Venous Partial O2 Saturation", The Oxygen Status of Arterial Blood, Zander, Mertzlufft (eds.), pp. 273-278 (Karger, Basel 1991).

PCT International Search Report and Written Opinion, dated Apr. 17, 2013, re: PCT Application No. PCT/US2013/020377, application dated Jan. 4, 2013, in 14 pages.

Philips' Claim Construction Hearing, Presentaion Materials, *MASIMO Corporation* v. *Philips Electronics North America Corporation and Philips Medizin Systeme Böblingen GMBH*, (District of Delaware, Case No. 1:09-cv-00080 (LPS/MPT) dated Dec. 1, 2010.

Philips' Opening Markman Brief, *MASIMO Corporation* v. *Philips Electronics North America Corporation and Philips Medizin Systeme Böblingen GMBH*, (District of Delaware, Case No. 1:09-cv-00080 (LPS/MPT) dated Oct. 19, 2010.

Philips' Responsive Markman Brief, *MASIMO Corporation* v. *Philips Electronics North America Corporation and Philips Medizin Systeme Böblingen GMBH*, (District of Delaware, Case No. 1:09-cv-00080 (LPS/MPT) dated Nov. 22, 2010.

Report and Recommendation re Claim Construction, *MASIMO Corporation* v. *Philips Electronics North America Corporation and Philips Medizin Systeme Böblingen GMBH*, (District of Delaware, Case No. 1:09-cv-00080 (LPS/MPT) dated Feb. 18, 2011.

Revised Joint Claim Construction Chart, *MASIMO Corporation* v. *Philips Electronics North America Corporation and Philips Medizin Systeme Böblingen GMBH*, (District of Delaware, Case No. 1:09-cv-00080 (LPS/MPT) dated Oct. 19, 2010.

Steinke, John M., Comparison of Mie Theory and the Light Scattering of Red Blood Cells:, Applied Optics, vol. 27, No. 19, Oct. 1, 1998, pp. 4027-4033.

Transcript of Markman Hearing, *MASIMO Corporation* v. *Philips Electronics North America Corporation and Philips Medizin Systeme Böblingen GMBH*, (District of Delaware, Case No. 1:09-cv-00080 (LPS/MPT) dated Dec. 1, 2010.

Vjayakumar, E. et al., "Pulse Oximetry in Infants of (1500 gm Birth Weight on Supplemental Oxygen: A national Survey", Journal of Perinatology, vol. 17, No. 5, 1997, pp. 341-345.

White, Katherine, "Completing the Hemodynamic Picture: SVox", Heart & Lung, May 1985, vol. 14, No. 3.

Wolf, Martin et al., "Continuous Noninvasive Measurement of Cerebral Arterial and Venous Oxygen Saturation at the Bedside in Mechanically Ventilated Neonates", Critical Care Med, 1997, vol. 25, No. 9, pp. 1579-1582.

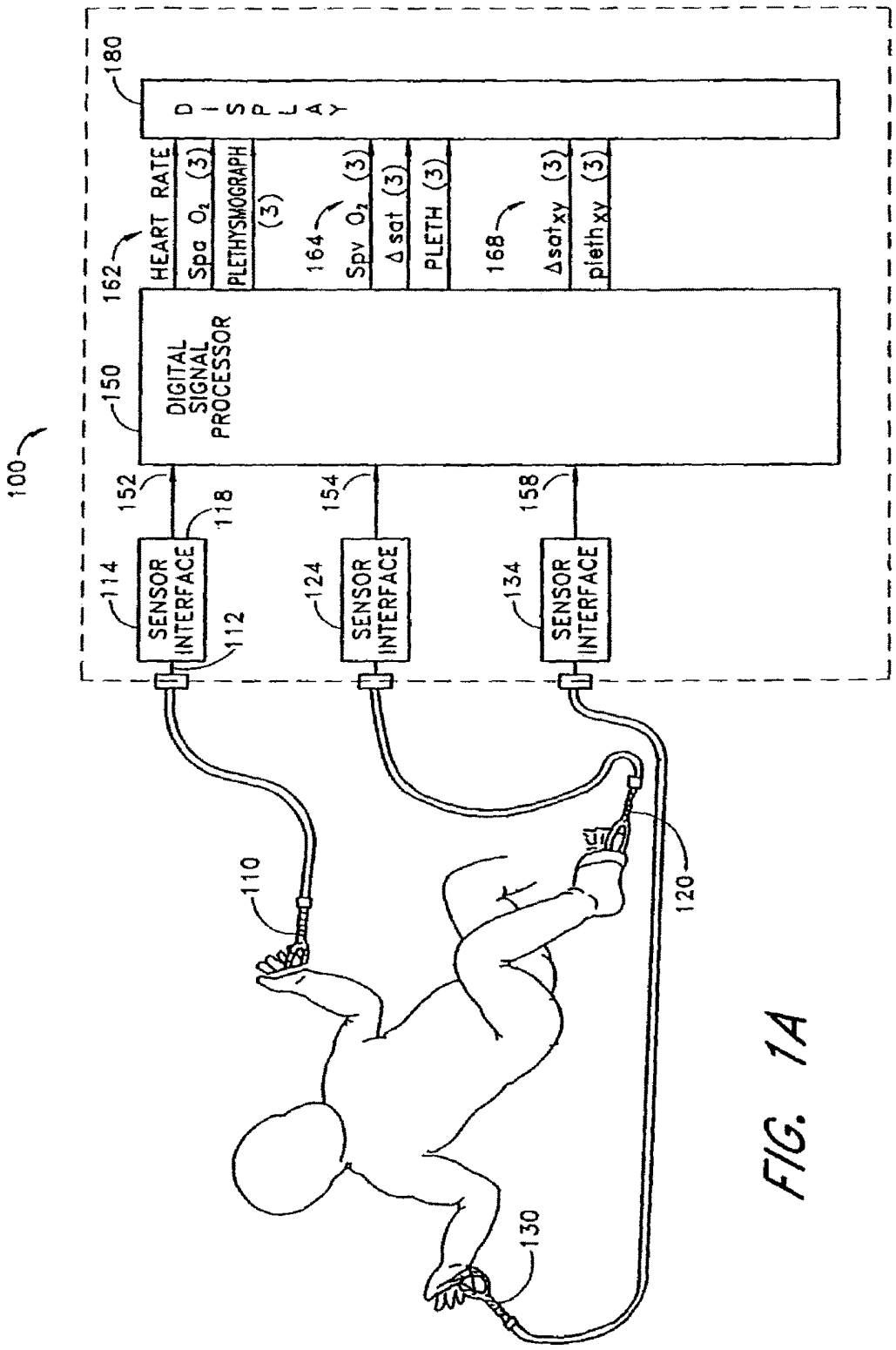
100
180
DISPLAY
HEART RATE
162
SpaO2 (3)
PLETHYSMOGRAPH (3)
164
SpvO2 (3)
Δsat (3)
PLETH (3)
168
Δsatxy (3)
plethxy (3)
150
DIGITAL SIGNAL PROCESSOR
152
154
158
118
114
SENSOR INTERFACE
112
124
SENSOR INTERFACE
134
SENSOR INTERFACE
110
120
130

FIG. 1A

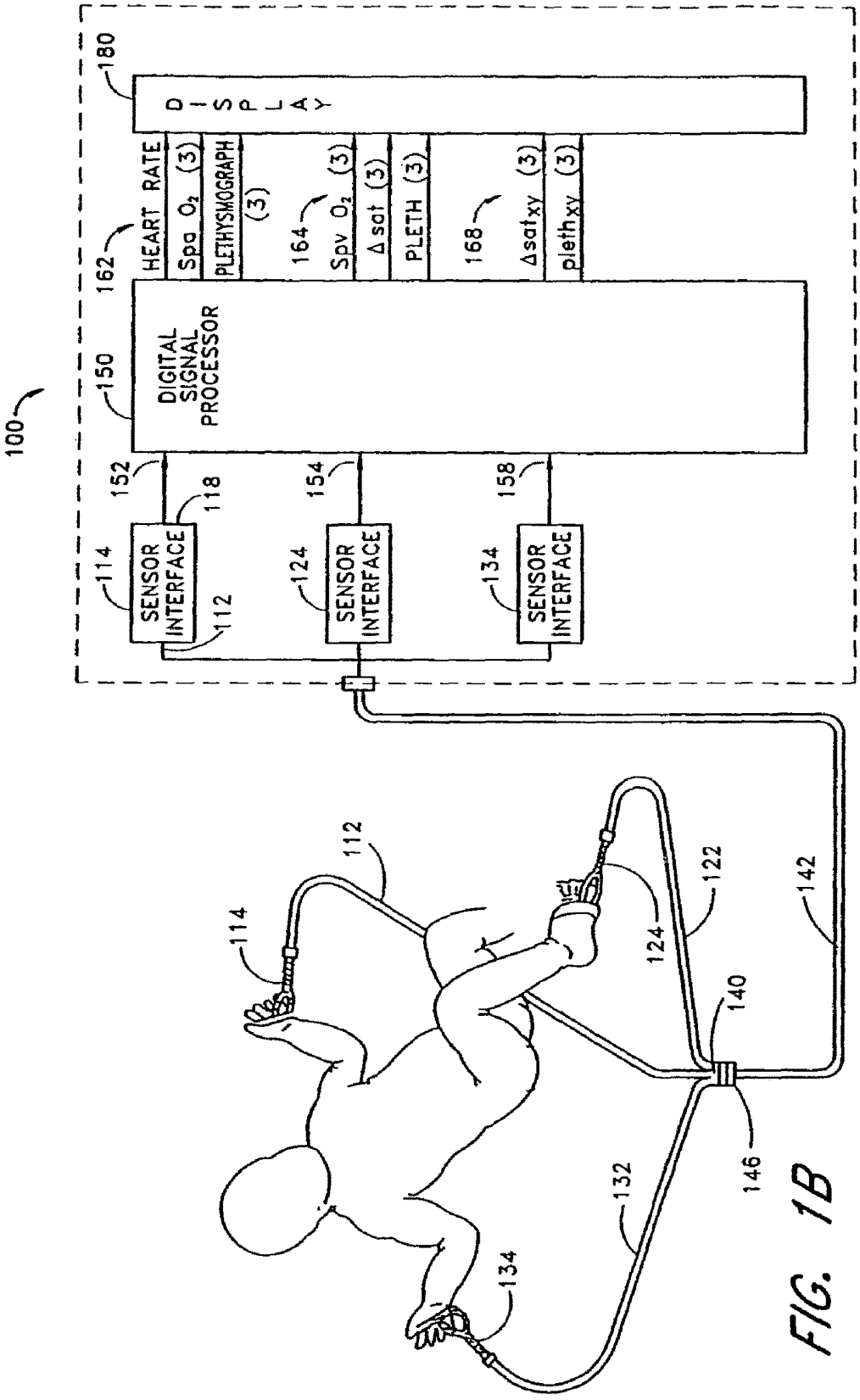
100
180
DISPLAY
HEART RATE
162
SpO2 (3)
PLETHYSMOGRAPH (3)
164
SpvO2 (3)
Δsat (3)
PLETH (3)
168
Δsatxy (3)
plethxy (3)
DIGITAL SIGNAL PROCESSOR
150
152
118
154
158
SENSOR INTERFACE
114
112
124
134
112
114
122
124
142
140
146
132
134

FIG. 1B

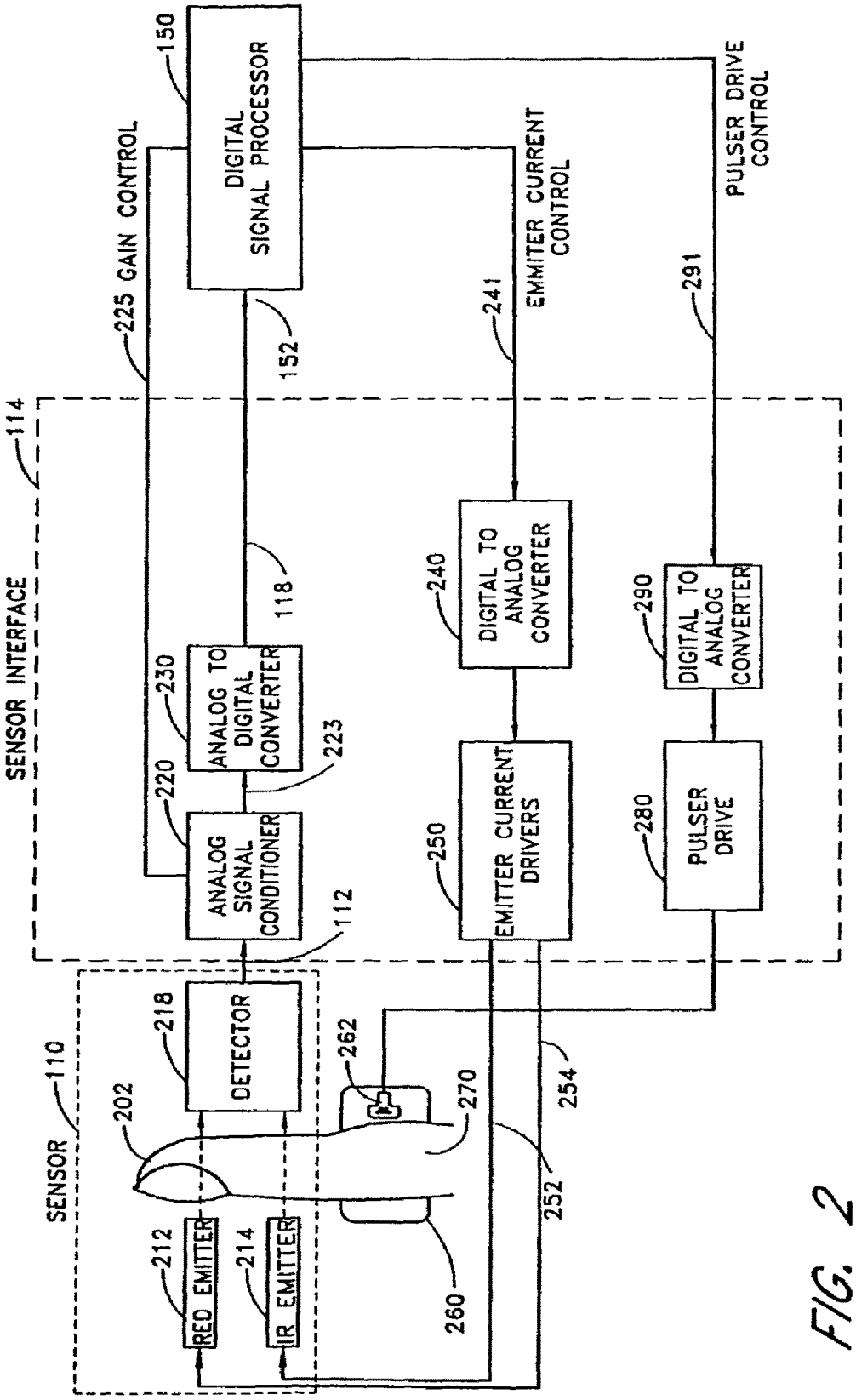
SENSOR INTERFACE
114
DIGITAL SIGNAL PROCESSOR
150
225 GAIN CONTROL
152
241
EMMITER CURRENT CONTROL
291
PULSER DRIVE CONTROL
ANALOG TO DIGITAL CONVERTER
230
118
223
ANALOG SIGNAL CONDITIONER
220
112
DIGITAL TO ANALOG CONVERTER
240
DIGITAL TO ANALOG CONVERTER
290
EMITTER CURRENT DRIVERS
250
PULSER DRIVE
280
DETECTOR
218
262
270
254
252
SENSOR
110
202
RED EMITTER
212
IR EMITTER
214
260

FIG. 2

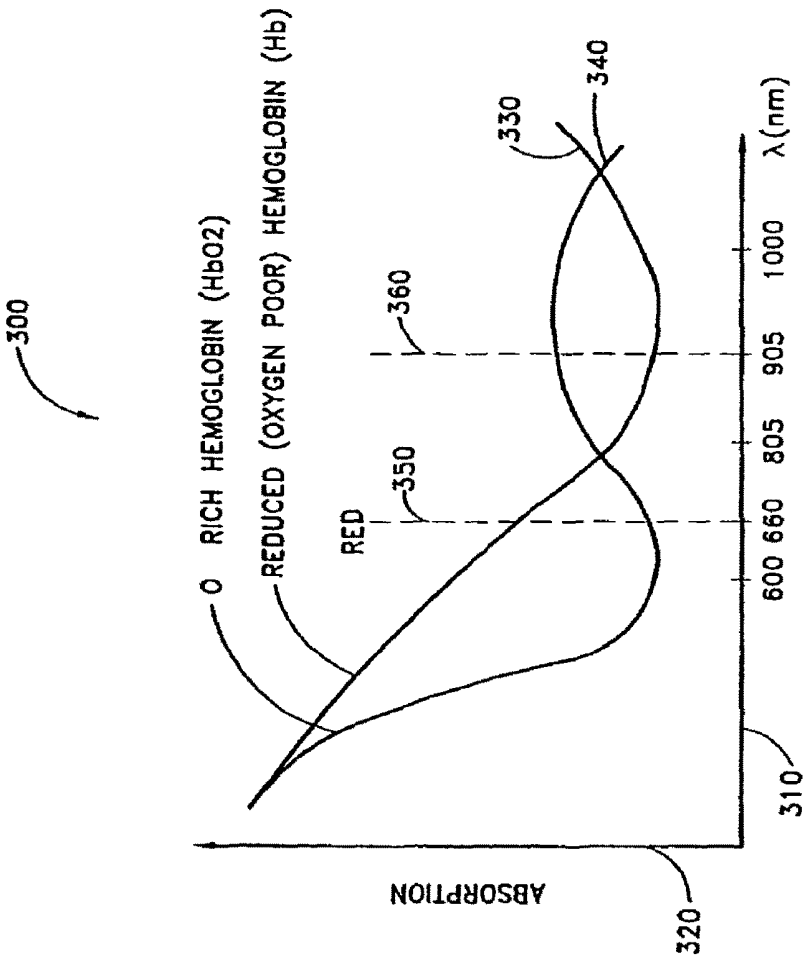
300
O RICH HEMOGLOBIN (HbO2)
REDUCED (OXYGEN POOR) HEMOGLOBIN (Hb)
RED
360
350
330
340
λ(nm)
1000
905
805
660
600
310
320
ABSORPTION

FIG. 3

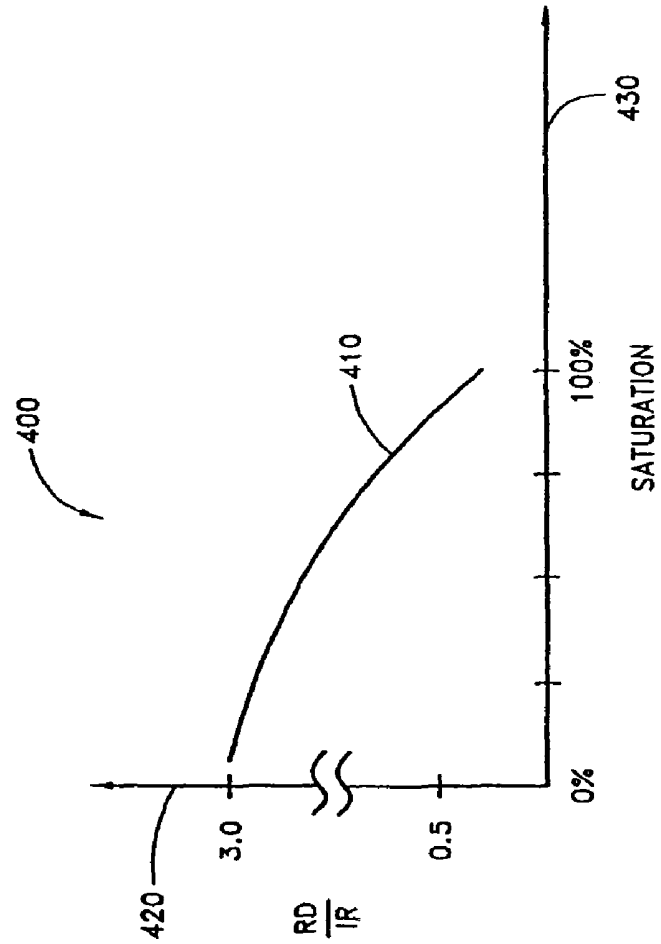

FIG. 4

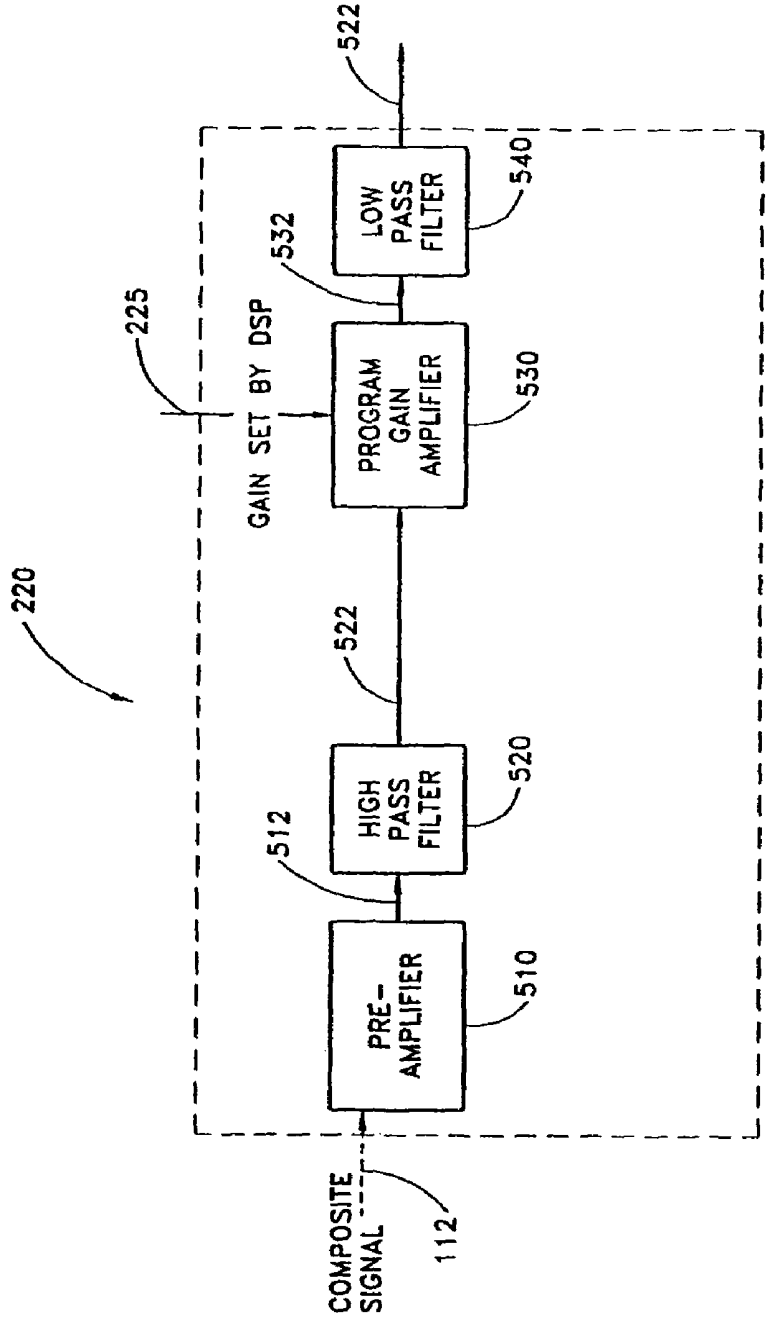
220
225
GAIN SET BY DSP
COMPOSITE SIGNAL
112
PRE-AMPLIFIER
510
512
HIGH PASS FILTER
520
522
PROGRAM GAIN AMPLIFIER
530
532
LOW PASS FILTER
540
522

FIG. 5

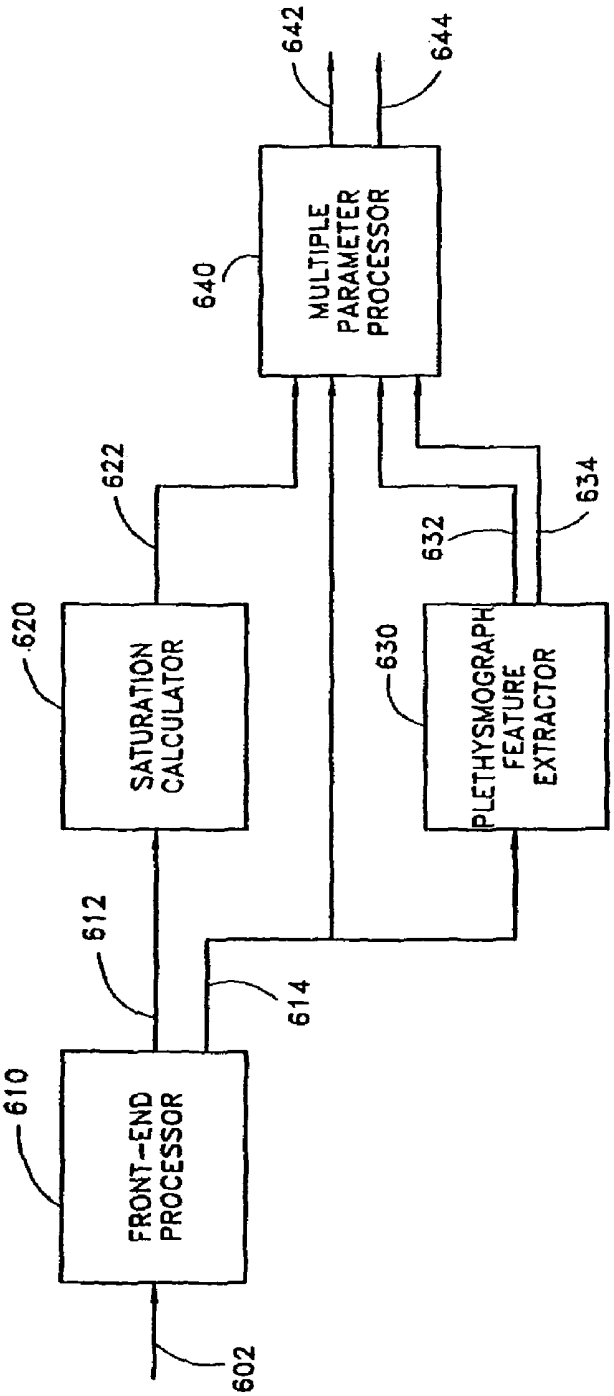
642
644
MULTIPLE PARAMETER PROCESSOR
640
622
634
632
620
SATURATION CALCULATOR
630
PLETHYSMOGRAPH FEATURE EXTRACTOR
612
614
610
FRONT-END PROCESSOR
602

FIG. 6

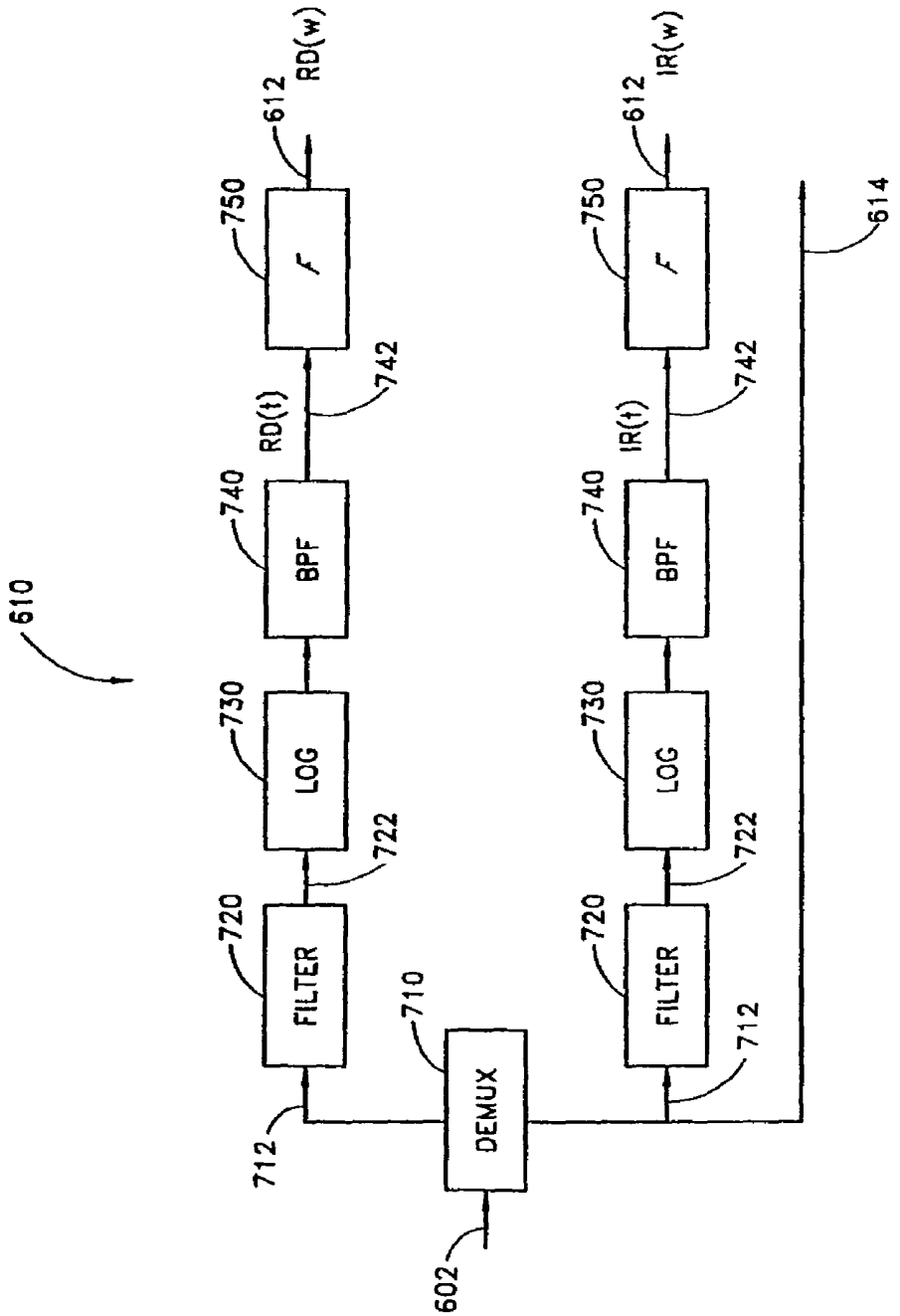
610
602
DEMUX
710
712
FILTER
720
LOG
730
722
BPF
740
RD(t)
742
F
750
612
RD(w)
IR(t)
IR(w)
614

FIG. 7

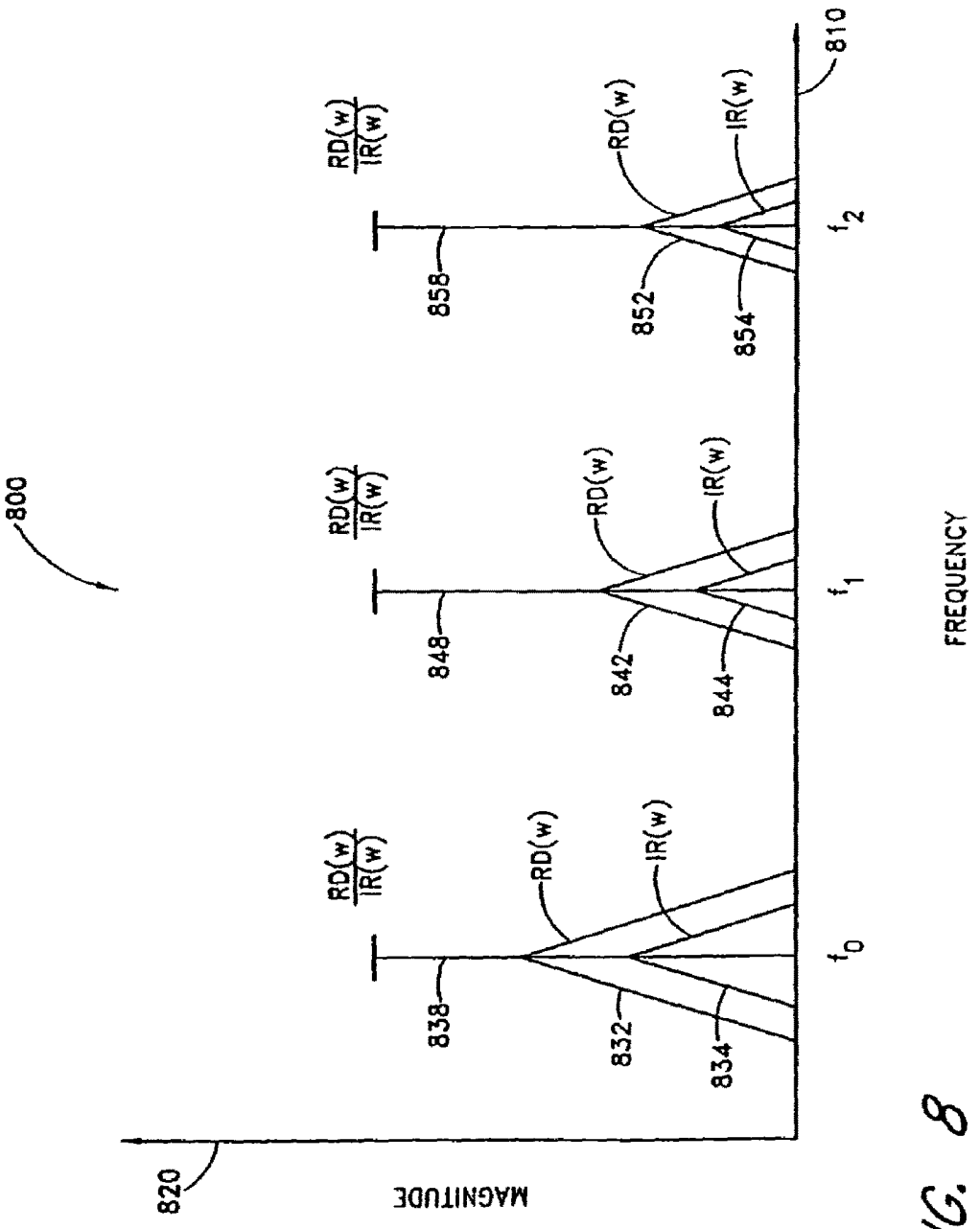
800
820
MAGNITUDE
810
FREQUENCY
f_0
f_1
f_2
838
832
834
848
842
844
858
852
854
RD(w)/IR(w)
RD(w)
IR(w)

FIG. 8

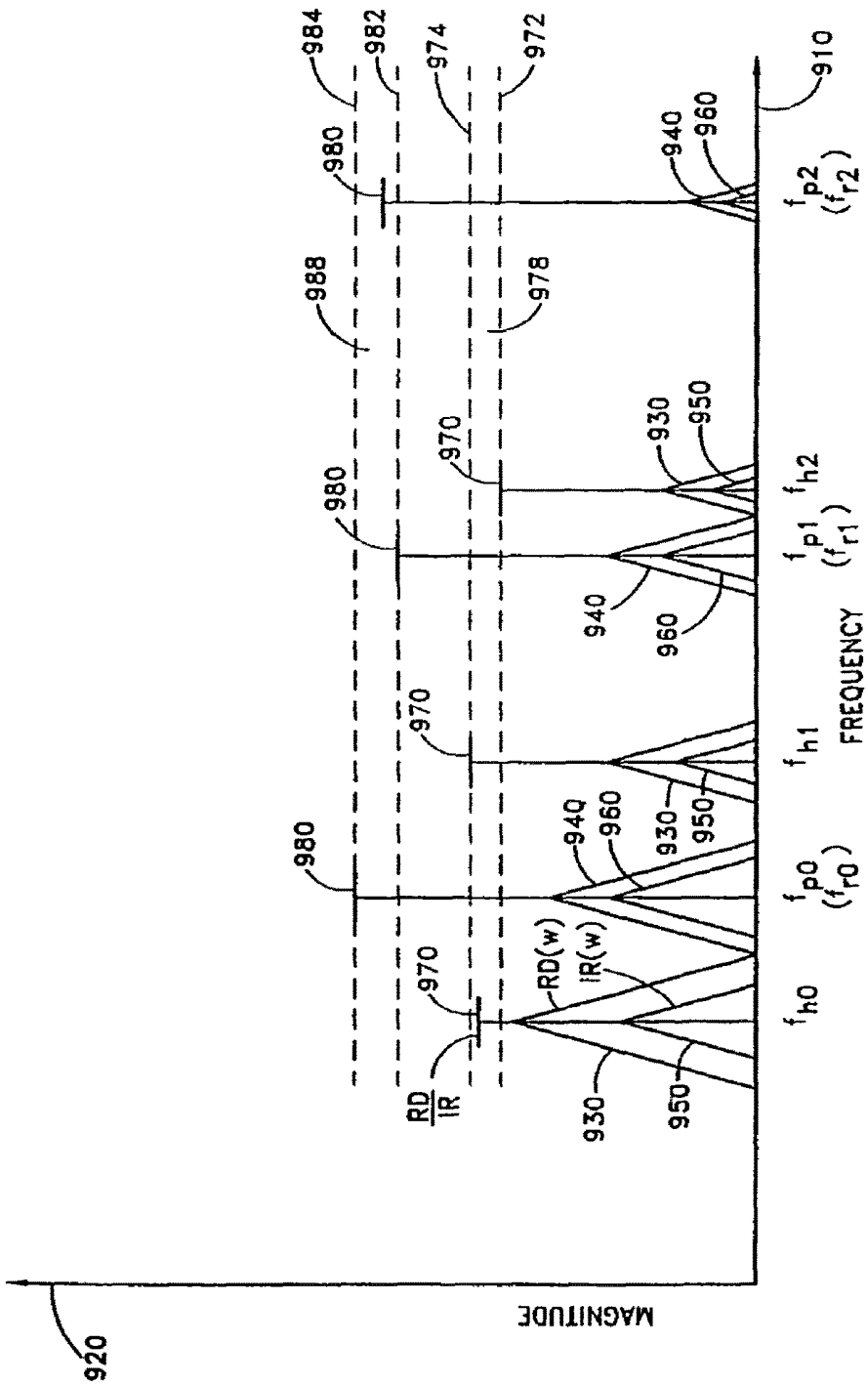
920
MAGNITUDE
FREQUENCY
910
984
982
974
972
980
988
978
970
980
930
950
940
960
970
980
940
960
930
950
970
RD
IR
930
950
RD(w)
IR(w)
940
960
930
950
980
970
970
980
940
960
930
950
f_{h0}
f_{p0} (f_{r0})
f_{h1}
f_{p1} (f_{r1})
f_{h2}
f_{p2} (f_{r2})

FIG. 9

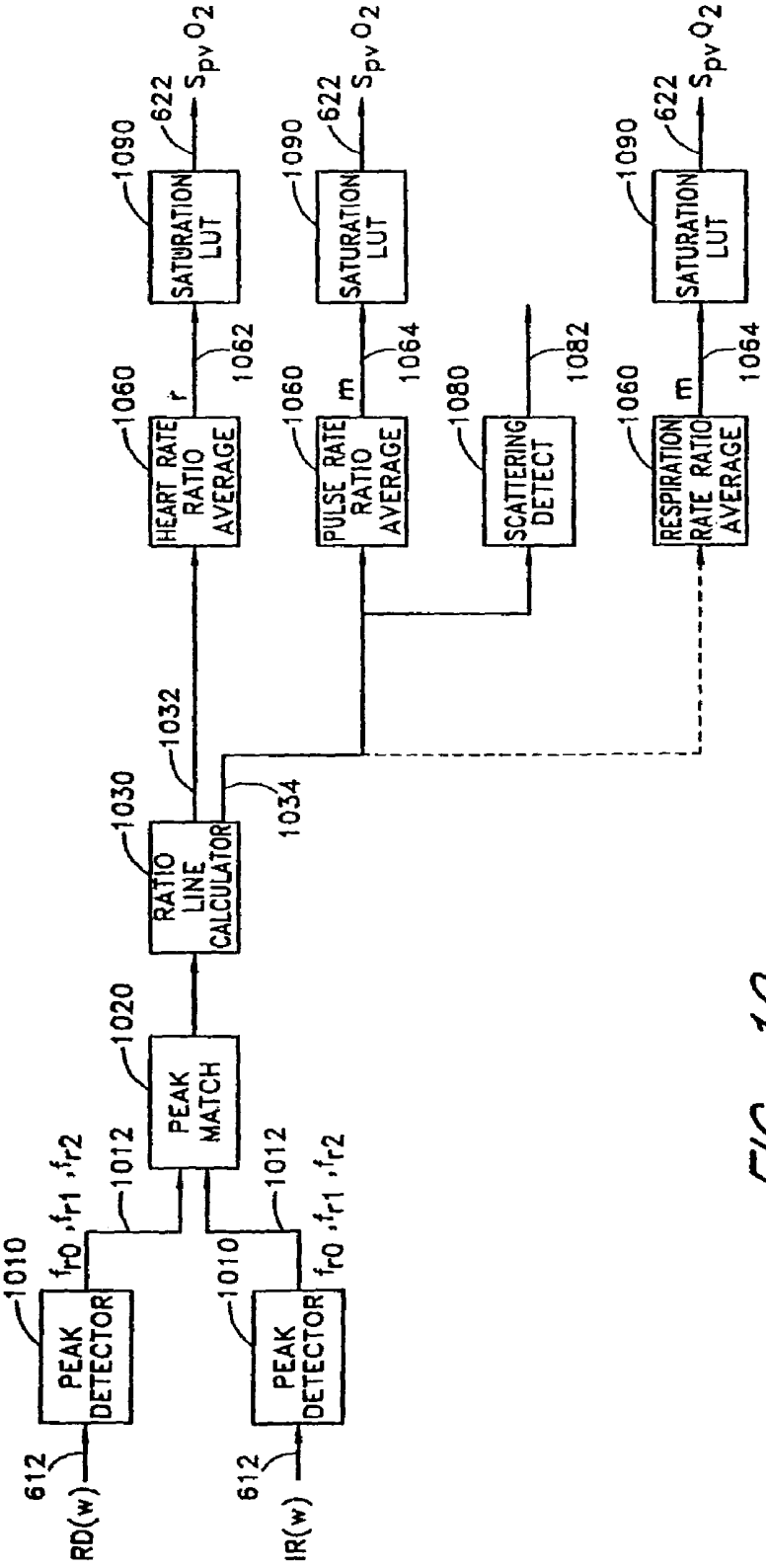
612
RD(w)
612
IR(w)
1010
PEAK DETECTOR
1010
PEAK DETECTOR
f_{r0}, f_{r1}, f_{r2}
1012
f_{r0}, f_{r1}, f_{r2}
1012
1020
PEAK MATCH
1030
RATIO LINE CALCULATOR
1032
1034
1060
HEART RATE RATIO AVERAGE
r
1062
1060
PULSE RATE RATIO AVERAGE
m
1064
1080
SCATTERING DETECT
1082
1060
RESPIRATION RATE RATIO AVERAGE
m
1064
1090
SATURATION LUT
622
$S_{pv}O_2$
1090
SATURATION LUT
622
$S_{pv}O_2$
1090
SATURATION LUT
622
$S_{pv}O_2$

FIG. 10

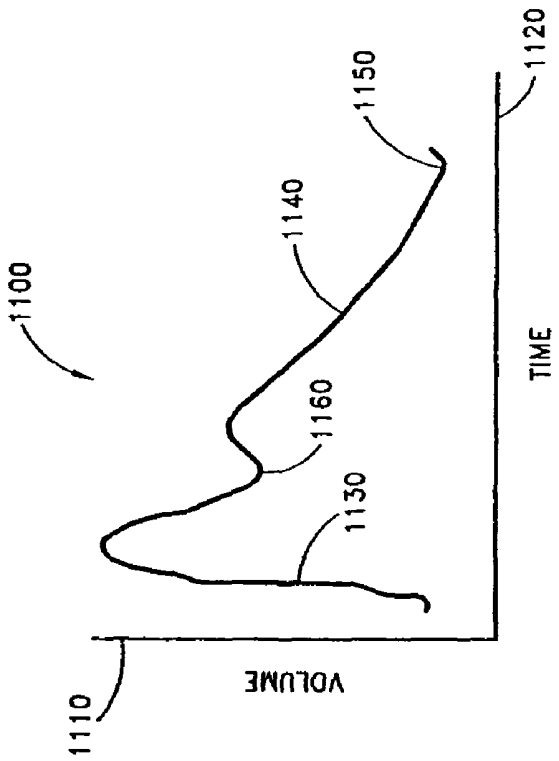

FIG. 11

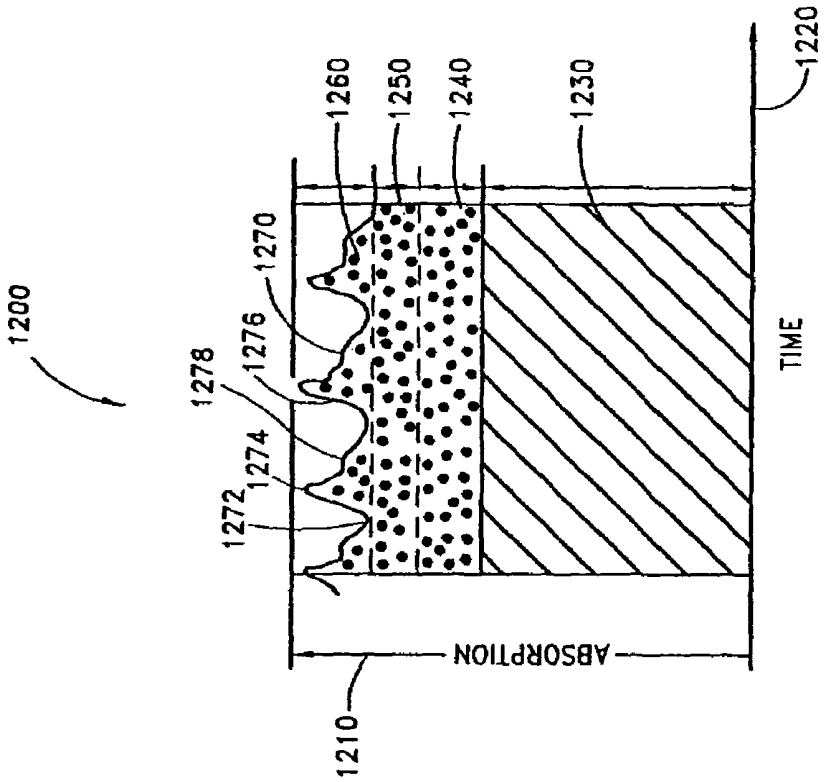
1200
1210
1220
1230
1240
1250
1260
1270
1272
1274
1276
1278
ABSORPTION
TIME

FIG. 12

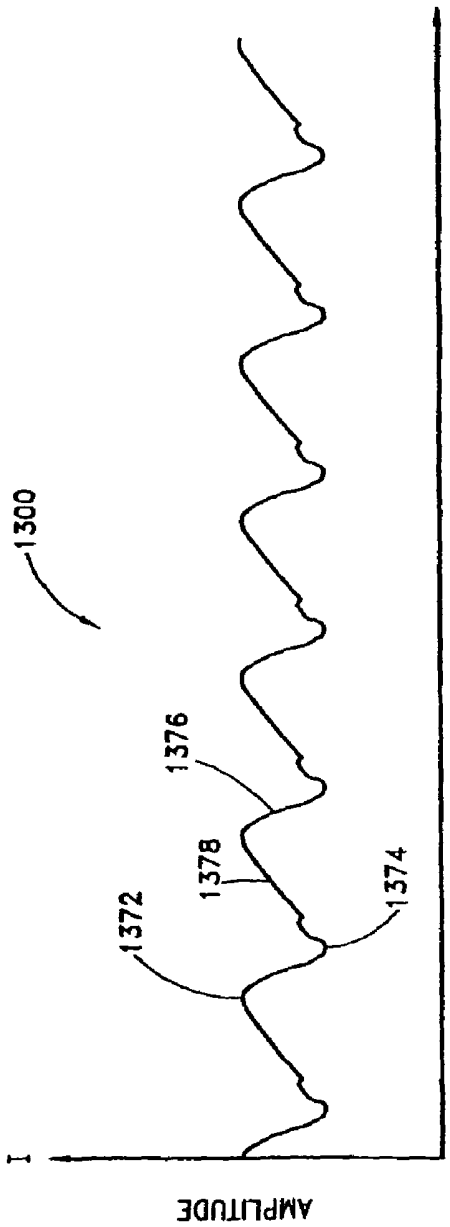

FIG. 13

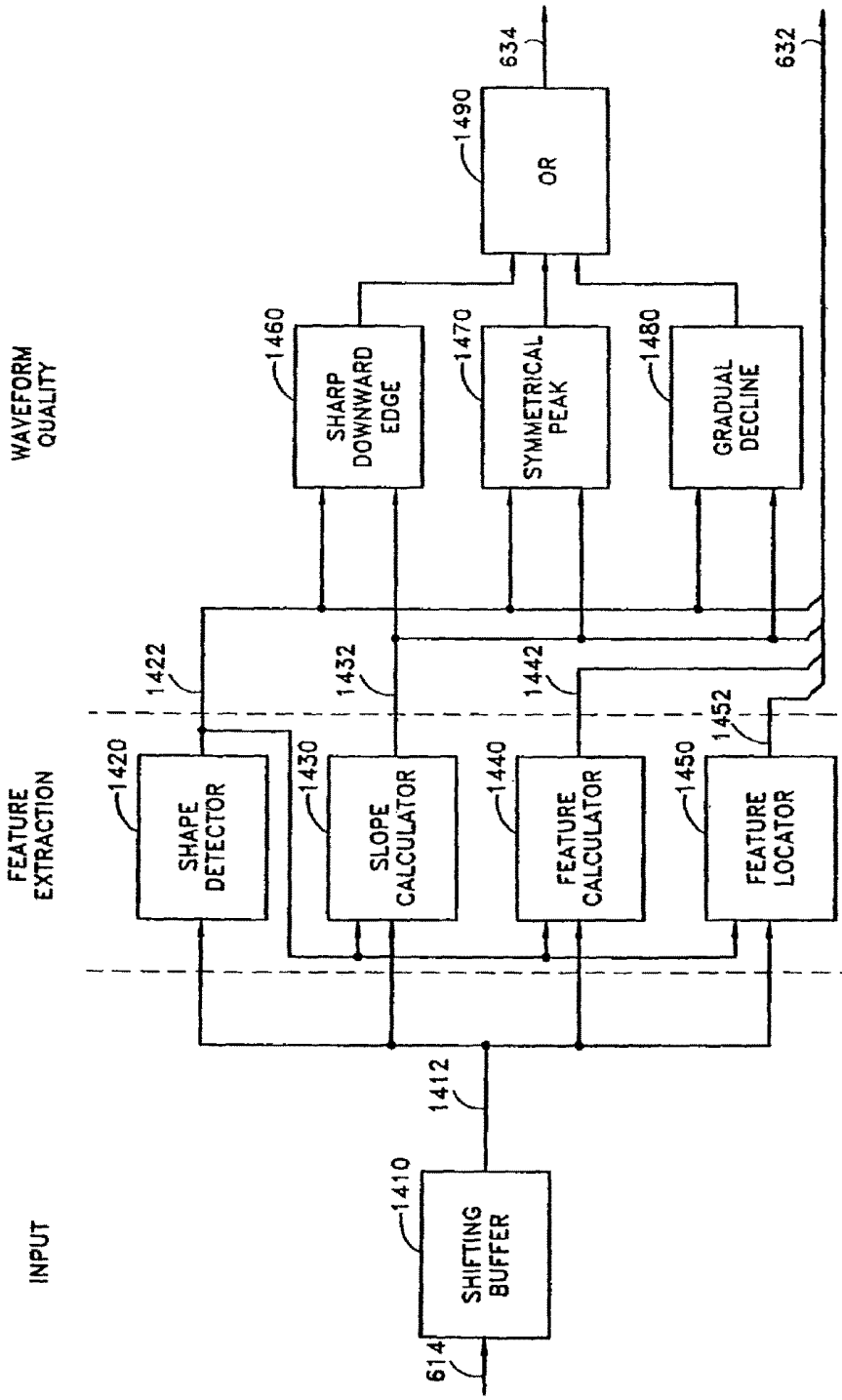
INPUT
FEATURE EXTRACTION
WAVEFORM QUALITY
SHIFTING BUFFER
SHAPE DETECTOR
SLOPE CALCULATOR
FEATURE CALCULATOR
FEATURE LOCATOR
SHARP DOWNWARD EDGE
SYMMETRICAL PEAK
GRADUAL DECLINE
OR
614
1410
1412
1420
1422
1430
1432
1440
1442
1450
1452
1460
1470
1480
1490
632
634

FIG. 14

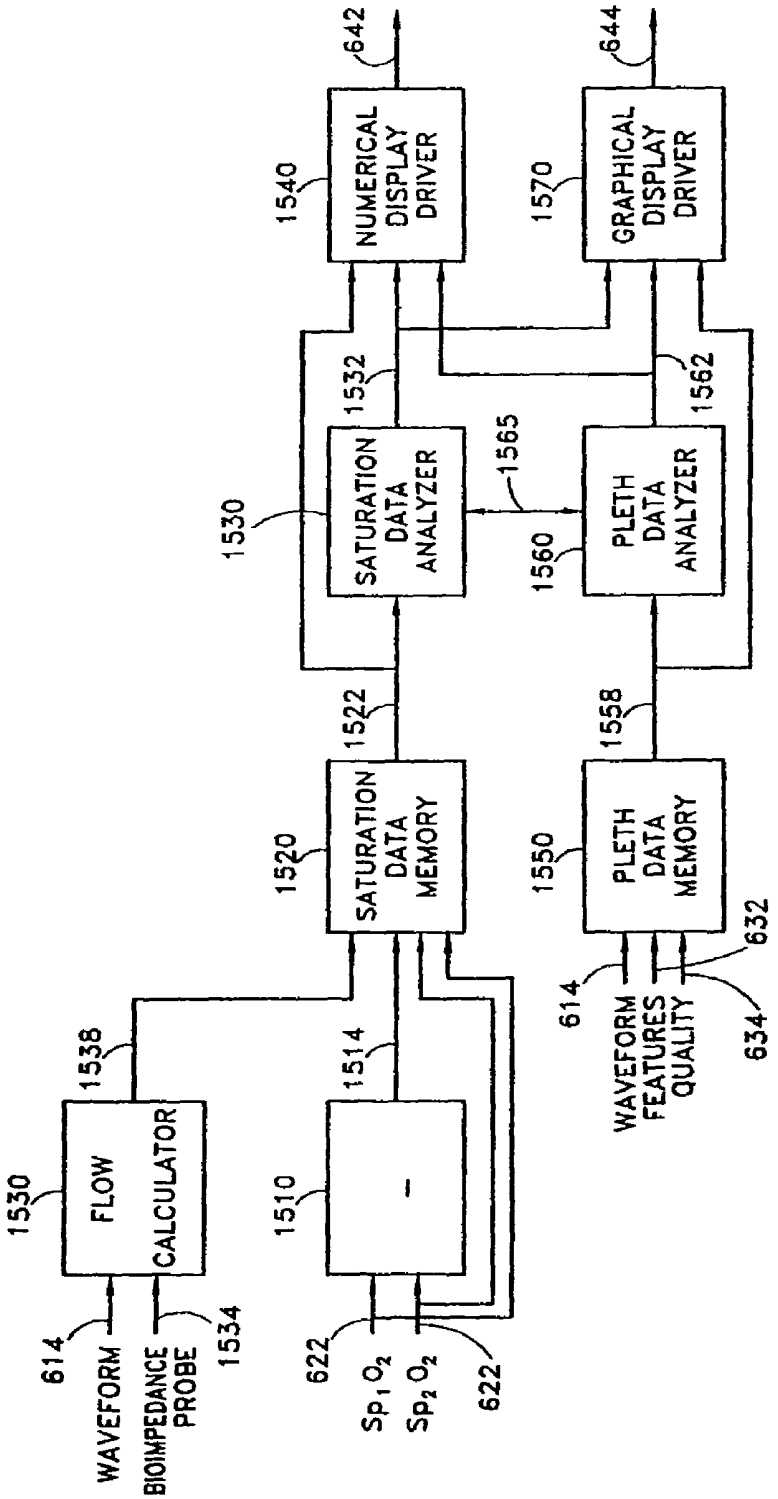
642
644
1540
NUMERICAL DISPLAY DRIVER
1570
GRAPHICAL DISPLAY DRIVER
1532
1562
1530
SATURATION DATA ANALYZER
1565
1560
PLETH DATA ANALYZER
1522
1558
1520
SATURATION DATA MEMORY
1550
PLETH DATA MEMORY
632
614
WAVEFORM FEATURES QUALITY
634
1538
1514
1530
FLOW CALCULATOR
1510
614
WAVEFORM
BIOIMPEDANCE PROBE
1534
622
Sp_1O_2
Sp_2O_2
622

FIG. 15

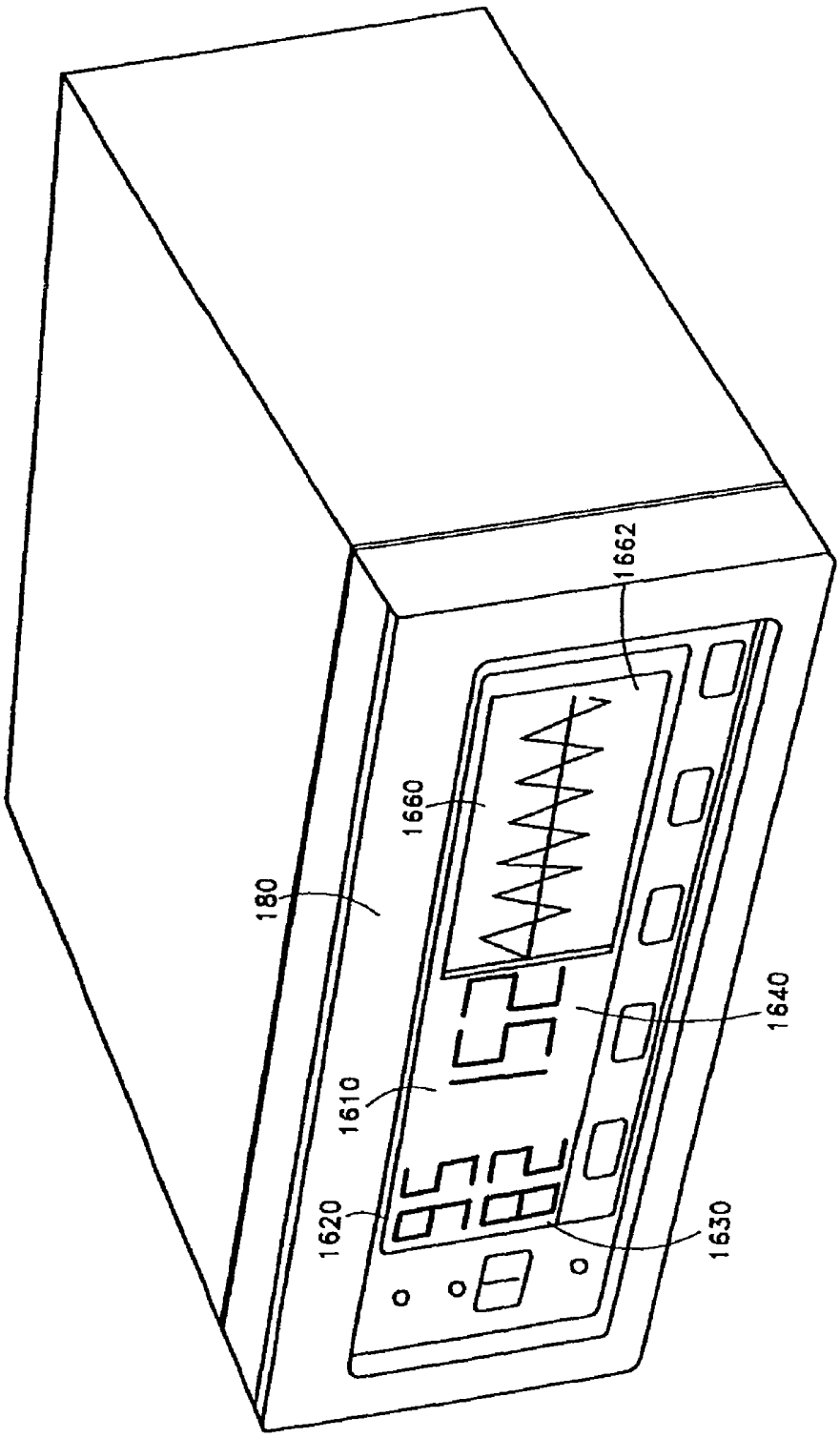

FIG. 16A

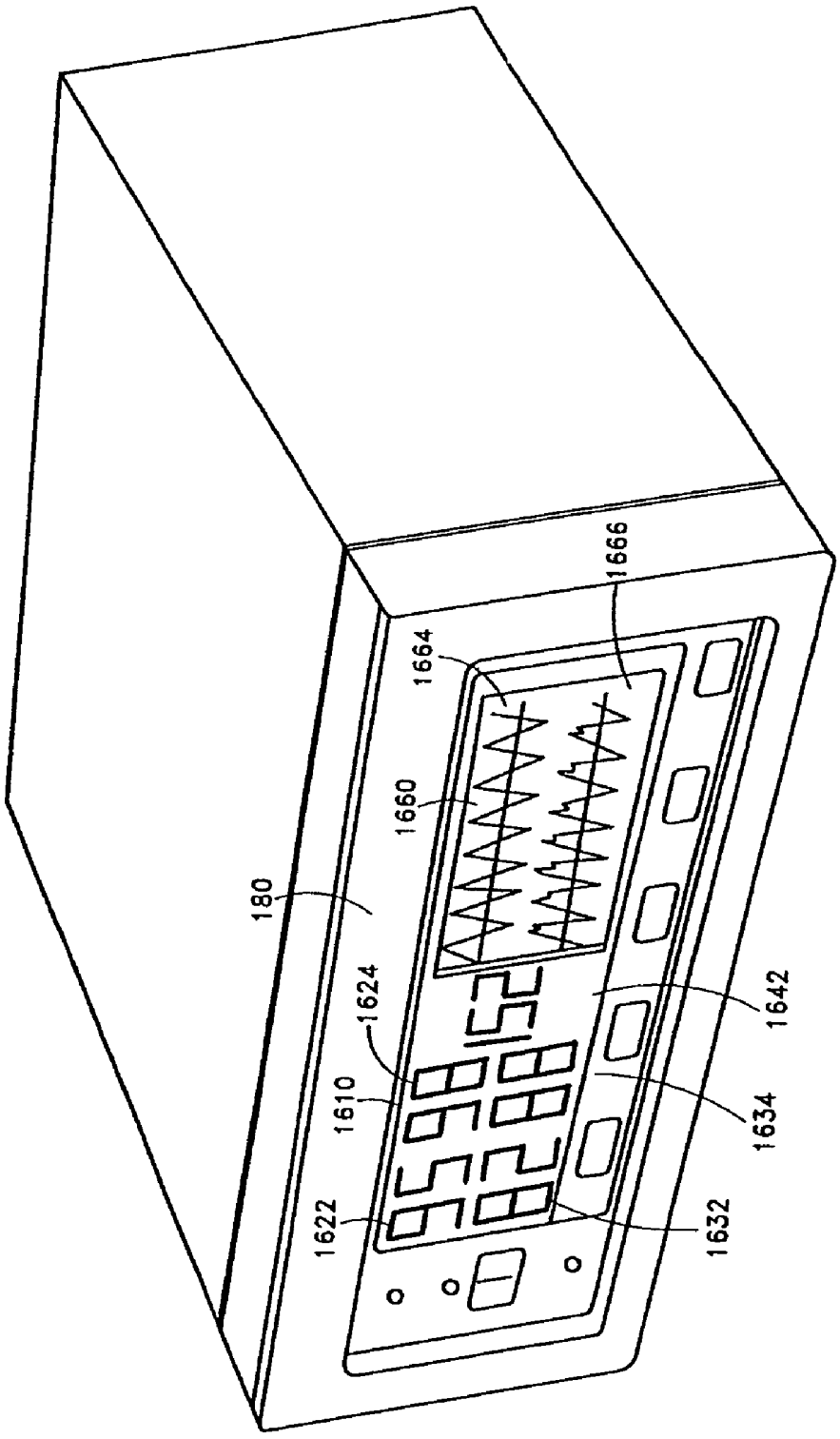

FIG. 16B

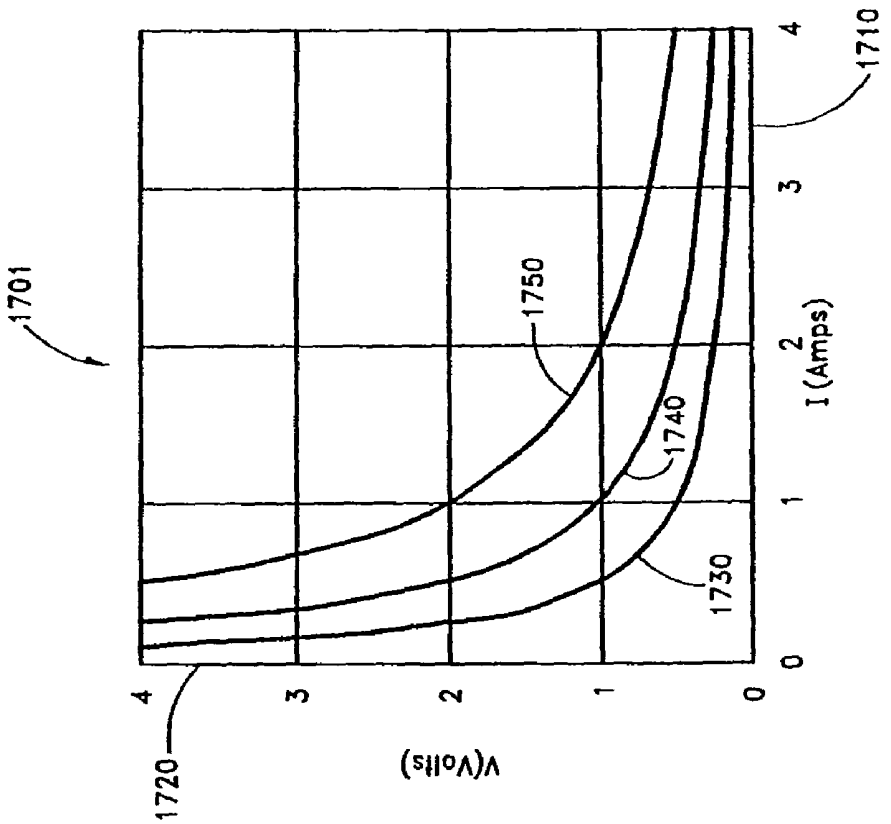

FIG. 17A

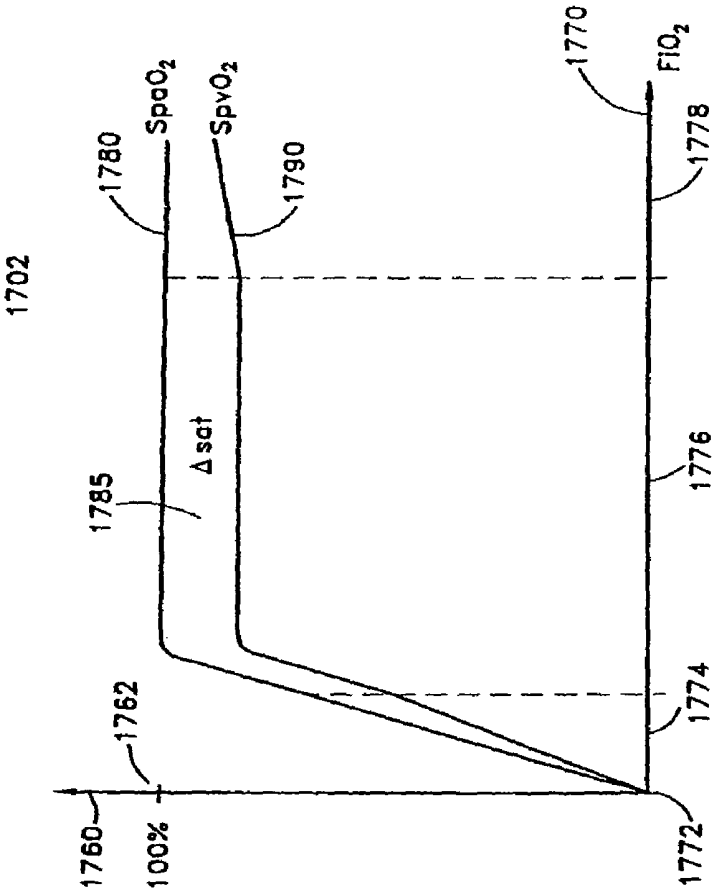
1702
1780
SpaO2
SpvO2
1790
1770
FiO2
1778
1785
Δsat
1776
1762
1774
1760
100%
1772

FIG. 17B

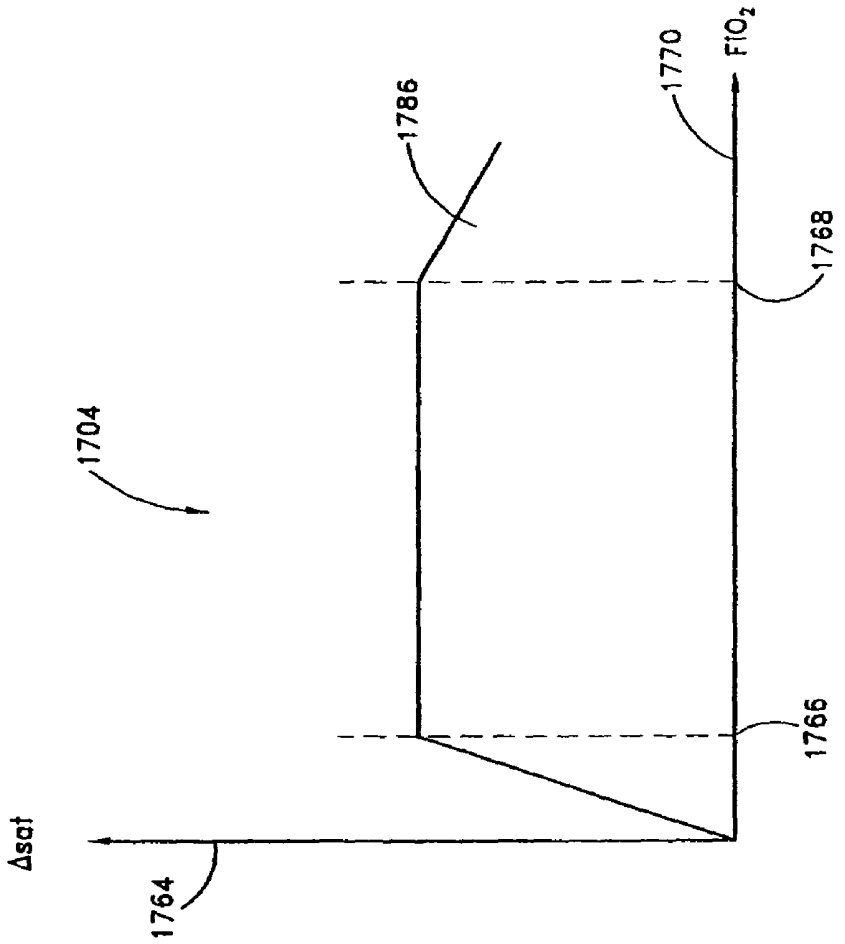

FIG. 17C

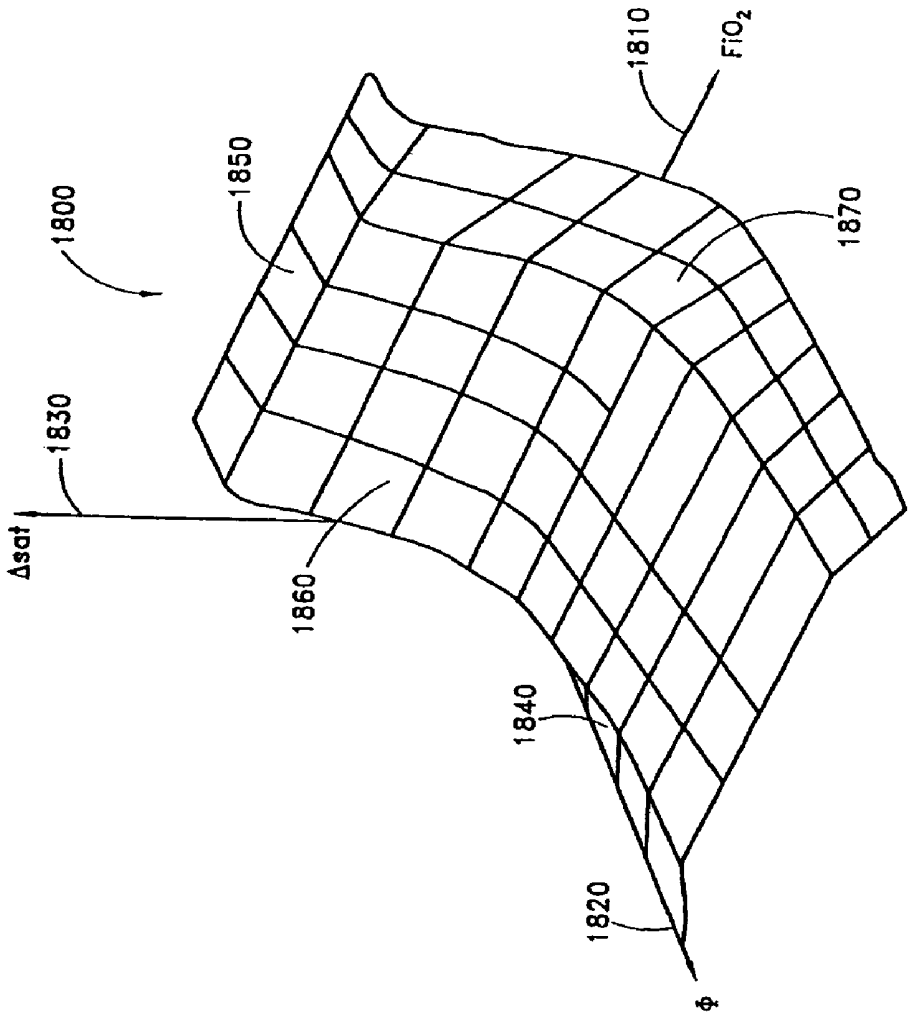

FIG. 18

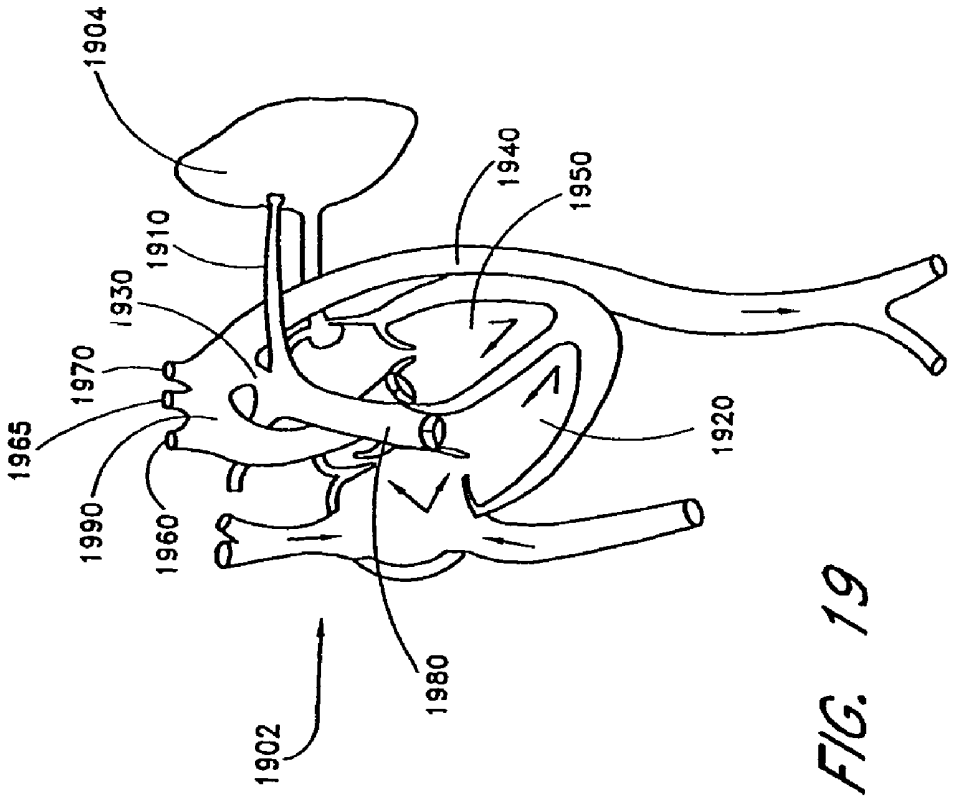

FIG. 19

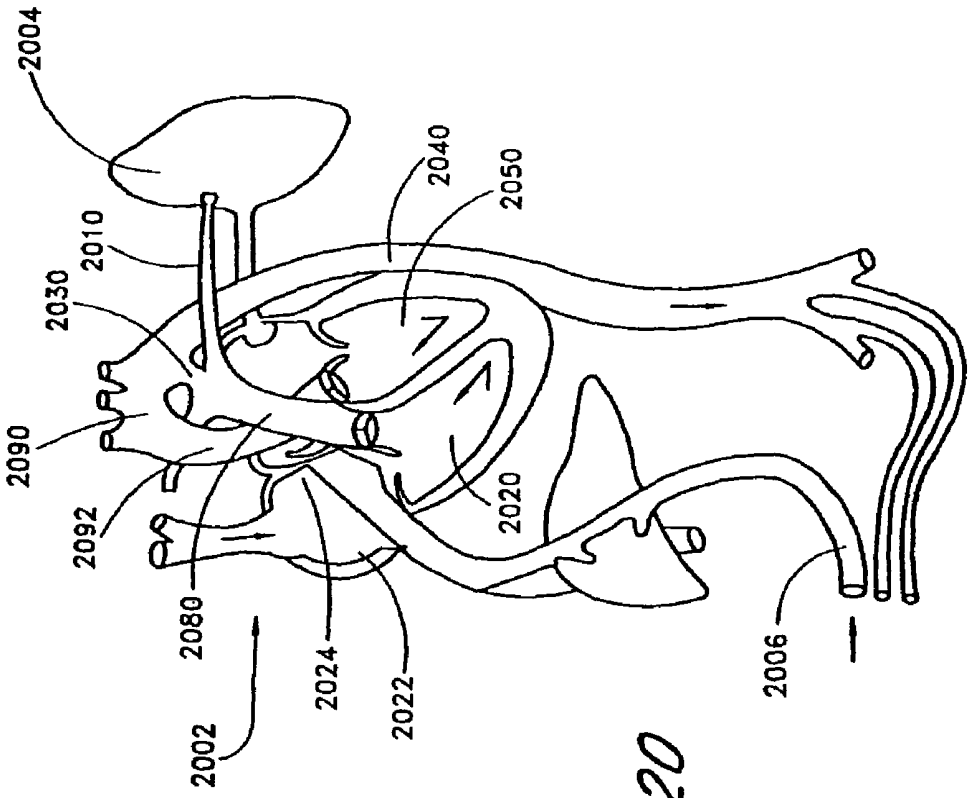
2004
2040
2050
2010
2030
2090
2092
2020
2080
2024
2022
2002
2006

FIG. 20

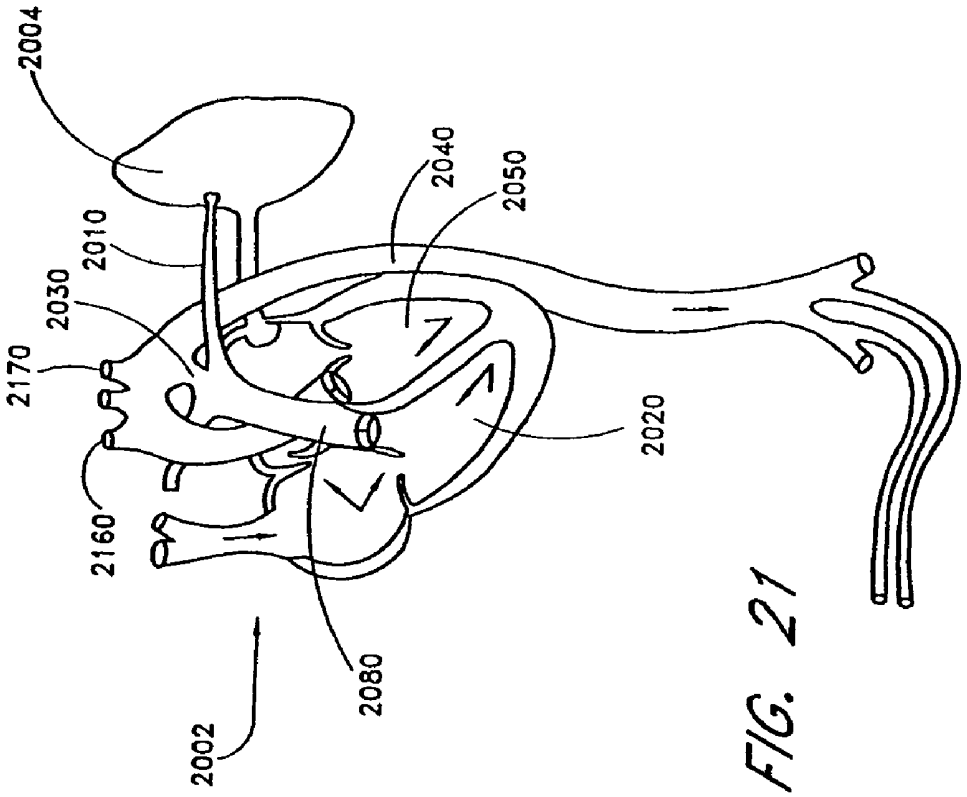

FIG. 21

PHYSIOLOGICAL MONITOR

INCORPORATION BY REFERENCE TO ANY PRIORITY APPLICATIONS

Any and all applications for which a foreign or domestic priority claim is identified in the Application Data Sheet as filed with the present application are incorporated by reference under 37 CFR 1.57 and made a part of this specification.

BACKGROUND

The measurement of oxygen delivery to the body and the corresponding oxygen consumption by its organs and tissues is vitally important to medical practitioners in the diagnosis and treatment of various medical conditions. Oxygen delivery, the transport of oxygen from the environment to organs and tissues, depends on the orchestration of several interrelated physiologic systems. Oxygen uptake is determined by the amount of oxygen entering the lung and the adequacy of gas exchange within the lung. This gas exchange is determined by the diffusion of oxygen from the alveolar space to the blood of the pulmonary capillaries. Oxygen is subsequently transported to all organs and tissues by blood circulation maintained by the action of the heart. The availability of oxygen to the organs and tissues is determined both by cardiac output and by the oxygen content in the blood. Oxygen content, in turn, is affected by the concentration of available hemoglobin and hemoglobin oxygen saturation. Oxygen consumption is related to oxygen delivery according to Fick's axiom, which states that oxygen consumption in the peripheral tissues is equal to oxygen delivery via the airway.

Oxygen delivery and oxygen consumption can be estimated from a number of measurable parameters. Because of the diagnostic impracticalities of measuring oxygen uptake and cardiac output, oxygen delivery is typically assessed from the oxygen status of arterial blood alone, such as arterial oxygen partial pressure, P_aO_2, and arterial oxygen saturation, S_aO_2. P_aO_2 represents the relatively small amount of oxygen dissolved in the blood plasma. S_aO_2 represents the much larger amount of oxygen chemically bound to the blood hemoglobin. Oxygen consumption is typically assessed from the oxygen status of mixed venous blood, i.e. the oxygen saturation of blood from the pulmonary artery, S_vO_2, which is used to estimate the O_2 concentration of blood returning from all tissues and organs of the body. These parameters can be measured by both invasive and non-invasive techniques, except S_vO_2, which requires an invasive measurement.

Invasive techniques include blood gas analysis using the in vitro measurement of extracted arterial or venous blood, drawn with a syringe and needle or an intervascular catheter. Arterial blood is commonly obtained by puncturing the brachial, radial or femoral artery. Venous blood can be obtained from an arm vein, but such a sample reflects only local conditions. To obtain mixed venous blood, which represents the composite of all venous blood, a long catheter is typically passed through the right heart and into the main pulmonary artery from a peripheral vein. Extracted blood gas analysis utilizes blood gas machines or oximeters. A blood gas machine measures the partial pressure of oxygen, PO_2, using a "Clark electrode" that detects the current generated by oxygen diffusing to a sealed platinum electrode across a gas permeable membrane. An oximeter measures the oxygen saturation, S_vO_2, of oxygenated and deoxygenated hemoglobin using spectrophotometry techniques that detect the differential absorption of particular wavelengths of light by these blood components.

Invasive monitoring also includes the in vivo monitoring of blood gas via a catheter sensor inserted into an artery or vein. Miniaturization of the Clark electrode allows placement of the electrode in a catheter for continuous measurement of PO_2. A fiber optic equipped catheter attached to an external oximeter allows continuous measurement of oxygen saturation. Because of risks inherent in catheterization and the promotion of blood coagulation by certain sensors, these techniques are typically only used when vitally indicated.

Non-invasive techniques include pulse oximetry, which allows the continuous in vivo measurement of arterial oxygen saturation and pulse rate in conjunction with the generation of a photoplethsymograph waveform. Measurements rely on sensors which are typically placed on the fingertip of an adult or the foot of an infant. Non-invasive techniques also include transcutaneous monitoring of PO_2, accomplished with the placement of a heated Clark electrode against the skin surface. These non-invasive oxygen status measurement techniques are described in further detail below.

SUMMARY

Prior art invasive oxygen assessment techniques are inherently limited. Specifically, in vitro measurements, that is, blood extraction and subsequent analysis in a blood gas machine or an oximeter, are non-simultaneous and non-continuous. Further, in vivo measurements through catheterization are not casual procedures and are to be particularly avoided with respect to neonates. Prior art noninvasive techniques are also limited. In particular, conventional pulse oximeters are restricted to measurement of arterial oxygen saturation at a single patient site. Also, transcutaneous monitoring is similarly restricted to the measurement of an estimate of arterial partial pressure at a single patient site, among other limitations discussed further below.

The stereo pulse oximeter according to the present invention overcomes many of the limitations of prior art oxygen status measurements. The word "stereo" comes from the Greek word stereos, which means "solid" or three-dimensional. For example, stereophonic systems use two or more channels to more accurately reproduce sound. The stereo pulse oximeter is similarly multi-dimensional, providing simultaneous, continuous, multiple-site and multiple-parameter oxygen status and plethysmograph (photoplethysmograph) measurements. The stereo pulse oximeter provides a benefit in terms of cost and patient comfort and safety over invasive oxygen status estimation techniques. The multi-dimensional aspects of this invention further provide oxygen status and plethysmograph measurements not available from current noninvasive techniques. In addition, the stereo pulse oximeter allows the isolation of noise artifacts, providing more accurate oxygen status and plethysmograph measurements than available from conventional techniques. The result is improved patient outcome based on a more accurate patient assessment and better management of patient care.

In one aspect of the stereo pulse oximeter, data from a single sensor is processed to advantageously provide continuous and simultaneous multiple-parameter oxygen status and plethysmograph measurements from a particular tissue site. This is in contrast to a conventional pulse oximeter that provides only arterial oxygen saturation data from a tissue site. In particular a physiological monitor comprises a sensor

interface and a signal processor. The sensor interface is in communication with a peripheral tissue site and has an output responsive to light transmitted through the site. The signal processor is in communication with the sensor interface output and provides a plurality of parameters corresponding to the oxygen status of the site, the plethysmograph features of the site or both. The parameters comprise a first value and a second value related to the peripheral tissue site. In one embodiment, the first value is an arterial oxygen saturation and the second value is a venous oxygen saturation. In this embodiment, another parameter provided may be the difference between arterial oxygen saturation and venous oxygen saturation at the tissue site. The venous oxygen saturation is derived from an active pulse generated at the site. The signal processor output may further comprise a scattering indicator corresponding to the site, and the sensor interface may further comprise a pulser drive, which is responsive to the scattering indicator to control the amplitude of the active pulse. One of the parameter values may also be an indication of perfusion.

In another aspect of the stereo pulse oximeter, data from multiple sensors is processed to advantageously provide continuous and simultaneous oxygen status measurements from several patient tissue sites. This is in contrast to a conventional pulse oximeter that processes data from a single sensor to provide oxygen status at a single tissue site. In particular, a physiological monitor comprises a plurality of sensor interfaces each in communications with one of a plurality of peripheral tissue sites. Each of the sensor interfaces has one of a plurality of outputs responsive to light transmitted through a corresponding one of the tissue sites. A signal processor is in communication with the sensor interface outputs and has a processor output comprising a plurality of parameters corresponding to the oxygen status of the sites, the plethysmograph features of the sites or both. The parameters may comprise a first value relating to a first of the peripheral tissue sites and a second value relating to a second of the peripheral tissue sites. In one embodiment, the first value and the second value are arterial oxygen saturations. In another embodiment, the first value and the second value are plethysmograph waveform phases. The physiological monitor may further comprise a sensor attachable to each of the tissue sites. This sensor comprises a plurality of emitters and a plurality of detectors, where at least one of the emitters and at least one of the detectors is associated with each of the tissue sites. The sensor also comprises a connector in communications with the sensor interfaces. A plurality of signal paths are attached between the emitters and the detectors at one end of the sensor and the connector at the other end of the sensor.

In yet another aspect of the stereo pulse oximeter, data from multiple sensors is processed to advantageously provide a continuous and simultaneous comparison of the oxygen status between several tissue sites. A conventional oximeter, limited to measurements at a single tissue site, cannot provide these cross-site comparisons. In particular a physiological monitoring method comprises the steps of deriving a reference parameter and a test parameter from oxygen status measured from at least one of a plurality of peripheral tissue sites and comparing that reference parameter to the test parameter so as to determine a patient condition. The reference parameter may be a first oxygen saturation value and the test parameter a second oxygen saturation value. In that case, the comparing step computes a delta oxygen saturation value equal to the arithmetic difference between the first oxygen saturation value and the second oxygen saturation value. In one embodiment, the reference parameter is an arterial oxygen saturation measured at a particular one the tissue sites and the test parameter is a venous oxygen saturation measured at that particular site. In another embodiment, the reference parameter is a first arterial oxygen saturation value at a first of the tissue sites, the test parameter is a second arterial oxygen saturation value at a second of the tissue sites. In yet another embodiment, the reference parameter is a plethysmograph feature measured at a first of the sites, the test parameter is a plethysmograph feature measured at a second of the sites and the monitoring method comparison step determines the phase difference between plethysmographs at the first site and the second site. In a further embodiment, the comparing step determines a relative amount of damping between plethysmographs at the first site and the second site. The multi-dimensional features of these embodiments of the stereo pulse oximeter can be advantageously applied to the diagnosis and managed medical treatment of various medical conditions. Particularly advantageous applications of stereo pulse oximetry include oxygen titration during oxygen therapy, nitric oxide titration during therapy for persistent pulmonary hypertension in neonates (PPHN), detection of a patent ductus arteriosis (PDA), and detection of an aortic coarctation.

BRIEF DESCRIPTION OF THE DRAWINGS

The present invention will be described in detail below in connection with the following drawing figures in which:

FIG. **1**A is a top-level block diagram of a stereo pulse oximeter according to the present invention;

FIG. **1**B shows a single-sensor alternative embodiment to FIG. **1**A;

FIG. **2** is a block diagram of the stereo pulse oximeter sensor interface;

FIG. **3** is a graph illustrating the absorption of red and infrared wavelengths by both oxygenated and deoxygenated hemoglobin;

FIG. **4** is a graph showing the empirical relationship between the "red over infrared" ratio and arterial oxygen saturation;

FIG. **5** is a block diagram of the analog signal conditioning for the sensor interface;

FIG. **6** is a functional block diagram of the stereo pulse oximeter signal processing;

FIG. **7** is a functional block diagram of the front-end signal processing;

FIG. **8** is a graph depicting the frequency spectrum of an arterial intensity signal;

FIG. **9** is a graph depicting the frequency spectrum of a combined arterial and venous intensity signal;

FIG. **10** is a functional block diagram of the saturation calculation signal processing;

FIG. **11** is a graph illustrating a plethysmograph waveform;

FIG. **12** is a graph illustrating the absorption contribution of various blood and tissue components;

FIG. **13** is a graph illustrating an intensity "plethysmograph" pulse oximetry waveform;

FIG. **14** is a functional block diagram of the plethysmograph feature extraction signal processing;

FIG. **15** is a functional block diagram of the multiple parameter signal processing;

FIG. **16**A is an illustration of a single-site stereo pulse oximeter display screen;

FIG. **16**B is an illustration of a multi-site stereo pulse oximeter display screen;

FIG. **17**A is a graph depicting a family of constant power curves for the electrical analog of constant oxygen consumption;

FIG. **17**B is a graph depicting arterial and venous oxygen saturation versus fractional inspired oxygen;

FIG. **17**C is a graph depicting arterial minus venous oxygen saturation versus fractional inspired oxygen;

FIG. **18** is a three-dimensional graph depicting a delta oxygen saturation surface;

FIG. **19** is an illustration of a neonatal heart depicting a pulmonary hypertension condition;

FIG. **20** is an illustration of a fetal heart depicting the ductus arteriosis; and

FIG. **21** is an illustration of a neonatal heart depicting a patent ductus arteriosis (PDA).

DETAILED DESCRIPTION

Stereo Pulse Oximetry

FIG. **1**A illustrates the multi-dimensional features of a stereo pulse oximeter **100** according to the present invention. Shown in FIG. **1**A is an exemplary stereo pulse oximeter configuration in which a first sensor **110** is attached to a neonate's left hand, a second sensor **120** is attached to one of the neonate's feet, and a third sensor **130** is attached to the neonate's right hand. In general, these sensors are used to obtain oxygen status and photoplethysmograph measurements at peripheral sites, including a person's ears and face, such as the nose and regions of the mouth in addition to hands, feet and limbs, but not including internal sites such as internal organs and the brain.

Each sensor **110**, **120**, **130** provides a stream of data through a corresponding sensor interface **114**, **124**, **134** to the digital signal processor (DSP) **150**. For example, the first sensor **110** is connected to an input **112** of the first sensor interface **114**, and the output **118** of the first sensor interface **114** is attached to a first data channel input **152** of the DSP **150**. Similarly, the second sensor **120** provides data to a second data channel input **154** and the third sensor **130** provides data to a third data channel input **158**.

FIG. **1**B illustrates an alternative embodiment of the separate sensors **110**, **120**, **130** (FIG. **1**A). A stereo sensor **140** has multiple branches **112**, **122**, **132** each terminating in a sensor portion **114**, **124**, **134**. Each sensor portion **114**, **124**, **134** has two light emitters and a light detector, as described below, and is attachable to a separate patient site. Thus, the stereo sensor **140** advantageously provides a single sensor device having multiple light emitters and multiple light detectors for attachment to multiple patient tissue sites. A combination of the stereo sensor **140** and a single patient cable **142** advantageously allows a single connection **144** at the stereo pulse oximeter **100** and a single connection **146** at the stereo sensor **140**.

The DSP **150** can independently process each data channel input **152**, **154**, **158** and provide outputs **162** typical of pulse oximetry outputs, such as arterial oxygen saturation, Sp_aO_2, the associated plethysmograph waveform and the derived pulse rate. In contrast with a conventional pulse oximeter, however, these outputs **162** include simultaneous measurements at each of several patient tissue sites. That is, for the configuration of FIG. **1**A, the stereo pulse oximeter **100** simultaneously displays Sp_aO_2 and an associated plethysmograph waveform for three tissue sites in addition to the patient's pulse rate obtained from any one of sites. Further, the DSP **150** can provide unique outputs unavailable from conventional pulse oximeters. These outputs **164** include venous oxygen saturation, Sp_vO_2, a comparison of arterial and venous oxygen saturation, $\Delta_{sat}=Sp_{av}O_2=Sp_aO_2-Sp_vO_2$, and pleth, which denotes plethysmograph shape parameters, for each site. In addition, the DSP **150** can provide cross-site outputs that are only available using stereo pulse oximetry. These unique cross-site outputs **168** include $\Delta sat_{xy}=Sp_{ax}O_2-Sp_{ay}O_2$, which denotes the arterial oxygen saturation at site x minus the arterial oxygen saturation at site y. Also included in these outputs **168** is $\Delta pleth_{xy}$, which denotes a comparison of plethysmograph shape parameters measured at site x and site y, as described in detail below. The stereo pulse oximeter also includes a display **180** capable of showing the practitioner the oxygen status and plethysmograph parameters described above. The display **180** has a multiple channel graphical and numerical display capability as described in more detail below.

Pulse Oximetry Sensor

FIG. **2** depicts one stereo pulse oximeter data channel having a sensor **110** and a sensor interface **114** providing a single data channel input **152** to the DSP **150**. The sensor **110** is used to measure the intensity of red and infrared light after transmission through a portion of the body where blood flows close to the surface, such as a fingertip **202**. The sensor **110** has two light emitters, each of which may be, for example, a light-emitting diode (LED). A red emitter **212**, which transmits light centered at a red wavelength and an infrared (IR) emitter **214**, which transmits light centered at an infrared wavelength are placed adjacent to, and illuminate, a tissue site. A detector **218**, which may be a photodiode, is used to detect the intensity of the emitted light after it passes through, and is partially absorbed by, the tissue site. The emitters **212**, **214** and detector **218** are secured to the tissue site, with the emitters **212**, **214** typically spaced on opposite sides of the tissue site from the detector **218**.

To distinguish between tissue absorption at the two wavelengths, the red emitter **212** and infrared emitter **214** are modulated so that only one is emitting light at a given time. In one embodiment, the red emitter **212** is activated for a first quarter cycle and is off for the remaining three-quarters cycle; the infrared emitter **214** is activated for a third quarter cycle and is off for the remaining three-quarters cycle. That is, the emitters **212**, **214** are cycled on and off alternately, in sequence, with each only active for a quarter cycle and with a quarter cycle separating the active times. The detector **218** produces an electrical signal corresponding to the red and infrared light energy attenuated from transmission through the patient tissue site **202**. Because only a single detector **218** is used, it receives both the red and infrared signals to form a time-division-multiplexed (TDM) signal. This TDM signal is coupled to the input **112** of the sensor interface **114**. One of ordinary skill in the art will appreciate alternative activation sequences for the red emitter **212** and infrared emitter **214** within the scope of this invention, each of which provides a time multiplexed signal from the detector **218** allowing separation of red and infrared signals and determination and removal of ambient light levels in downstream signal processing.

To compute Sp_aO_2, pulse oximetry relies on the differential light absorption of oxygenated hemoglobin, HbO_2, and deoxygenated hemoglobin, Hb, to compute their respective concentrations in the arterial blood. This differential absorption is measured at the red and infrared wavelengths of the sensor **110**. The relationship between arterial oxygen saturation and hemoglobin concentration can be expressed as:

$$Sp_aO_2 = 100\frac{C_{HbO2}}{C_{Hb} + C_{HbO2}} \quad (1)$$

That is, arterial oxygen saturation is the percentage concentration of oxygenated hemoglobin compared to the total concentration of oxygenated hemoglobin and deoxygenated hemoglobin in the arterial blood. Sp_aO_2 is actually a measure of the partial oxygen saturation of the hemoglobin because other hemoglobin derivatives, such as COHb and MetHb, are not taken into consideration.

FIG. **3** shows a graph **300** of the optical absorption properties of HbO_2 and Hb. The graph **300** has an x-axis **310** corresponding to wavelength and a y-axis **320** corresponding to hemoglobin absorption. An Hb curve **330** shows the light absorption properties of deoxygenated hemoglobin. An HbO_2 curve **340** shows the light absorption properties of oxygenated hemoglobin. Pulse oximetry measurements are advantageously made at a red wavelength **350** corresponding to 660 nm and an infrared wavelength **360** corresponding to 905 nm. This graph **300** shows that, at these wavelengths **350**, **360**, deoxygenated hemoglobin absorbs more red light than oxygenated hemoglobin, and, conversely, oxygenated hemoglobin absorbs more infrared light than deoxygenated hemoglobin.

In addition to the differential absorption of hemoglobin derivatives, pulse oximetry relies on the pulsatile nature of arterial blood to differentiate hemoglobin absorption from absorption of other constituents in the surrounding tissues. Light absorption between systole and diastole varies due to the blood volume change from the inflow and outflow of arterial blood at a peripheral tissue site. This tissue site might also comprise skin, muscle, bone, venous blood, fat, pigment, etc., each of which absorbs light. It is assumed that the background absorption due to these surrounding tissues is invariant and can be ignored. Thus, blood oxygen saturation measurements are based upon a ratio of the time-varying or AC portion of the detected red and infrared signals with respect to the time-invariant or DC portion. This AC/DC ratio normalizes the signals and accounts for variations in light pathlengths through the measured tissue. Further, a ratio of the normalized absorption at the red wavelength over the normalized absorption at the infrared wavelength is computed:

$$\frac{RD}{IR} = \frac{\left(\frac{\mathrm{Red}_{AC}}{\mathrm{Red}_{DC}}\right)}{\left(\frac{IR_{AC}}{IR_{DC}}\right)} \quad (2)$$

where Red_{AC} and IR_{AC} are the root-mean-square (RMS) of the corresponding time-varying signals. This "red-over-infrared, ratio-of-ratios" cancels the pulsatile signal. The desired Sp_aO_2 measurement is then computed from this ratio.

FIG. **4** shows a graph **400** depicting the relationship between RD/IR and Sp_aO_2. This relationship can be approximated from Beer-Lambert's Law, as outlined below. However, it is most accurately determined by statistical regression of experimental measurements obtained from human volunteers and calibrated measurements of oxygen saturation. The result can be depicted as a curve **410**, with measured values of RD/IR shown on a y-axis **420** and corresponding saturation values shown on an x-axis **430**. In a pulse oximeter device, this empirical relationship can be stored in a read-only memory (ROM) look-up table so that Sp_aO_2 can be directly read-out from input RD/IR measurements.

According to the Beer-Lambert law of absorption, the intensity of light transmitted through an absorbing medium is given by:

$$I = I_0\exp\left(-\sum_{i=1}^{N}\varepsilon_{i\lambda}c_i x_i\right) \quad (3)$$

where I_0 is the intensity of the incident light, $\varepsilon_{i,\lambda}$ is the absorption coefficient of the i^{th} constituent at a particular wavelength λ, c_i is the concentration coefficient of the i^{th} constituent and x_i is the optical path length of the i^{th} constituent. As stated above, assuming the absorption contribution by all constituents but the arterial blood is constant, taking the natural logarithm of both sides of equation (3) and removing time invariant terms yields:

$$\ln(I) = -[\varepsilon_{HbO2,\lambda}C_{HbO2} + \varepsilon_{Hb,\lambda}C_{hb}]X(t) \quad (4)$$

Measurements taken at both red and infrared wavelengths yield:

$$RD(t) = -[\varepsilon_{HbO2,RD}C_{HbO2} + \varepsilon_{hb,RD}C_{hb}]x_{RD}(t) \quad (5)$$

$$IR(t) = -[\varepsilon_{HbO2,IR}C_{HbO2} + \varepsilon_{Hb,IR}C_{hb}]x_{IR}(t) \quad (6)$$

Taking the ratio RD(t)/IR(t) and assuming $x_{RD}(t) \approx x_{IR}(t)$ yields:

$$RD/IR = [\varepsilon_{HbO2,RD}C_{HbO2} + \varepsilon_{Hb,RD}C_{Hb}]/[\varepsilon_{HbO2,IR}C_{HbO2} + \varepsilon_{Hb,IR}C_{hb}] \quad (7)$$

Assuming further that:

$$C_{HbO2} + C_{Hb} = 1 \quad (8)$$

then equation (1) can be solved in terms of RD/IR yielding a curve similar to the graph **400** of FIG. **4**.

Sensor Interface

FIG. **2** also depicts the sensor interface **114** for one data channel. An interface input **112** from the sensor **110** is coupled to an analog signal conditioner **220**. The analog signal conditioner **220** has an output **223** coupled to an analog-to-digital converter (ADC) **230**. The ADC output **118** is coupled to the DSP **150**. The analog signal conditioner also has a gain control input **225** from the DSP **150**. The functions of the analog signal conditioner **220** are explained in detail below. The ADC **230** functions to digitize the input signal **112** prior to further processing by the DSP **150**, as described below. The sensor interface **114** also has an emitter current control input **241** coupled to a digital-to-analog converter (DAC) **240**. The DSP provides control information to the DAC **240** via the control input **241** for a pair of emitter current drivers **250**. One driver output **252** couples to the red emitter **212** of the sensor **110**, and another driver output **254** couples to the IR emitter **214** of the sensor **110**.

FIG. **5** illustrates one embodiment of the analog signal conditioner **220**. The analog signal conditioner **220** receives a composite intensity signal **112** from the sensor detector **218** (FIG. **2**) and then filters and conditions this signal prior to digitization. The embodiment shown has a preamplifier **510**, a high pass filter **520**, a programmable gain amplifier **530** and a low pass filter **540**. The low pass filter output **223** is coupled to the ADC **230** (FIG. **2**). The preamplifier **510** converts the current signal **112** from the detector **218** (FIG. **2**) to a corresponding amplified voltage signal. The gain in the preamplifier **510** is selected in order to prevent ambient

light in the signal **112** from saturating the preamplifier **510** under normal operating conditions. The preamplifier output **512** is coupled to the high pass filter **520**, which removes the DC component of the detector signal **112**. The corner frequency of the high pass filter **520** is set well below the multiplexing frequency of the red and infrared emitters **212**, **214** (FIG. **2**). The high pass filter output **522** couples to the programmable gain amplifier **530**, which also accepts a programming input **225** from the DSP **150** (FIG. **2**). This gain is set at initialization or at sensor placement to compensate for variations from patient to patient. The programmable gain amplifier output **532** couples to a low-pass filter **540** to provide anti-aliasing prior to digitization.

As described above, pulse oximetry measurements rely on the existence of a pulsatile signal. The natural heart beat provides a pulsatile signal that allows measurement of arterial oxygen saturation. In the systemic circulation, all arterial pulsations are damped before flow enters the capillaries, and none are transmitted into the veins. Thus, there is no arterial pulse component in the venous blood and absorption caused by venous blood is assumed canceled by the ratio-of-ratio operation described above. Venous blood, being at a relatively low pressure, will "slosh back and forth" during routine patient motions, such as shivering, waving and tapping. This venous blood sloshing creates a time-varying signal that is considered "noise" and can easily overwhelm conventional ratio-based pulse oximeters. Advanced pulse oximetry techniques allow measurement of Sp_vO_2 under these circumstances. For example, such advanced techniques are disclosed in U.S. Pat. No. 5,632,272, which is assigned to the assignee of the current application. This measurement is only available during motion or other physiological events causing a time-varying venous signal.

The venous blood may also have a pulsatile component at the respiration rate, which can be naturally induced or ventilator induced. In adults, the natural respiration rate is 10-15 beats per minute (bpm). In neonates, this natural respiration rate is 30-60 bpm. The ventilator induced pulse rate depends on the ventilator frequency. If this respiration induced venous pulse is of sufficient magnitude, advanced pulse oximetry techniques, described below, allow measurement of Sp_vO_2.

A controlled physiological event, however, can be created that allows for a continuous measurement of venous oxygen saturation, independent of motion or respiration. U.S. Pat. No. 5,638,816, which is assigned to the assignee of the current application discloses a technique for inducing an intentional active perturbation of the blood volume of a patient, and is referred to as an "active pulse." Because peripheral venous oxygen saturation, Sp_vO_2, is a desirable parameter for stereo pulse oximetry applications, it is advantageous to provide for a continuous and controlled pulsatile venous signal.

FIG. **2** depicts an active pulse mechanism used in conjunction with a pulse oximetry sensor. An active pulser **260** physically squeezes or otherwise perturbs a portion of patient tissue **270** in order to periodically induce a "pulse" in the blood at the tissue site **202**. A pulser drive **280** generates a periodic electrical signal to a transducer **262** attached to the patient. The transducer **262** creates a mechanical force against the patient tissue **270**. For example, the pulser **260** could be a solenoid type device with a plunger that presses against the fleshy tissue to which it is attached. The DSP **150** provides pulse drive control information to a digital to analog converter (DAC) **290** via the control input **291**. The DAC output **292** is coupled to the pulser drive **280**. This allows the processor to advantageously control the magnitude of the induced pulse, which moderates scattering as described below. The pulser **260** could be a pressure device as described above. Other pressure mechanisms, for example a pressure cuff, could be similarly utilized. Other methods, such as temperature fluctuations or other physiological changes, which physiologically alter a fleshy medium of the body on a periodic basis to modulate blood volume at a nearby tissue site could also be used. Regardless of the active pulse mechanism, this modulated blood volume is radiated by a pulse oximeter sensor and the resulting signal is processed by the signal processing apparatus described below to yield Sp_vO_2.

Signal Processor

FIG. **6** illustrates the processing functions of the digital signal processor (DSP) **150** (FIG. **1**A). Each data channel input **152**, **154**, **158** (FIG. **1**A) is operated on by one or more of the front-end processor **610**, saturation calculator **620**, plethysmograph feature extractor **630** and multiple parameter processor **640** functions of the DSP **150**. First, a digitized signal output from the ADC **230** (FIG. **2**) is input **602** to the front-end processor **610**, which demultiplexes, filters, normalizes and frequency transforms the signal, as described further below. A front-end output **612** provides a red signal spectrum and an IR signal spectrum for each data channel as inputs to the saturation calculator **620**. Another front-end output **614** provides a demultiplexed, normalized IR plethysmograph for each data channel as an input to the feature extractor **630**. The saturation calculator output **622** provides arterial and venous saturation data for each data channel as input to the multiple parameter processor **640**. One feature extractor output **632** provides data on various plethysmograph shape parameters for each data channel as input into the multiple parameter processor **640**. Another feature extractor output **634**, also coupled to multiple parameter processor **640**, provides an indication of plethysmograph quality and acts as a threshold for determining whether to ignore portions of the input signal **602**. The multiple parameter processor has a numerical output **642** that provides same-channel Δsat parameters and cross-channel parameters, such as Δsat_{xy} or $\Delta pleth_{xy}$ to a display **180** (FIG. **1**A). The numeric output **642** may also provide saturation and plethysmograph parameters directly from the saturation calculator **620** or the feature extractor **630** without further processing other than data buffering. The multiple parameter processor also has a graphical output **644** that provides plethysmograph waveforms for each data channel in addition to graphics, depending on a particular application, the indicate the trend of the numerical parameters described above.

Front-End Processor

FIG. **7** is a functional block diagram of the front-end processor **610** for the stereo pulse oximeter. The digitized sensor output **118** (FIG. **2**) is an input signal **602** to a demultiplexer **710**, which separates the input signal **602** into a red signal **712** and an infrared signal **714**. The separated red and infrared signals **712**, **714** are each input to a filter **720** to remove unwanted artifacts introduced by the demultiplexing operation. In one embodiment, the filter **720** is a finite-impulse-response, low-pass filter that also "decimates" or reduces the sample rate of the red and infrared signals **712**, **714**. The filtered signals **722** are then each normalized by a series combination of a log function **730** and bandpass filter **740**. The normalized signals, RD(t), IR(t) **742** are coupled to a Fourier transform **750**, which provides

red frequency spectrum and infrared frequency spectrum outputs, RD(ω), IR(ω) **612**. A demultiplexed infrared signal output **614** is also provided.

Saturation Calculator

FIG. **8** shows a graph **800** illustrating idealized spectrums of RD(t) and IR(t) **752** (FIG. **7**). The graph has an x-axis **810** that corresponds to the frequency of spectral components in these signals and a y-axis **820** that corresponds to the magnitude of the spectral components. The spectral components are the frequency content of RD(t) and IR(t), which are plethysmograph signals corresponding to the patient's pulsatile blood flow, as described below. Thus, the frequencies shown along the x-axis **810**, i.e. f_0, f_1, f_2, are the fundamental and harmonics of the patient's pulse rate. The spectrum of RD(t), denoted RD(ω) **612** (FIG. **7**), is shown as a series of peaks, comprising a first peak **832** at a fundamental frequency, f_0, a second peak **842** at a first harmonic, f_1 and a third peak **852** at a second harmonic, f_2. Similarly, the spectrum of IR(t), denoted IR(ω) **612** (FIG. **7**), is shown as another series of peaks, comprising a first peak **834** at a fundamental frequency, f_0, a second peak **844** at a first harmonic, f_1 and a third peak **854** at a second harmonic, f_2. Also shown in FIG. **8** is the ratio of the spectral peaks of RD(t) and IR(t), denoted RD(ω)/IR(ω). This ratio is shown as a first ratio line **838** at the fundamental frequency f_0, a second ratio line **848** at the first harmonic f_1, and a third ratio line **858** at the second harmonic f_2.

The magnitude of these ratio lines RD(ω)/IR(ω) corresponds to the ratio RD/IR defined by equation (2), and, hence, can be used to determine Sp_aO_2. This can be seen from Parseval's relation for a periodic signal, x(t), having a period T, where X_k is the spectral component at the kth harmonic of x(t):

$$\frac{1}{T}\int_0^T (|x(t)|)^2 dt = \sum_k (|X_k|)^2 \tag{9}$$

Equation (9) relates the energy in one period of the signal x(t) to the sum of the squared magnitudes of the spectral components. The term $|X_k|^2$ can be interpreted as that part of the energy per period contributed by the kth harmonic. In an ideal measurement, the red and infrared signals are the same to within a constant scale factor, which corresponds to the arterial oxygen saturation. Likewise, the red and infrared spectra are also the same to within a constant scale factor. Thus, in an ideal measurement, all of the ratio lines **838**, **848**, **858** have substantially the same amplitude. Any differences in the amplitude of the ratio lines is likely due to motion, scattering or other noise contaminations, as discussed further below. Accordingly, any of the RD(ω)/IR(ω) ratio lines is equivalent to the ratio, RD/IR, of equation (2) and can be used to derive Sp_aO_2.

One skilled in the art will recognize that the representations in FIG. **8** are idealized. In particular, in actual measured data, especially if contaminated by noise, the frequencies of the peaks of RD(ω) do not correspond exactly to the frequencies of the peaks of IR(ω). For example, the fundamental frequency, f_0, found for RD(ω) will often be different from the fundamental frequency, f_0', found for IR(ω) and similarly for the harmonics of f_0.

FIG. **9** shows a graph **900** illustrating idealized spectrums RD(ω) and IR(ω) and associated ratio lines measured with an active pulse sensor. The graph **900** has an x-axis **910** that corresponds to the frequency of spectral components in these signals and a y-axis **920** that corresponds to the magnitude of the spectral components. The spectrum, RD(ω), is shown as two series of peaks. One series of peaks **930** occurs at a fundamental frequency, f_{h0}, and associated harmonics, f_{h1} and f_{h2}, of the patient's pulse (heart) rate. Another series of peaks **940** occurs at a fundamental frequency, f_{p0}, and associated harmonics, f_{p1} and f_{p2}, of the active pulse rate. Similarly, the spectrum, IR(ω), is shown as two series of peaks. One series of peaks **950** occurs at a fundamental frequency, f_{h0}, and associated harmonics, f_{h1} and f_{h2}, of the patient's pulse rate. Another series of peaks **960** occurs at a fundamental frequency, f_{p0}, and associated harmonics, f_{p1} and f_{p2}, of the active pulse rate. Accordingly, there are two series of RD/IR ratio lines. One series of ratio lines **970** are at the patient's pulse rate and associated harmonics, and another series of ratio lines **980** are at the active pulser rate and associated harmonics.

Because only the arterial blood is pulsatile at the patient's pulse rate, the ratio lines **970** are only a function of the arterial oxygen saturation. Accordingly, Sp_aO_2 can be derived from the magnitude of these ratio lines **970**, as described above. Further, a modulation level for the active pulse is selected which insignificantly perturbates the arterial blood while providing a measurable venous signal. This is possible because the arterial blood pressure is significantly larger than the venous pressure. The modulation level is regulated as described above with respect to FIG. **2**, i.e. the DSP **150**, via a pulser drive control **291**, sets the magnitude of the pulser drive **280** to the pulse inducing mechanism **262**. Assuming that the active pulse modulation of the arterial blood is insignificant, only the venous blood is pulsatile at the active pulser rate. Hence, the ratio lines **980** are only a function of the venous oxygen saturation. Accordingly, Sp_aO_2 can be derived from the magnitude of the pulse rate related ratio lines **980** in the same manner as Sp_aO_2 is derived from the magnitude of the pulse rate related ratio lines.

Scattering

Propagation of optical radiation through tissue is affected by absorption and scattering processes. The operation of pulse oximeters was described qualitatively above using an analysis based on the Beer-Lambert law of absorption, equation (3). This approach, however, fails to account for the secondary effects of light scattering at pulse oximeter wavelengths. The primary light scatterer in blood is erythrocytes, i.e. red blood cells. A qualitative understanding of the effects of scattering on pulse oximetry is aided by a description of red blood cell properties within flowing blood.

Human blood is a suspension of cells in an aqueous solution. The cellular contents are essentially all red blood cells, with white cells making up less the $1/600^{th}$ of the total cellular volume and platelets less than $1/800^{th}$ of the total cellular volume. Normally the hematocrit, which is the percentage of the total volume of blood occupied by cells, is about 50% in large vessels and 25% in small arterioles or venules.

Red blood cells are extremely deformable, taking on various shapes in response to the hydrodynamic stresses created by flowing blood. For example, assuming a laminar blood flow within a vessel, a parabolic velocity profile exists that is greatest in the vessel center and smallest along the vessel walls. Nominally, red blood cells are shaped as biconcave disks with a diameter of 7.6 um and thickness of 2.8 um. Exposed to this velocity profile, the red blood cells become parachute-shaped and aligned in the direction of the blood flow. Thus, during systole, transmitted light is scat-

tered by aligned, parachute-shaped cells. During diastole, the light is scattered by biconcave disks having a more or less random alignment.

The time-varying shape and alignment of the red blood cells can have a significant effect on measured values of oxygen saturation if scattering is ignored. Analogous to the analysis using the Beer-Lambert absorption law, scattering can be qualitatively understood as a function of the scattering coefficients of various tissues. Specifically, the bulk scattering coefficient can be written as:

$$\mu_s = V_b \mu_b + V_t \mu_t \quad (10)$$

where V_b is the blood volume, $.\mu_b$ is the scattering coefficient of blood, V_t is the surrounding tissue volume and $.\mu_t$ is the scattering coefficient of the surrounding tissue. The volume, V_t, and scattering coefficient, $.\mu_t$, of the surrounding tissue are time invariant. The blood volume, V_b, however, is pulsatile. The ratio of ratios computation, RD/IR, results in normalization of the time invariant or DC tissue absorption and cancellation of the time varying or AC pulsatile blood volume absorption to yield a number related to oxygen saturation. This computational approach is valid because the absorption coefficients of blood, ε_{HbO2}, λ, ε_{Hb}, λ given in equation (4) were assumed to change only slowly over time. The scattering coefficient of blood $.\mu_b$, however, is time variant. As described above, this variation is due to the time-varying alignment and shape of the red blood cells. This time variation in the detected intensity of light transmitted through a tissue site is not normalized or canceled by the RD/IR calculation. Further, because the magnitude of the scattering coefficient variations is a function of blood flow, these variations become more pronounced with larger pulses in the blood supply. As a result, scattering produces frequency-dependent magnitude variations in the ratio lines RD(ω)/IR(ω).

FIG. **9** illustrates the effect of scattering on the spectra of the detected red and infrared intensity waveforms. When these waveforms are transformed into the frequency domain, the time varying component of scattering manifests itself as spreads **978**, **988** in the RD/IR ratio lines at each harmonic of the plethysmograph or active pulse rate. The magnitude of the ratio lines **970** at the fundamental and harmonics of the patient's pulse rate varies between a minimum **972** and a maximum **974**, resulting in a magnitude spread **978**. Similarly, the magnitude of the ratio lines **980** at the fundamental and harmonics of the active pulse rate varies between a minimum **982** and a maximum **984**, resulting in a magnitude spread **988**. Normally, absent motion artifact or noise contamination, the spread **978**, **988** in the ratio lines is quiet small, but the magnitude of these spreads **978**, **988**, increases with larger blood flows or pulse magnitudes. Scattering attributable to an active pulse can be regulated by adjusting the magnitude of the active pulse modulation based upon the amount of spread **978**, **988** of the ratio line magnitudes. Thus, the active pulse magnitude can be increased to obtain a larger detected AC signal, but limited to below the point at which scattering becomes significant.

FIG. **10** depicts an embodiment of the signal processing for determining oxygen saturation from the ratio lines of RD(ω)/RD(ω). The red spectrum RD(ω) **612** and infrared spectrum IR(ω) **612**, computed as described above with respect to FIG. **7**, are input to a peak detector **1010**. The peak detector **1010** separately calculates localized maximums for RD(ω) and IR(ω). The peak detector output **1012** is a series of frequencies corresponding to the patient pulse rate fundamental and harmonics. If an active pulse is used, the peak detector output **1012** is also a series of frequencies corresponding to the active pulse rate. Although the active pulse rate is known, the detected peaks may have been shifted due to noise, motion artifact or other signal contamination. The peak detector output **1012** is coupled to a series combination of peak matcher **1020** and ratio line calculator **1030**. The ratio lines RD/IR are calculated by matching the frequency peaks of RD(ω) with the nearest frequency peaks of IR(ω). The ratio lines associated with the pulse rate harmonics **1032** are then separated into a different set from the ratio lines associated with the active pulse harmonics **1034**, assuming an active pulse is utilized. An average ratio line for each set **1032**, **1034** is calculated by averaging **1060** all ratio lines in a set. The magnitude of the average ratio line r **1062** for the pulse rate set **1032** is then fed to a look-up table (LUT) **1090**, which provides an output **622** of the measured value of Sp_aO_2. Similarly, if an active pulse is used, the magnitude of the average ratio line μ **1064** for the active pulse rate set **1034** is then fed to a LUT **1090**, which provides an output **622** of the measured value of Sp_vO_2. A scattering detector **1080** computes the spread **988** (FIG. **9**) in the set of ratio lines associated with the active pulse and provides this value **1082** to the DSP **150** (FIG. **2**) so that the DSP can set the pulser drive control **291** (FIG. **2**) to regulate the magnitude of the active pulse.

Alternatively, Sp_vO_2 may be measured from respiration-induced pulses in the venous blood, described above, without utilizing an active pulse sensor. Specifically, a series of ratio lines **980** (FIG. **9**) would occur at a fundamental frequency, f_{r0}, and associated harmonics, f_{r1} and f_{r2}, of the respiration rate, which is either known from the ventilator frequency or derived from a separate measurement of the natural respiration. As shown in FIG. **10**, the ratio lines associated with the respiration rate harmonics **1034** are then separated into a different set from the ratio lines associated with the pulse rate harmonics **1032**. An average ratio line for the respiration rate set **1034** is calculated by averaging **1060** all ratio lines in that set. The magnitude of the average ratio line μ **1064** for the respiration rate set **1034** is then fed to a look-up table (LUT) **1090**, which provides an output **622** of the measured value of Sp_vO_2.

Plethysmograph Feature Extractor

FIG. **11** illustrates the standard plethysmograph waveform **1100**, which can be derived from a pulse oximeter. The waveform **1100** is a visualization of blood volume change in the illuminated peripheral tissue caused by arterial blood flow, shown along the y-axis **1110**, over time, shown along the x-axis **1120**. The shape of the plethysmograph waveform **1100** is a function of heart stroke volume, pressure gradient, arterial elasticity and peripheral resistance. The ideal waveform **1100** displays a broad peripheral flow curve, with a short, steep inflow phase **1130** followed by a 3 to 4 times longer outflow phase **1140**. The inflow phase **1130** is the result of tissue distention by the rapid blood volume inflow during ventricular systole. During the outflow phase **1140**, blood flow continues into the vascular bed during diastole. The end diastolic baseline **1150** indicates the minimum basal tissue perfusion. During the outflow phase **1140** is a dicrotic notch **1160**, the nature of which is disputed. Classically, the dicrotic notch **1160** is attributed to closure of the aortic valve at the end of ventricular systole. However, it may also be the result of reflection from the periphery of an initial, fast propagating, pressure pulse that occurs upon the opening of the aortic valve and that precedes the arterial flow wave. A double dicrotic notch can sometimes be observed, although its explanation is obscure, possibly the result of reflections reaching the sensor at different times.

FIG. **12** is a graph **1200** illustrating the absorption of light at a tissue site illuminated by a pulse oximetry sensor. The graph **1200** has a y-axis **1210** representing the total amount of light absorbed the tissue site, with time shown along an x-axis **1220**. The total absorption is represented by layers including the static absorption layers due to tissue **1230**, venous blood **1240** and a baseline of arterial blood **1250**. Also shown is a variable absorption layer due to the pulse-added volume of arterial blood **1260**. The profile **1270** of the pulse-added arterial blood **1260** is seen as the plethysmograph waveform **1100** depicted in FIG. **11**.

FIG. **13** illustrates the photoplethysmograph intensity signal **1300** detected by a pulse oximeter sensor. A pulse oximeter does not directly detect absorption, and hence does not directly measure the standard plethysmograph waveform **1100** (FIG. **11**). However, the standard plethysmograph can be derived by observing that the detected intensity signal **1300** is merely an out of phase version of the absorption profile **1270**. That is, the peak detected intensity **1372** occurs at minimum absorption **1272** (FIG. **12**), and minimum detected intensity **1374** occurs at maximum absorption **1274** (FIG. **12**). Further, a rapid rise in absorption **1276** (FIG. **12**) during the inflow phase of the plethysmograph is reflected in a rapid decline **1376** in intensity, and the gradual decline **1278** (FIG. **12**) in absorption during the outflow phase of the plethysmograph is reflected in a gradual increase **1378** in detected intensity.

FIG. **14** illustrates the digital signal processing for plethysmograph feature extraction **630** (FIG. **6**). The input **614** is the IR signal output from the demultiplexer **710** (FIG. **7**). This signal is shifted into a first-in, first-out (FIFO) buffer, which allows fixed-length portions of the input signal **614** to be processed for feature extraction. The buffered output signal **1412** is coupled to a shape detector **1420**, slope calculator **1430**, feature width calculator **1440** and a notch locator **1450**, which perform the core feature extraction functions. The shape detector **1420** determines if a particular buffered signal portion **1412** contains specific gross features, such as a peak, a valley, an upward slope, a downward slope, a dicrotic notch or a multiple dicrotic notch. A detected shape output **1422** containing one or more flags indicating the gross feature content of the current signal portion **1412** is coupled to the other feature extraction functions **1430**, **1440**, **1450** and to the waveform quality determination functions **1460**, **1470**, **1480**. A slope calculator **1430** determines the amount of positive or negative slope in the signal portion **1412** if the shape detector output **1422** indicates a slope is present. The output slope value **1432** is coupled to the waveform quality functions **1460**, **1470**, **1480** in addition to the feature extraction output **632**. A feature calculator **1440** quantifies a feature in one or more signal portions **1412** specified by the shape detector **1420**, such as the magnitude, the area under, or the width of a peak or notch. The feature calculator output **1442** is a code indicating the feature and its value, which is coupled to the feature extraction output **632**. A feature locator **1450** quantifies the time of occurrence of one or more features of a signal portion **1412** as specified by the shape detector **1420**. The feature locator output **1452**, which is coupled to the feature extraction output **632**, is a code indicating a feature and an associated code indicating time of occurrence in reference to a particular epoch. The feature locator output **1452** allows a determination of the relative location of plethysmograph features in addition to a phase comparison of plethysmographs derived from two or more tissue sites. Another feature extraction output **634**, which is coupled to the multiple parameter processor **640** (FIG. **6**), provides an indication of waveform quality. Input signals portions **1412** not having either a sharp downward edge **1460**, a symmetrical peak **1470** or a gradual decline **1480** are not processed further.

Multiple Parameter Processor

FIG. **15** illustrates the multiple parameter processing portion **640** (FIG. **6**) of the signal processing. A differencing function **1510** has as inputs a first saturation value, Sp_1O_2, and a second saturation value, Sp_2O_2, **622**. The saturation input values **622** can be arterial and venous saturation values from a single data channel, arterial saturation values from two different data channels or venous saturation values from two different data channels. The differences of the saturation value inputs **622** are provided as an output **1514**, which is coupled to a saturation data memory **1520**. The saturation values **622** are also directly coupled to the saturation data memory **1520**. The memory **1520** stores a record of saturation values, SpO_2, for each channel, delta saturation values, Δsat, for each channel and cross-channel delta saturation values, Δsat_{xy}, as required for a particular application. A flow calculator **1530** utilizes a plethysmograph input **614** or a bio-impedance probe input **1534** to provide a flow value **1538**, which is also coupled to the saturation data memory **1520**. For example, the flow value **1538** may be a perfusion index, PI, defined as follows:

$$PI = \frac{IR_{max} - IR_{min}}{IR_{DC}} \tag{11}$$

where IR_{max} is the maximum value, IR_{min} is the minimum value, and IR_{DC} is the average value of the IR plethysmograph signal **614** (FIG. **7**).

The saturation data memory **1520** provides a buffered output **1522** that is coupled to a numerical display driver **1540**. The numerical display driver **1540** provides an output **642** to a standard display, such as LED or LCD numerical display modules or a CRT monitor. The memory output **1522** is also coupled to a saturation data analyzer **1530**, one function of which calculates a long-term trend of the values in memory **1520**. For example, the saturation data analyzer may average a saturation value over time, or provide samples of the saturation values taken at regular time intervals. The output **1532** can either be numerical, which is coupled to the numerical display driver **1540**, or graphical, which is coupled to the graphical display driver **1570**. The graphical display driver **1570** provides an output **644** to a standard graphical display device, such as LED or LCD graphical display modules or a CRT monitor.

A pleth data memory **1550** has as inputs the IR plethysmograph signals **614** (FIG. **7**) from each data channel and the associated extracted features **632** (FIG. **14**). The memory **1550** also has an input indicating waveform quality **634** (FIG. **14**). The pleth memory **1550** provides a buffered output **1558** that is coupled to the graphical display driver **1570**, allowing display of the plethysmograph waveforms for each data channel. The memory output **1558** is also coupled to a pleth data analyzer **1560**, one function of which calculates a long-term trend of the plethysmograph and shape parameters in pleth memory **1520**. For example, the pleth data analyzer **1560** may provide an average of particular shape parameters over time. As another example, the pleth data analyzer **1560** may provide a graphic showing an accumulation of many overlaid plethysmographs. The output **1562** can either be numerical, which is coupled to the numerical display driver **1540**, or graphical, which is coupled to the graphical display driver **1570**.

Another function of the saturation data analyzer **1530** and the pleth data analyzer **1560** is to compare oxygen status and plethysmograph parameters derived from multiple sites in order to isolate noise artifacts and to derive a more accurate estimate of these parameters. For example, it is unlikely that motion artifact will affect each peripheral site in the same manner. If the quality input **634** indicates a noisy plethysmograph for one channel during a particular time period, the pleth data analyzer **1560** can exchange this information **1565** with the saturation data analyzer **1530**. The saturation data analyzer **1530** can then ignore the saturation data for that channel for that time period in lieu of saturation data from another channel. In a similar fashion, noisy data from multiple channels can be averaged, correlated or otherwise processed to provide an estimate of Sp_aO_2, Sp_vO_2 or pulse rate, or to provide a plethysmograph that is more accurate than can be derived from a single data channel.

FIG. **16**A illustrates detail of a single-site display screen **180** for the stereo pulse oximeter. The display has a numerical display portion **1610** controlled by the numerical display driver **1540** (FIG. **15**) and a graphical display portion **1660** controlled by the graphical display driver **1570** (FIG. **15**). The numerical display portion **1610** displays a value for Sp_aO_2 **1620**, Sp_vO_2 **1630** and pulse rate **1640** for a particular tissue site. The graphical display portion **1660** displays a plethysmograph **1662** for the corresponding tissue site, which can be displayed as a single waveform or an accumulated multiple of overlayed waveforms that may reveal a waveform trend. A push button or menu selection allows the user to switch to a display of data from any single one of the multiple tissue sites to which a sensor is attached.

FIG. **16**B illustrates detail of a multi-site display screen **180** for the stereo pulse oximeter. The numerical display portion **1610** displays a value for Sp_aO_2 **1622** and Sp_vO_2 **1632** for a first tissue site. Also displayed is a value for Sp_aO_2 **1624** and Sp_vO_2 **1634** for a second tissue site. In addition, a value for pulse rate **1642** derived from either the first or second tissue site, or both, is displayed. The graphical display portion **1660** displays a first plethysmograph **1664** and a second plethysmograph **1666** corresponding to the first and second tissue sites, respectively. A push button, menu selection allows the user to manually switch between the single site display (FIG. **16**A) and the multi-site display (FIG. **16**B). Also, a triggering event, such as an alarm based on multiple-site oxygen status parameters, causes the display to automatically switch from the single-site display to the multi-site display, enabling the user better view the conditions that caused the triggering event.

One of ordinary skill will appreciate many display screens variations from those shown in FIGS. **16**A and **16**B that are within the scope of this invention. For example, the stereo pulse oximeter could be configured to provide several push button or menu selectable display screens. One display screen might display more than two channels of oxygen status data. Another display screen could display cross-channel parameters such as Δsat_{xy} or a comparison of plethysmograph shape parameters from two channels. One of ordinary skill will also appreciate many variations and modifications of layout and design for the graphical and numerical displays within the scope of this invention.

Stereo Pulse Oximetry Applications

Oxygen Titration

Oxygen is one of the most commonly used drugs in an intensive care unit and is an integral part of all respiratory support. The goal of oxygen therapy is to achieve adequate delivery of oxygen to the tissues without creating oxygen toxicity. Too little oxygen results in organ damage and, in particular, brain damage. Too much oxygen can result in, for example, pulmonary edema and, in neonates, retinopathy of prematurity (ROP). Infants receiving oxygen therapy, in particular, must have inspired oxygen concentration and blood oxygen levels monitored closely.

Oxygen titration in neonates is currently accomplished with either transcutaneous monitoring or monitoring with a conventional pulse oximeter. As mentioned above, transcutaneous monitoring involves the placement of a heated Clark electrode against the skin surface. The electrode is secured to the skin surface with an airtight seal to eliminate contamination by room air gases. The skin surface beneath the electrode is then heated, which opens pre-capillary sphincters allowing localized arteriolar blood flow beneath the sensor. The so-called T_cO_2 value that is measured correlates well with P_aO_2. However, there are several drawbacks to this approach. Because the skin surface must be heated, a fifteen minute elapsed time after application is necessary before stable readings are acquired. Further, the required temperature is 43-45° C. (110° F.), with an associated risk of burns. In addition, titration is often accomplished by simply maintaining T_cO_2 within acceptable limits for this parameter, e.g. an equivalent P_aO_2 of 50-80 mm Hg for neonates. However, P_aO_2 alone does not provide an indication of balance between inspired oxygen and the rate of tissue oxygen consumption. If the patient is particularly anemic or hypovolemic, has an abnormal hemoglobin, or a small cardiac output, then oxygen delivery may be inadequate even in the presence of a normal P_aO_2. Titration with a conventional pulse oximeter is similarly accomplished by maintaining Sp_aO_2 within acceptable limits, which also fails to consider tissue oxygen consumption.

Oxygen titration can be more adequately monitored with a continuous indication of oxygen consumption, which is equal to oxygen delivery according to Fick's algorithm, as noted above. Further, continuous monitoring of oxygen consumption at a peripheral tissue site, although not necessarily indicative of overall oxygen consumption, may be indicative of an oxygen supply dependency. A measure of peripheral oxygen consumption can be expressed in terms of $\Delta sat = Sp_aO_2 - Sp_vO_2$ and perfusion, which, as noted above, are parameters advantageously provided by the stereo pulse oximeter according to the present invention. Oxygen consumption at a peripheral site is obtained by multiplying the difference between peripheral arterial and venous oxygen content by perfusion at the site.

$$VpO_2 = [O_2 \text{ content (arterial)} - O_2 \text{ content (venous)}]\Phi \quad (12)$$

where oxygen content is measured in milliliters (ml) of O_2 per deciliters (dl) of blood and Φ denotes perfusion in deciliters per minute. Oxygen content, however, can be expressed in terms of the amount of oxygen bound to the hemoglobin plus the amount of oxygen dissolved in the plasma. The amount of bound oxygen is equal to the hemoglobin concentration, C_{hb}, in grams per deciliter of blood, times the hemoglobin carrying capacity, which is 1.34 milliliters of O_2 per gram of hemoglobin times the hemoglobin oxygen saturation, SO_vO_2. The amount of dissolved oxygen is simply the partial pressure of oxygen, PO_2, times the O_2 solubility coefficient in blood, which is 0.003 milliliters of O_2 per deciliter. The sum of these two terms yields:

$$O_2 \text{ content} = 1.34 C_{Hb} SO_2 + 0.003 PO_2 \quad (13)$$

Substituting equation (13) into equation (12) yields the following equation for tissue oxygen consumption:

$$VpO_2 = [1.34 C_{Hb}(Sp_aO_2 - Sp_vO_2) + 0.003(P_aO_2 - P_vO_2)]\Phi \quad (14)$$

Except when the fractional inspired oxygen, FiO_2, is high, blood plasma plays a minimal role in oxygen delivery. Thus, peripheral oxygen consumption is approximately:

$$VpO_2=[1.34C_{Hb}\Delta sat]\Phi \quad (15)$$

In order to illustrate a schema of oxygen titration, it is convenient to characterize the relationship between oxygen supplied at the airway to oxygen consumed at a peripheral tissue site. Specifically, characterization of the relationship between Δsat, Φ and FiO_2 is useful. Assuming constant oxygen consumption at the tissue site, equation (15) is:

$$\Delta sat\ \Phi=constant \quad (16)$$

Equation (16) has a simple analog in electronic circuits, i.e. a variable resistor across a current or voltage source adjusted to maintain constant power. In this analog circuit, the current through the resistor, I, is equivalent to perfusion, the voltage across the resistor, V, is equivalent to Δsat and the constant of equation (16) is equivalent to the constant power, P, consumed by the resistor. The equation representing this electrical analog is:

$$V\times I=P \quad (17)$$

FIG. **17**A shows a graph **1701** that depicts a family of curves each corresponding to different values of P in equation (17). The graph **1701** has an x-axis **1710** indicating current, I, and a y-axis **1720** indicating voltage, V. A first curve **1730** shows V versus I for a constant power, P, of 0.5 watts; a second curve **1740** shows V versus I for a constant P of 1 watt; and a third curve **1750** shows V versus I for a constant P of 2 watts. Using the analogy between equations (16) and equation (17), whenever Φ (current) is small, the Δsat (voltage) is large and vice-a-versa. Also, a change in consumption (power) causes a shift in the curve along with a change in its curvature. That is, if the body suddenly changes its metabolic rate at the peripheral tissue site, the curve will accordingly shift up or shift down and will change its shape. Equation (16) and the analogous constant consumption curves of FIG. **17**A assume a supply independent condition, i.e. that peripheral oxygen consumption is satisfied by peripheral oxygen delivery. If the peripheral tissue site is starved for oxygen, then the locus of points for Δsat versus Φ is quite different from a hyperbola The amount of tissue oxygen extraction is at a maximum and is independent of Φ. Accordingly Δsat is at a maximum and independent of Φ. The above analysis provides insight into the relationship between Δsat and Φ. The relationship between Δsat and FiO_2 can also be characterized.

FIG. **17**B shows a graph **1702** of saturation along a y-axis **1760** and fractional inspired oxygen along an x-axis **1770**. A curve of Sp_aO_2 **1780** and a curve of Sp_aO_2 **1790** are depicted versus FiO_2. The difference between these curves **1780**, **1790** yields Δsat **1785** versus FiO_2. When FiO_2 is zero **1772**, oxygen saturation and, hence, both Sp_aO_2 **1780** and Sp_vO_2 **1790** are zero. As FiO_2 is increased, Sp_aO_2 **1780** also increases until virtually reaching 100 percent saturation **1762**. As FiO_2 increases further, Sp_aO_2 **1780** stays at virtually 100 percent saturation **1762**. As FiO_2 is increased from zero **1772**, Sp_vO_2 **1790** also increases. In this low FiO_2 region **1774**, the peripheral tissue site is supply dependent and Δsat **1785** also increases. At a certain point, the tissue site oxygen demand is met by supply. In this supply independent region **1776**, oxygen consumption is constant and equation (16) is valid. Also, Δsat **1785** is at a constant maximum, which is a function of the metabolism at the tissue site. As FiO_2 increases further, eventually the partial pressure of oxygen becomes significant and the second term of equation (14) must be considered. In this high FiO_2 region **1778**, Δsat **1785** decreases because some of the tissue oxygen consumption is supplied by oxygen dissolved in the plasma.

FIG. **17**C shows a graph **1704** of saturation difference along a y-axis **1764** and fractional inspired oxygen along an x-axis **1770**. A curve of Δsat **1786** is depicted versus FiO_2, corresponding to the region Δsat **1785** depicted in FIG. **17**B. The curve **1786** has a first deflection point **1766** occurring at the transition between the low FiO_2 region **1774** (FIG. **17**B) and the supply independent region **1776** (FIG. **17**B). The curve **1786** also has a second deflection point **1768** occurring at the transition between the supply independent region **1776** (FIG. **17**B) and the high FiO_2 region **1778** (FIG. **17**B). The curve **1786** illustrates how the trend for Δsat, as measured by the stereo pulse oximeter, can be used to accurately titrate oxygen. The goal of oxygen titration is to supply sufficient oxygen to supply tissue demand and avoid unnecessarily high amounts of FiO_2. Thus, the Δsat parameter should be monitored so that FiO_2 is adjusted between the two deflection points **1766**, **1768**. For neonates, FiO_2 should be adjusted just beyond the first deflection point **1766**. For adults, FiO_2 should be adjusted just before the second deflection point **1768**.

FIG. **18** illustrates a graph having a three-dimensional surface **1800** generally depicting the relationship between Δsat, Φ and FiO_2 from the combined graphs of FIGS. **17**A and **17**C. The graph has an x-axis **1810** showing FiO_2, a y-axis **1820** showing Φ and a z-axis **1830** showing Δsat. The surface **1800** has a supply dependent region **1840**, a perfusion-limited region **1850**, a constant consumption region **1860** and a plasma dependent region **1870**. The surface describes the oxygen status of a peripheral tissue site. The supply dependent region **1840** corresponds to the low FiO_2 region **1774** (FIG. **17**B) described above. That is, inspired oxygen into the lungs is so low that, at the tissue site, oxygen extraction by the tissues is limited by oxygen delivery, and Δsat falls rapidly as FiO_2 is reduced. The perfusion-limited region **1850** along the x-axis **1810** represents a low perfusion state where equation (16) is not valid. That is, perfusion at the tissue site is so low that oxygen extraction by the tissues is at a maximum, and, hence, Δsat is at a maximum and is independent of FiO_2. A cross-section of the surface taken parallel to the y-axis **1820** yields a hyperbole-shaped constant consumption region **1860**, consistent with the constant metabolic rate curves illustrated above with respect to FIG. **17**A. The plasma dependent region **1870** corresponds to the high FiO_2 region **1778** (FIG. **17**B) described above. That is, inspired oxygen into the lungs is so high that the tissue site is partially dependent on oxygen dissolved in the plasma The surface **1800** illustrates that perfusion should be monitored simultaneously with Δsat to avoid the perfusion-limited region **1850**, where Δsat is an unresponsive indicator of FiO_2, and to avoid misinterpreting hyperbolic changes in Δsat that result from changes in perfusion.

Persistent Pulmonary Hypertension in Neonates

FIG. **19** illustrates the heart/lung circulation of a hypertensive neonate. Persistent Pulmonary Hypertension in Neonates (PPHN) is a neonatal condition with persistent elevation of pulmonary vascular resistance and pulmonary artery pressure. Shown is a neonatal heart **1902** and a portion of a neonatal lung **1904**. The pulmonary artery **1910** that normally feeds oxygen depleted "blue" blood from the right ventricle **1920** to the lung **1904** is constricted. The back pressure from the constricted artery **1910** results in a right-to-left shunting of this oxygen depleted blood through the ductus arteriosus **1930**, causing it to mix with oxygen rich

"red" blood flowing through the descending aorta **1940**. PPHN treatment options include vasodilators, such as nitric oxide (NO). Inhaled exogenous NO causes a dose-dependent decrease in pulmonary artery pressure and pulmonary vascular resistance, as well as a parallel increase in pulmonary blood flow, without affecting systemic arterial pressure. However, the response to NO therapy is a function of the cause of the PPHN as well as the time elapsed before initiation of therapy. Potential toxic effects of NO dictate the proper titration of NO gas. Too little NO may not effectively relieve pulmonary hypertension, and too much NO may cause cellular injury or toxicity. NO therapy is currently monitored using intermittent ultrasound imaging and/or in vitro blood gas measurements. The drawbacks to these techniques are noncontinuous monitoring and disturbances to the neonate that can exacerbate or not reflect the hypertension in the non-disturbed state.

The stereo pulse oximeter according to the present invention allows noninvasive, continuous monitoring of a neonate for detection and managed treatment of PPHN that does not disturb the patient. A right hand sensor **130** (FIG. **1**) provides arterial oxygen saturation and a plethysmograph for blood circulating from the left ventricle **1950** through the innominate artery **1960**, which supplies the right subclavian artery. Because the innominate artery **1960** is upstream from the shunt at the ductus arteriosus **1930**, the oxygen saturation value and plethysmograph waveform obtained from the right hand are relatively unaffected by the shunt and serve as a baseline or reference for comparison with readings from other tissue sites. Alternatively, a reference sensor can be placed on a facial site, such as an ear, the nose or the lips. These sites provide arterial oxygen saturation and a plethysmograph for blood circulating from the left ventricle **1950** to the innominate artery **1960**, which supplies the right common carotid artery (not shown), or to the left common carotid artery **1965**.

A foot sensor **120** (FIG. **1**) provides oxygen status for blood supplied from the descending aorta **1940**. The shunt **1930** affects both the oxygen saturation and the blood flow in the descending aorta **1940**. As stated above, the shunt **1930** causes oxygen-depleted blood to be mixed with oxygen-rich blood in the descending aorta **1940**. Because the descending aorta **1940** supplies blood to the legs, the oxygen saturation readings at the foot will be lowered accordingly. The PPHN condition, therefore, is manifested as a higher arterial oxygen saturation at the right hand reference site and a lower saturation at the foot site.

The shunt also allows a transitory left to right flow during systole, which distends the main pulmonary artery **1980** as the result of the blood flow pressure at one end from the right ventricle and at the other end from the aortic arch **1990**. A left-to-right flow through the shunt **1930** into the distended artery **1980** alters the flow in the descending aorta **1940** and, as a result, the plethysmograph features measured at the foot. The PPHN condition, therefore, also is manifested as a plethysmograph with a narrow peak and possibly a well-defined dicrotic notch at the left hand baseline site and a broadened peak and possibly no notch at the foot site.

An optional left hand sensor **110** (FIG. **1**) provides oxygen status for blood circulating from the left ventricle through the left subclavian artery **1970** that supplies the left arm. Because the left subclavian artery **1970** is nearer the shunt **1930** than the further upstream innominate artery **1960**, it may experience some mixing of deoxygenated blood and an alteration in flow due to the shunt **1930**. The PPHN condition, therefore, may also be manifested as a reduced saturation and an altered plethysmograph waveform at the left hand site as compared with the right hand baseline site, although to a lesser degree than with a foot site. Thus, the PPHN condition can be detected and its treatment monitored from Δsat and plethysmograph morphology comparisons between a right hand baseline sensor site and one or more other sites, such as the left hand or foot.

Patent Ductus Arteriosus

FIG. **20** illustrates the fetal heart/lung circulation. Shown is a fetal heart **2002** and a portion of a fetal lung **2004**. The lung **2004** is non-functional and fluid-filled. Instead, oxygenated blood is supplied to the fetus from gas-exchange in the placenta with the mother's blood supply. Specifically, oxygenated blood flows from the placenta, through the umbilical vein **2006** and into the right atrium **2022**. There, it flows via the foramen **2024** into the left atrium **2052**, where it is pumped into the left ventricle **2050** and then into the aortic trunk **2092**. Also, oxygenated blood is pumped from the right atrium **2022** into the right ventricle **2020** and directly into the descending aorta **2040** via the main pulmonary artery **2080** and the ductus arteriosus **2030**. Normally, the ductus arteriosus **2030** is only open (patent) during fetal life and the first 12 to 24 hours of life in term infants. The purpose of the ductus arteriosus **2030** is to shunt blood pumped by the right ventricle **2020** past the constricted pulmonary circulation **2010** and into the aorta **2040**.

FIG. **21** illustrates a neonatal heart **2002** with a patent ductus arteriosus **2030**. The ductus arteriosus frequently fails to close in premature infants, allowing left-to-right shunting, i.e. oxygenated "red" blood flows from the aorta **2040** to the now unconstricted pulmonary artery **2010** and recirculates through the lungs **2004**. A persistent patent ductus arteriosus (PDA) results in pulmonary hyperperfusion and an enlarged right ventricle **2020**, which leads to a variety of abnormal respiratory, cardiac and genitourinary symptoms. Current PDA diagnosis involves physical examination, chest x-ray, blood gas analysis, echocardiogram, or a combination of the above. For example, large PDAs may be associated with a soft, long, low-frequency murmur detectable with a stethoscope. As another example, two-dimensional, color Doppler echocardiography may show a retrograde flow from the ductus arteriosus **2030** into the main pulmonary artery **2080**. Once a problematic PDA is detected, closure can be effected medically with indomethacin or ibuprofen or surgically by ligation. Multiple doses of indomethacin are commonplace but can still result in patency, demanding ligation. A drawback to current diagnostic techniques is that clinical symptoms of a PDA can vary on an hourly basis, requiring extended and inherently intermittent testing.

The stereo pulse oximeter according to the present invention allows for continuous evaluation of PDA symptoms using non-invasive techniques. A right hand sensor **130** (FIG. **1**) provides arterial oxygen saturation and a plethysmograph for blood circulating from the left ventricle **2050** through the innominate artery **2160**, which supplies the right subclavian artery leading to the right arm. Because the innominate artery **2160** is upstream from the shunt at the ductus arteriosus **2030**, the oxygen saturation value and plethysmograph waveform obtained from the right hand are relatively unaffected by the shunt and serve as a baseline for comparison with readings from other tissue sites.

A foot sensor **120** (FIG. **1**) provides oxygen status for blood supplied from the descending aorta **2040**. Unlike a PPHN condition, the shunt **2030** does not affect oxygen saturation in the descending aorta **2040**, because the relatively low pressure in the pulmonary artery **2010** does not allow a mixing of deoxygenated blood into the relatively

high pressure flow of oxygenated blood in the aorta **2040**. However, like a PPHN condition, the shunt **2030** does affect the aortic flow. In particular, the shunt allows a transitory left-to-right flow during systole from the high pressure aorta **2040** to the low pressure pulmonary circulation **2010**. This left-to-right flow through the shunt **1930** alters the flow in the descending aorta **1940** and, as a result, the plethysmograph features measured at the foot. The PDA condition, therefore, is manifested as a normal plethysmograph with a characteristically narrow peak and well-defined dicrotic notch at the right-hand baseline site compared with a damped plethysmograph with a broadened peak and reduced or missing notch at the foot site. Further, the foot site waveform is phase shifted from the baseline waveform. These plethysmograph differences are accompanied by comparable arterial oxygen saturation values between the right-hand site and the foot site.

An optional left hand sensor **110** (FIG. **1**) provides oxygen status for blood circulating from the left ventricle through the left subclavian artery **2170** that supplies the left arm. Because the left subclavian artery **2170** is nearer the shunt **2030** than the further upstream innominate artery **2160**, it may experience some alteration in flow due to the shunt **2030**. The PDA condition, therefore, may also be manifested as an altered plethysmograph waveform at a left hand site as compared with the right hand baseline site, although to a lesser degree than with a foot site. Thus, the PDA condition can be detected and its treatment monitored from $\Delta sat_{xy} \approx 0$ and plethysmograph morphology and phase comparisons between a right hand baseline sensor site and one or more other sites, such as the left hand or foot. One of ordinary skill will recognize that multiple site comparisons using the stereo pulse oximeter of the current invention may also be used to detect other cardiac abnormalities that cause mixing of oxygenated and deoxygenated blood, such as a ventricular hole or a patent foramen. Further, abnormal mixing of oxygenated and deoxygenated blood may also be manifested in measurements provided by the stereo oximeters other than Δsat_{xy} and .$\Delta pleth_{xy}$ as described above. For example, an inversion in Δsat at a particular tissue site, i.e., Sp_vO_2 being larger than Sp_aO_2 at that site, would indicate such an abnormal condition.

Aortic Coarctation

Coarctation of the aorta is a congenital cardiac anomaly in which obstruction or narrowing occurs in the distal aortic arch or proximal descending aorta. It occurs as either an isolated lesion or coexisting with a variety of other congenital cardiac anomalies, such as a PDA. If the constriction is preductal, lower-trunk blood flow is supplied predominantly by the right ventricle via the ductus arteriosus, and cyanosis, i.e. poorly oxygenated blood, is present distal to the coarctation. This can be detected by the stereo pulse oximeter from a comparison of Sp_aO_2 between an upper body and a lower body site. If the constriction is postductal, blood supply to the lower trunk is supplied via the ascending aorta Differential plethysmographs between the upper and lower extremities may not exist if the ductus is widely patent. If the ductus closes, however, this condition can be detected by the stereo pulse oximeter as a reduced amplitude and phase delay between the plethysmographs measured at a lower body site with respect to an upper body site.

The stereo pulse oximeter has been disclosed in detail in connection with various embodiments of the present invention. These embodiments are disclosed by way of examples only and are not to limit the scope of the present invention, which is defined by the claims that follow. One of ordinary skill in the art will appreciate many variations and modifications within the scope of this invention.

What is claimed is:

1. A physiological monitor comprising:

interface componentry in communication with at least two sensors adapted to be positioned on tissue sites of a patient, the interface componentry having at least two outputs corresponding to signals received from the at least two sensors and responsive to light transmitted through corresponding tissue sites; and

at least one signal processor in communication with the interface componentry outputs, the at least one signal processor configured to:

receive a first output, from the interface componentry, associated with a first tissue site of a first limb of the patient;

receive a second output, from the interface componentry, associated with a second tissue site on a second limb of the patient;

determine at least one first oxygen saturation measurement from the first tissue site and at least one second oxygen saturation measurement from the second tissue site in response to the first output and the second output;

determine the presence of a heart abnormality of an infant based at least in part on a comparison of the at least one first oxygen saturation measurement with the at least one second oxygen saturation; and

display an indication of the heart abnormality.

2. The physiological monitor of claim **1**, wherein the at least one signal processor is further configured to determine the heart abnormality is a patent ductus arteriosus, based, at least in part, on a determination that a difference between the at least one first oxygen saturation measurement and the at least one second oxygen saturation measurement is substantially zero.

3. The physiological monitor of claim **2**, wherein the at least one signal processor is further configured to:

determine plethysmograph measurements from the first tissue site and the second tissue site; and

compare at least one first plethysmograph measurement from the first tissue site with a second plethysmograph measurement from the second tissue site,

wherein the determination of the patent ductus arteriosus is further based on the comparison between the at least one first plethysmograph measurement and the at least one second plethysmograph measurement.

4. The physiological monitor of claim **3**, wherein the comparison between the at least one first plethysmograph measurement and the at least one second plethysmograph measurement identifies a phase difference between the at least one first plethysmograph measurement and the at least one second plethysmograph measurement.

5. The physiological monitor of claim **4**, wherein the determination of the patent ductus arteriosus is based at least in part on a determination that the phase difference is substantially non-zero.

6. The physiological monitor of claim **3**, wherein the comparison between the at least one first plethysmograph measurement and the at least one second plethysmograph measurement identifies a relative amount of damping between the at least one first plethysmograph measurement and the at least one second plethysmograph measurement.

7. The physiological monitor of claim **6**, wherein the determination of the patent ductus arteriosus is based at least in part on a determination that the relative amount of damping is substantially non-zero.

8. The physiological monitor of claim 1, wherein a first sensor of the at least two sensors is configured to output the first output and be positioned on a right arm and a second sensor of the at least two sensors is configured to output the second output and be positioned on one of a left foot or a left hand.

9. A method for determining a heart abnormality in an infant, the method comprising:

using a pulse oximeter to determine a first oxygen saturation measurement from a first tissue site on a first limb of a patient;

using the pulse oximeter to determine a second oxygen saturation measurement from at least one additional tissue site on a second limb of the patient;

determining the presence of a heart abnormality of an infant based at least in part on a comparison of the first oxygen saturation measurement with the second oxygen saturation measurement; and

determining and displaying an indication of the heart abnormality on a display device of the pulse oximeter.

10. The method of claim 9, further comprising detecting a patent ductus arteriosus, based at least in part, on a determination that the difference between the first oxygen saturation measurement and the second oxygen saturation measurement is substantially zero.

11. The method of claim 10, wherein detecting a patent ductus arteriosus is further based on a determination of a phase difference between a first plethysmograph measurement at the first tissue site and a second plethysmograph measurement at the second tissue site.

12. The method of claim 11, wherein the phase difference is substantially non-zero.

13. The method of claim 10, wherein detecting a patent ductus arteriosus is further based on a determination of a relative amount of damping between a first plethysmograph measurement at the first tissue site and a second plethysmograph measurement at the second tissue site.

14. The method of claim 13, wherein the relative amount of damping is substantially non-zero.

15. The method of claim 9, wherein the first limb of the patient is a right arm and the second limb of the patient is one of a left foot or a left hand.

* * * * *

专利名称(译)	生理监测		
公开(公告)号	US10335072	公开(公告)日	2019-07-02
申请号	US15/351181	申请日	2016-11-14
[标]申请(专利权)人(译)	梅西莫股份有限公司		
申请(专利权)人(译)	Masimo公司		
当前申请(专利权)人(译)	Masimo公司		
[标]发明人	AL ALI AMMAR DIAB MOHAMED K KIANI MASSI E KOPOTIC ROBERT JAMES TOBLER DAVID		
发明人	AL-ALI, AMMAR DIAB, MOHAMED K. KIANI, MASSI E. KOPOTIC, ROBERT JAMES TOBLER, DAVID		
IPC分类号	A61B5/1455 A61B5/0205 A61B5/1459 A61B5/00 A61B5/024 A61M16/00 A61B5/145		
CPC分类号	A61B5/14551 A61B5/1459 A61B5/6814 A61B5/6815 A61B5/6819 A61B5/6825 A61B5/6826 A61B5/6829 A61B5/6838 A61B5/742 A61B5/746 A61B5/0205 A61M2230/205 A61B5/02416 A61M16/00 A61M16/021		
优先权	10/026013 2004-03-30 US 60/087802 1998-06-03 US		
其他公开文献	US20170188919A1		
外部链接	Espacenet		

摘要(译)

患者监测器具有多个适于附着到活体的组织部位的传感器。传感器产生传感器信号，其在组织部位内的脉动血液衰减之后响应于至少两个波长的光辐射。